# Study on Verification of Nuclear Data for Nuclear Design of Next Generation Thermal Reactors

Hironobu Unesaki

# Study on Verification of Nuclear Data for Nuclear Design of Next Generation Thermal Reactors

*November, 2001*

Hironobu Unesaki

# CONTENTS

# Chapter 1

# Introduction

## 1.1 NUCLEAR DATA AND ITS IMPACT ON NEUTRONICS DESIGN OF NEXT GENERATION THERMAL REACTORS

Nuclear energy is indispensable to secure the required energy for maintaining the civilized life of mankind. At the same time, there is also no doubt that further development of nuclear energy is inevitable with respect to the limitation in available resources and its impact to environment. The estimated uranium resource today is considered to be exhausted in approximately 70 to 80 years if it were continued to be only utilized in a frame of the current nuclear energy technology, namely in the light water reactors. The reduction and elimination of potential risk due to the radiological hazard from the spent fuel and high level wastes are with no doubt indispensable to achieve better public acceptance. Together with the request for enhanced safety, these two major concerns - the effective utilization of nuclear materials and the reduction of radiological hazard from the high level wastes - have been the strong motivation for promoting the investigation on the new concepts of nuclear reactors[1]-[8].

In accordance with the current delay in the realization of fast reactors, it is considered to be realistic that the current thermal reactors, represented by light water reactors (LWRs), would still be the dominating nuclear energy system in the near future. Under this circumstance, the effective utilization of nuclear materials and the reduction of radiological hazard from the high level wastes in the conventional thermal reactors have gathered great

interest worldwide, not only from viewpoints of the energy resource and the environmental impact, but also from a viewpoint of the nuclear security. This situation leads to the proposal of various new concepts of thermal reactors, which hereafter will be called as "next generation thermal reactors".

Among the various concepts of the nuclear reactors, considerable efforts have been focused on the uranium-fueled LWRs. Having a rich operation experience, practical and effective design routes, including both nuclear data and calculation codes, have been developed for uranium-fueled LWRs worldwide. However, these design routes are not always guaranteed to be successfully applied to the nuclear design of the next generation thermal reactors, since the nuclear characteristics of the next generation thermal reactors are often considerably different from those of the conventional LWRs. This is attributable to the differences in the operation targets of the next generation thermal reactors to the conventional ones, which result in the differences in the material composition and then lead to the differences in the neutronics behavior. Thus, the applicability and the performance of the design routes need to be verified before the application to an actual design of the next generation thermal reactors.

However, the uncertainty (or reliability) of the design route should be examined with much care, since the uncertainty in the calculated nuclear parameter obtained through design routes generally consists of two components, *i.e.* uncertainty from the nuclear data and that from the calculation method employed in the code. These two components cannot always be treated separately in the actual design of nuclear reactor and are often treated together in gross. The typical example of such feature is the so-called "bias factor", which is widely used as a practical measure of the accuracy of the design route. The bias factor is simply the difference between the calculated and the actual nuclear parameters of the system under investigation. This factor could be derived from the analysis of mock-up experiments,

provided that the mock-up experiments were sufficiently simulating the nuclear characteristics of the actual system. This, on the other hand, means that a bias factor for a certain core system cannot be directly applied to other systems, even its accuracy and uncertainty have been proven to be satisfactory for the system under investigation. Therefore, the uncertainty from the nuclear data and that from the calculation method should be separately treated and verified in order to generalize and assure the overall prediction accuracy for the nuclear system.

The recent compilation of new evaluated nuclear data libraries, represented by JENDL-3.2[9] of Japan, ENDF/B-VI[10] of the Unites States and JEF2.2[11] of European countries has acted to improve the reliability of the nuclear data used in reactor design. Also, it should be noted that the recent emergence of sophisticated design methodology, together with the notable progress in computation environment has acted to improve the reliability of the calculation methods. The combination of these latest nuclear data libraries and calculation methods seems to be promising to provide nuclear parameters with the improved accuracy. However, recent analyses show that there still exist considerable discrepancies in the core parameters obtained by using different nuclear data libraries. Even for a close relative of the current LWRs, the uncertainty in the prediction accuracy of nuclear parameters sometimes become rather remarkable, as will be shown in the following section. For the nuclear design of any nuclear systems whose material composition and neutronic balance differ from those of the conventional LWRs, such situation may be occasionally observed.

As mentioned above, the uncertainties in the calculation method can now be decreased to a great extent if desired; for example, the use of continuous energy Monte Carlo codes[12],[13] can eventually reduce the uncertainty in the calculation method. This decrease in the calculation uncertainty has act to unveil the uncertainty due to the nuclear data itself, which was hidden in the total uncertainty in the past. Consequently, importance of the precise

knowledge on the reliability of the nuclear data is even more emphasized, especially for the design of nuclear systems based on the new concept, where experimental data are less available.

Therefore, for the accurate and reliable design of next generation thermal reactors, it is inevitable as a first step to verify the accuracy and reliability of the nuclear data to be used in the nuclear design. The precise knowledge on the accuracy and reliability of the nuclear data will serve to further clarify the need for sophisticated methodologies to be used in the design calculations, and eventually will serve to improve the overall reliability of the nuclear design of next generation thermal reactors. From this point of view, studies on verification of nuclear data relevant to the nuclear design of next generation thermal reactors have been performed in the present thesis. In the studies, the two major objectives of the next generation thermal reactors, namely, the effective utilization of nuclear energy resources and reduction of potential radiological hazard in the nuclear wastes, will be focused. Study on verification of nuclear data relevant to the use of plutonium and thorium in thermal reactors will be treated from the viewpoint of effective utilization of nuclear energy resources, and those relevant to the incineration of minor actinides in thermal reactors will be treated from the viewpoint of reducing the potential radiological hazard from the nuclear wastes.

## 1.2 REACTOR DESIGN OF NEXT GENERATION THERMAL REACTORS AND NUCLEAR DATA

In this section, present status of reactor design as well as the nuclear data relevant to the next generation thermal reactors are briefly reviewed for mixed-oxide (MOX) fueled thermal reactors, thorium fueled thermal reactors and thermal systems for minor actinides incineration. Detailed overview on each topic will be given in the following chapters 2, 3 and 4, respectively.

### 1.2.1 MOX FUELED THERMAL REACTORS

The importance of the nuclear data for plutonium isotopes in LWR design was greatly focused through the research and development activities on high conversion light water reactors (HCLWR)[14],[15] mainly in the 1980s, which were the first major attempt in the world to actively utilize plutonium in LWRs. Verification of the nuclear data of plutonium isotopes was intensively performed through the analysis of critical experiments and international benchmark problems[16]. Although the interest on HCLWR programme gradually decreased in the world by the end of 1980s, the activities on research and development of HCLWR have contributed to emphasize the need for better understanding on the behavior of plutonium isotopes in thermal systems. The detailed description of the important contributions of HCLWR activities will be given in Chapter 2.

After HCLWR, the utilization of plutonium in thermal systems has shifted to the use in conventional light water reactors; the so-called Pu-thermal concept[17]-[24], where plutonium is used in the form of MOX fuel which is loaded either partially or fully into the conventional light water reactor. In addition to the increased difficulties in calculation method, it has been

pointed out that considerable fraction of the uncertainty in calculated nuclear parameters of MOX fueled LWRs may be attributable to the uncertainty in the nuclear data itself[25]. This is due to the fact that various heavy nuclides form a complicated situation from the viewpoint of neutronics in the system, and the uncertainties of the isotopes with less importance in conventional uranium-fueled LWRs become significant in MOX fueled systems. Such difficulties have been also pointed out in the feasibility studies of reduced-moderation water reactor (RMWR) concept[26]-[28] recently initiated by Japan Atomic Energy Research Institute, which represent the latest activities on the next-generation thermal reactors.

### 1.2.2 THORIUM FUELED THERMAL REACTORS

Use of thorium as energy resource was intensively carried out from the very beginning of the peaceful use of atomic energy. Although extensive studies have been performed during the 60s and 70s worldwide[29], the interest has declined until recently; it was from the mid 90s when the thorium fuel cycle has re-gained an increasing interest as a promising energy resource[30]. This is due to the potential superiority of thorium-based fuel cycle to the uranium-plutonium cycle from the viewpoint of resource availability and the reduced amount of actinides produced by the burnup of the fuel.

In addition to these aspects, the increasing concerns about the non-proliferation of nuclear materials and the strong demand for eliminating long-lived radiotoxic isotopes in the nuclear fuel cycle have also acted as strong motivations to pay attention and to reexamine the use of thorium-based fuel cycles. The renewed international interest on the thorium-based fuel cycles has led to various new activities, as will be described later in Chapter 3.

These activities are mainly based on neutronics calculations, and the results of design studies on the thorium-based fuel cycles could certainly be affected by the scheme of

calculation, including both the nuclear data and the neutronics design code. However, investigation on the sensitivity of the calculation scheme to the nuclear characteristics of thorium-based fuel cycle has not been performed intensively. It should be noted that, compared to the uranium-plutonium fuel cycle, less attention has been paid to the nuclear data related to the thorium-based fuel cycle. Therefore, to conduct further the feasibility studies on neutronic performance in consideration of the various candidates in the thorium-based fuel cycle, it is considered to be necessary to assess the current nuclear data and to clarify how the uncertainty of nuclear data affects the nuclear characteristics of thorium-based fuel cycle.

### 1.2.3 INCINERATION OF MINOR ACTINIDES USING THERMAL SYSTEMS

Studies on the methods to cope with the minor actinides (MAs) generated in the fuel cycle have been intensively carried out in the recent years[31]. These include studies on incineration of MAs using nuclear reactors or accelerator-driven subcritical systems by means of nuclear transmutation. Among them, the concept of incineration of MAs in LWRs has recently been intensively studied as a realistic option.

Among the MAs produced in nuclear reactors, major interest has been paid to Np and Am[32]. These two nuclides are the most burdensome ones from the viewpoint of production rate in the reactor, half life and hazard index. They are also important from the viewpoint of nuclear characteristics of the incineration system.

In the research and development of the incineration system, reliability of the nuclear data of MAs is important for the evaluation of the nuclear characteristics and the incineration performance. Although the experimental activities on MA nuclear data have been extensively performed from the 60s to 80s, the disagreement among the measured data is rather significant. Consequently, the differences among the evaluated data in the compiled

libraries are considerably large in general. This situation is also the same for Np and Am isotopes; compared to the major heavy nuclides (*i.e.* uranium and some plutonium isotopes), the evaluated nuclear data for Np and Am available still show remarkable discrepancies, as will be shown in Chapter 4.

These discrepancies in the nuclear data of MAs directly influence the incineration performance of the system. Therefore, in order to attain the reliability in the evaluation of nuclear characteristics and incineration performance of the MA incineration system, assessment of the nuclear data of MAs will be indispensable.

## 1.3 PURPOSE AND OUTLINE OF THE PRESENT THESIS

The goal of the present research work is to provide quantitative measures on the validity of the current nuclear data relevant to the nuclear design of next generation thermal reactors described in the preceding section, and also to provide suggestions for the anticipated reevaluation of nuclear data for the nuclides with major importance. In order to achieve this goal, data analysis and experimental methods relevant to the validation of nuclear data should also be developed.

For this purpose, the following studies were performed and summarized in the present thesis.

a) Analysis of benchmark problem devoted for void coefficient predictions in MOX fueled tight pitch light water reactor cells[33]:

This study is aimed at the verification of nuclear data relevant to nuclear design of next generation thermal reactors based on plutonium fuel. Detailed analysis of the calculated results obtained by Japanese SRAC/JENDL-3.2 and French APOLLO-2/JEF2.2 code systems has been performed to investigate the possible causes of the observed discrepancies in $k_\infty$ and void coefficients of MOX fueled light water fuel lattices. Although several activities on benchmark analysis of MOX fueled light water fuel lattice do exist, the intercomparison between the obtained results was mostly restricted to integrated nuclear parameters such as $k_\infty$ and reactivity coefficients. On the contrary, a detailed intercomparison of the results based on decomposition of reactivity difference into contributing nuclide, reaction and energy group has been performed in this study, which is the first attempt to be applied to major code systems. This study will be summarized in Chapter 2.

b) Criticality analysis of thorium-loaded thermal reactor critical experiments[34]:

This study is aimed at the verification of nuclear data relevant to nuclear design of next generation thermal reactors using thorium-based fuel. Criticality analysis of the experiments on thorium-loaded thermal reactors performed at the Kyoto University Critical Assembly (KUCA) of the Research Reactor Institute, Kyoto University, Japan, has been performed. Through the analysis of the KUCA experiments, assessment of $^{232}$Th cross section compiled in current evaluated nuclear data libraries has been performed. Recent activities related to thorium-based fuel systems are concentrated on the conceptual design studies of the reactor systems, and basic studies such as cross section measurement are rather scarce. Under this situation, the present study could be considered as the only major activity on verification of nuclear data based on integral experiments directly aiming at the thorium-based fuel cycle. This study will be summarized in Chapter 3.

c) Measurement and analysis of $^{237}$Np and $^{241}$Am fission rate ratios relative to $^{235}$U in thermal neutron fields of KUCA[35][36]:

This study is aimed at the verification of nuclear data relevant to nuclear design of MA incineration systems based on next generation thermal reactors. The measurements of $^{237}$Np and $^{241}$Am fission rate ratios relative to $^{235}$U have been performed at five cores having different neutron spectrum by using the KUCA. Assessment of $^{237}$Np and $^{241}$Am fission cross sections compiled in current evaluated nuclear data libraries has been performed through the analysis. The recent activities related to MA incineration studies are mostly either basic studies on cross section measurement, or application studies on the conceptual design of the incineration system.

Activities on the integral evaluation of MA nuclear data, such as measurement of MA reaction rate, are very scarce, and no activity has been reported in thermal neutron systems. The systematic measurement of MA reaction rates in thermal neutron systems performed in this study is the first activity ever reported on integral evaluation of MA nuclear data in thermal neutron systems. This study will be summarized in Chapter 4.

Finally, the conclusions drawn from the present thesis will be summarized in Chapter 5.

## References for Chapter 1


[1] Papers in *Proc. Int'l. Conf. on Future Nuclear Systems GLOBAL'97*, Yokohama, Kanagawa, Japan, Oct. 5-10, 1997 (1997).

[2] Papers in *Proc. Int'l. Conf. on Future Nuclear Systems GLOBAL'99*, Jackson Hole, USA, Aug. 29- Sept.3, 1999 (1999).

[3] BARANAEV, Yu. D., DOLGOV, V. V. and SEGEEV, Yu. A.: *Nucl. Eng. Design*, **173**, 159(1997).

[4] BIRKHOFER, A.: *Appl. Radiation and Isotopes*, **46**, 701 (1995).

[5] KUPITZ, J.: *Progress in Nucl. Energy*, **29**, 11 (1995).

[6] BANERJEE, S., ORTIZ, M. G., LARSON, T. K. and REEDER, D. L.: *Nucl. Eng. Design*, **186**, 111 (1998).

[7] OKA, Y.: JAERI-Conf-98-13, 3 (1998).

[8] CHO, S. J., KIM, B. S., KANG, M. G. *et al.*: *Nucl. Eng. Design*, **201**, 259 (2001).

[9] NAKAGAWA, T. *et al.*: *J. Nucl. Sci. Technol.*, **32**, 1259 (1995).

[10] ROSE, P. F. (comp. and ed.) : BNL-NCS-17541 (4th Ed.) (1991).

[11] NORDBORG, C. and SALVATORES, M. : *Proc. International Conf. on Nuclear Data for Science and Technology*, Gatlinburg, Tennessee, USA, May 9-13, 1994, Vol. **2**, 680 (1994).

[12] MORI, T. and NAKAGAWA, M.: JAERI-Data/Code 94-007, Japan Atomic Energy Research Institute (1994).

[13] BRIESMEISTER, J. F.: LA-12625-M, Ver. 4B, Los Alamos National Lab. (1997).

[14] OKUMURA, K. *et al.*: JAERI-M 90-96 (1990)

[15] OKUBO, T.: JAERI-Conf 98-13, 8 (1998)

[16] BERNNAT, W., ISHIGURO, Y. *et al.*: *Proc. Int, Conf. on the Physics of Reactors : Operation, Design and Computation PHYSOR90*, Marseille, France, April 23-27,

1990, Vol. **1**, p. I-54 (1990).

[17] KANDA, K. *et al.*: *Trans. Am. Nucl. Soc.*, **66**, 459 (1992)

[18] SASAKI, M., IWASE, T. and KANDA, K.: *Trans. Am. Nucl. Soc.*, **66**, 464 (1992)

[19] SAKURAI, S., MASUMI, R., MASUDA, F. and OKA, Y.: *Trans. Am. Nucl. Soc.*, **66**, 463 (1992)

[20] VAN DER MEER, K. *et al.*: *Trans. Am. Nucl. Soc.*, **77**, 366(1997).

[21] KANDA, K. *et al.*: *J. Atomic Energy Soc. Japan*, **40**, 834 (1998) (In Japanese).

[22] KLOOSTERMAN, J. L.: *Nucl. Technol.*, **130**, 227 (2000).

[23] PORTA, J. and DORIATH, J. -Y.: *J. Nucl. Mater.*, **274**, 153 (1999).

[24] PARATTE, J. M. *et al.*: *Prog. Nucl. Energy*, **38**, 335 (2001).

[25] CATHALAU, S., BENSLIMANE, A. *et al.*: *Nucl. Sci. Eng.*, **121**, 326 (1995).

[26] IWAMURA, T. *et al.*: JAERI-Research 99-058 (1999).

[27] ISHIKAWA, N. *et al.* eds.: JAERI-Conf 2000-010 (2000).

[28] IWAMURA, T. *et al.*: *Nuclear Engineering International*, Vol. **46**, Issue 560, 25 (2001).

[29] LUNG, M. and GREMM, O.: *Nucl. Eng. Design.*, **180**, 133 (1998).

[30] "*Thorium Based Fuel Options for the Generation of Electricity: Developments in the 1990s* ", IAEA-TECHDOC-1155, International Atomic Energy Agency (2000).

[31] "*Present Status of Transmutation Research and Development*", Atomic Energy Soc. Japan (1994) (In Japanese).

[32] "*Actinide and Fission Product Partitioning and Transmutation*", OECD-NEA (1999).

[33] UNESAKI, H., SHIROYA, S., KANDA, K., CATHALAU, S. *et al.*: *Nucl. Sci. Eng.*, **135**, 1 (2000).

[34] UNESAKI, H., KOBAYASHI, K. and SHIROYA, S.: *J. Nucl Sci. Technol.*, **38**, 370 (2001).

[35] UNESAKI, H., IWASAKI, T., KITADA, T. *et al.*: *J. Nucl Sci. Technol.*, **37**, 627 (2000).

[36] UNESAKI, H., IWASAKI, T., KITADA, T. *et al.*: *J. Nucl Sci. Technol.*, **38**, 600 (2001).

# Chapter 2

# Analysis of Differences in Void Coefficient Predictions for Mixed-Oxide-Fueled Tight-Pitch Light Water Reactor Cells

## 2.1 INTRODUCTION

The introduction of plutonium isotopes to the conventional uranium fuel results in a completely different behavior of the system in terms of neutronics balance. This phenomena has attracted interest in the reactor physics study.

The first major activities on the analysis of plutonium fueled thermal reactors were performed during the period of the research and development of high conversion light water reactors (HCLWRs)[1]-[4], where the plutonium oxide is used as mixed-oxide (MOX) fuel in tight-pitch fuel lattice with reduced moderator-to-fuel volume ratio.

During the activities on HCLWR development, the accurate prediction of void reactivity coefficient was one of the major concerns in the nuclear design with respect to safety aspects. Through the studies, it became clear that a complex neutronics balance is governing the void reactivity coefficient of tight-pitch MOX fuel lattices[5]-[8]. This is due to the fact that the void reactivity coefficient is a result of a complicated trade-off of both negative and positive contributions of various isotopes to the reactivity[9],[10]. Consequently, the void reactivity coefficient could be sensitive and be largely influenced by the nuclear data and the methods adopted in the cell calculation codes.

The impact of different nuclear data and codes on core parameters of plutonium fueled

thermal reactors, especially on the void reactivity coefficient, has been emphasized in the analysis of void reactivity coefficient of PROTEUS-HCLWR experiments[11]-[17] and also during the international benchmark program on HCLWR[18] sponsored by the Reactor Physics Committee of NEA (NEA/CRP). These activities have lead to improvements on both nuclear data libraries and calculation schemes, which served to decrease the discrepancies among different analyses [19],[20] and to reduce the uncertainty in nuclear design of plutonium fueled thermal reactors. Furthermore, the results of these studies are implemented in the compilation activities of newly evaluated nuclear data libraries, including JENDL-3.2 of Japan, JEF-2.2 of the European countries and ENDF/B-VI of the USA. Together with these efforts, development or refinement of reactor analysis codes with sophisticated calculation schemes has been proceeded.

The combination of these latest nuclear data libraries and codes seems to be promising to provide the estimation of nuclear parameters with increased accuracy[21],[22]. However, for MOX cells where various heavy nuclides form a complicated situation from the viewpoint of neutronics, the uncertainty in the integrated core parameters caused by the uncertainty in nuclear cross sections alone could be still considerable. It has been recently reported that the uncertainty in $k_\infty$ of a standard pressurized light-water reactor MOX cell will reach up to 1500 pcm (1 pcm = $1 \times 10^{-5} \Delta k / k$) due to the uncertainty in the cross sections.[23] The uncertainty due to the calculation scheme employed in the cell codes will further increase the overall uncertainty of the core parameters.

Thus it is worthwhile to perform a detailed comparison among the results obtained by latest code systems in order to check the discrepancy in the calculated nuclear characteristics and to provide possible physical interpretations on them. Such efforts are anticipated to provide invaluable information for the improvement of both the nuclear data and the methodology adopted in the code systems. Because of the complexity arising from the

isotopic composition and the emphasis on the resonance reactions, void reactivity coefficient for MOX fueled tight-pitch light water lattice could be considered to be a suitable benchmark problem for this purpose.

From these points of view, analysis of the benchmark calculations for void coefficient predictions for MOX fueled tight-pitch LWR cells has been performed in this study[1]. Detailed intercomparison of the results based on decomposition of reactivity difference into contributing nuclide, reaction type and energy group has been performed, which is the first attempt to be applied to major code systems.

[1] This study has been performed within the framework of collaborative studies between the French Atomic Energy Commission (CEA) and University Association in Japan. The University Association in Japan comprises researchers involved in the field of nuclear science and engineering from Hokkaido Univ., Tohoku Univ., Tokyo Institute of Technology, Musashi Institute of Technology, Tokai Univ., Nagoya Univ., Osaka Univ., Kyoto Univ., Kinki Univ. and Kyushu University.

## 2.2 SPECIFICATION OF THE BENCHMARK PROBLEM

The system investigated is an infinite array of light-water moderated hexagonal cells loaded with MOX fuels. The configuration of the cell is illustrated in **Fig. 2.1**. The diameter of the fuel pellet, outer diameter of the stainless cladding, and the hexagonal pitch of the cell are 0.82 cm, 0.95 cm and 1.22 cm, respectively. These values correspond to the moderator-to-fuel volume ratio ($V_m/V_f$) of approximately 1.1. The temperature of the fuel, clad and moderator were set to 873 K, 573 K and 573 K, respectively.

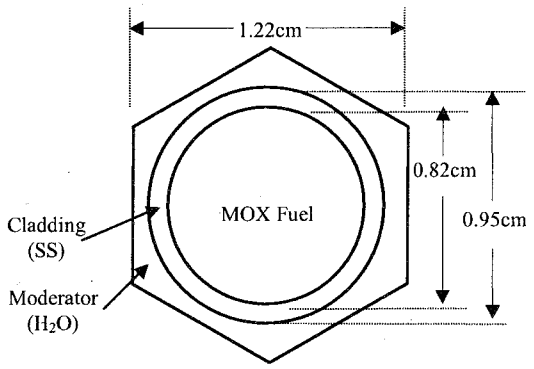


Figure 2.1 Configuration of the benchmark cell.

In order to illustrate the impact of isotopic composition of Pu on the void reactivity coefficient, two types of MOX fuels (Cell 1 and 2) having different Pu isotopic compositions have been studied. The isotopic compositions of the heavy nuclides of two cells[2] are shown in **Table 2.1**. Compared to Cell 1, Cell 2 has a more "clean" Pu isotopic composition free of higher Pu isotopes; the most significant difference is the small fraction of Pu-241 in Cell 2.

The void fraction of the light water moderator region of the fuel cell has been varied between 0% and 100%, namely, 0% to 90% with increment of 10%, and 95%, 97.5%, 99% and 100%. The small void fraction increment steps in the highly voided state are to cope

[2] Pu composition of Cell 1 corresponds to a "standard" Pu coming from reprocessed standard $UO_2$ fuel of PWR at about 33GWd/t, whereas that of Cell 2 corresponds to Pu coming from a reprocessed gas-cooled reactor fuel.

with the significant change in the neutron spectrum in this void region.

Table 2.1 Isotopic composition (wt%) of the MOX fuels

| Isotope | Cell 1 | Cell 2 |
|---|---|---|
| Pu-238 | 1.8% | 1.1% |
| Pu-239 | 57.9% | 79.2% |
| Pu-240 | 22.6% | 17.2% |
| Pu-241 | 10.8% | 1.4% |
| Pu-242 | 5.7% | 0.5% |
| Am-241 | 1.2% | 0.6% |
| Total(Pu+Am) | 100% | 100% |
| U-235 | 0.2% | 0.2% |
| U-238 | 99.8% | 99.8% |
| Total(U) | 100% | 100% |

## 2.3 CODES AND LIBRARIES

The Japanese SRAC code system[24] developed at JAERI with 107-group cross section library based on JENDL-3.2 (SRAC/JENDL-3.2) and the French APOLLO-2 code[25] developed at CEA with 172-group cross section library CEA93 based on JEF-2.2 (APOLLO-2/JEF2.2) were used for the analysis of the benchmark. A continuous-energy Monte Carlo code MVP[26] developed at JAERI together with cross section library based on JENDL-3.2 was also used.

The calculations were performed based on a 1-D cylindrical model with white (isotropic reflection) boundary condition. It should be noted that such cylindrical approximation together with the white boundary condition currently adopted may yield a considerable error compared to the exact 2-D hexagonal calculations[27] ; however, the essential feature of the two code systems are considered to be illustrated by the present analysis.

### 2.3.1 SRAC/JENDL-3.2 AND MVP/JENDL-3.2

The SRAC calculations were performed using the 107-group library based on JENDL-3.2. The thermal cutoff energy has been chosen to be 3.93 eV, which gives 59 fast groups and 48 thermal groups. The resonance calculations for the major resonant nuclides in the energy range of 961 eV to 3.93 eV were carried out with a ultra-fine $P_{ij}$ routine PEACO[28] incorporated in SRAC. This enables to treat the interaction between the resonance of different nuclides with more accuracy. The spatial dependence of resonance self-shielding effect was not taken into account; namely, the fuel region was treated as a single resonant material.

The reaction rates were calculated using the heterogeneous flux obtained by the eigenvalue calculation and the effective cross sections. The $k_\infty$ values used in this study were calculated based on the reaction rate balance by $k_\infty = P / (F+C-N)$, where $P$, $F$, $C$ and $N$ denote the production, fission, capture and $(n,2n)$ rates integrated over the entire energy and space, respectively. Note that the $(n,2n)$ reactions were treated as negative absorption and were subtracted from the actual absorption rate $(F+C)$ for calculating $k_\infty$ values.

The MVP calculations were executed in order to provide the complementary results so as to validate the SRAC calculations. Because of the limitations in the nuclear data provided for MVP, the temperatures of the fuel, clad and moderator were set to 900 K, 600 K and 600 K, respectively. 500,000 neutrons were tallied for each calculation, which gave the statistical error of less than 0.1% ($1\sigma$) for $k_\infty$ values.

### 2.3.2 APOLLO-2 / JEF2.2

The APOLLO-2 calculations were performed by using the 172-group CEA93 library (version 0) which is based on JEF-2.2 library. Thermal cutoff energy for this library is 4 eV, which gives 92 fast groups and 80 thermal groups. The resonance calculations were performed based on an improved self-shielding scheme (background matrix formalism method[29]). In order to take the spatial dependence of the resonance self-shielding into account, the fuel pellet was subdivided into six regions, each being treated as a separate resonance region. The space-dependent effective cross section for each resonant region was calculated based on background matrix formalism together with the wide resonance approximation. The interaction among the resonances was taken into account by iterating the whole self-shielding calculation by using the calculated effective cross section as the background cross section in the subsequent iteration. The number of this iteration was fixed

to two, which had been proven to give sufficient convergence in the effective cross section and the $k_\infty$ values. The $k_\infty$ values used in this study were calculated based on the reaction rate balance as described above.

It should be mentioned that the first analysis of MISTRAL experiments[30],[31] using SRAC/JENDL-3.2 and APOLLO-2/JEF2.2 shows that the $k_{eff}$ values are satisfactory predicted by the two codes[32],[33], assuring the overall quality and the performance of the two code systems. However, it should be noted that the two code systems give different tendency on the prediction of $k_{eff}$ for MOX cores; $k_{eff}$ is overpredicted by SRAC/JENDL-3.2 and is underpredicted by APOLLO-2/JEF2.2.

## 2.4 RESULTS AND DISCUSSION

### 2.4.1 COMPARISON OF INFINITE MULTIPLICATION FACTOR AND TOTAL VOID REACTIVITY

**Figure 2.2** shows the $k_\infty$ values of Cell 1 and Cell 2 and their dependence on the void fraction obtained by the two code systems. The $k_\infty$ values decrease with increasing void fraction up to approximately 60% to 70%, and then turn to increase with void fraction. The void fraction values corresponding to the minimum $k_\infty$ values are slightly different between the two cells; approximately 60% for Cell 1 and 70% for Cell 2. SRAC/JENDL-3.2 gives larger $k_\infty$ values for both cells for the entire void range. Especially, there is a clear difference in the shape of the $k_\infty$ curve for Cell 1 in void fraction above 90%; APOLLO-2/JEF2.2 gives a monotonous variation of $k_\infty$ versus the void fraction, whereas the $k_\infty$ values given by SRAC/JENDL-3.2 present some perturbations between 50 and 100% void which will be explained in the following paragraphs. It should be mentioned that the discrepancies between the SRAC and MVP results, both based on the JENDL-3.2 library, are sufficiently small compared with the statistical error of the MVP calculations. Especially, the overall shape of the $k_\infty$ curve is in good agreement, including the difference of the curve shapes between the two cells above 90% void.

The $k_\infty$ discrepancy between the two codes are shown in **Fig. 2.3**. The discrepancies have a clear dependence on the fuel composition and also have a large dependence on the void fraction. Cell 2, which is more free of higher Pu isotopes, shows large reactivity discrepancy than Cell 1. The maximum discrepancy is observed at void fraction range near 80%, which reaches up to approximately $1\% \Delta k/k$ and $1.35\% \Delta k/k$ for Cell 1 and Cell 2, respectively.

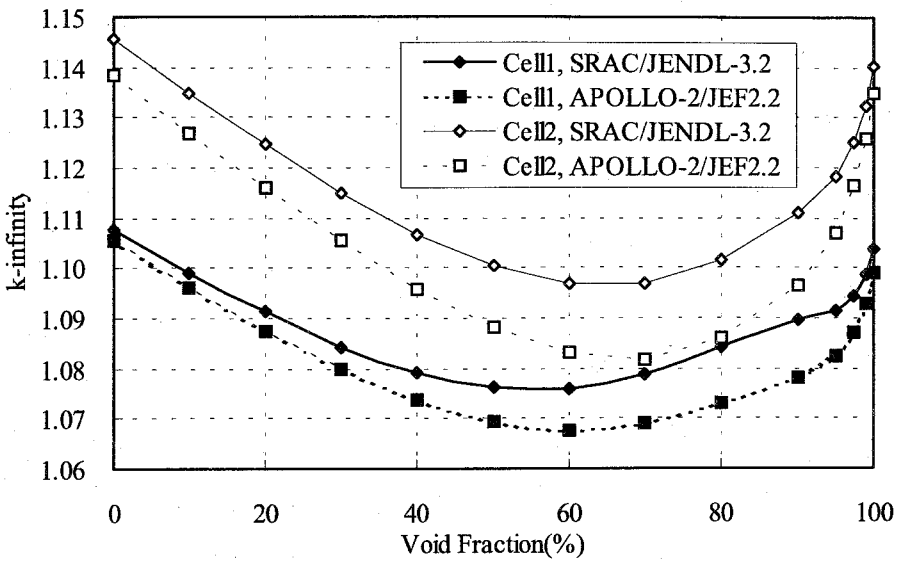


Figure 2.2 Comparison of $k_\infty$ values obtained by APOLLO-2/JEF2.2 and SRAC/JENDL-3.2.

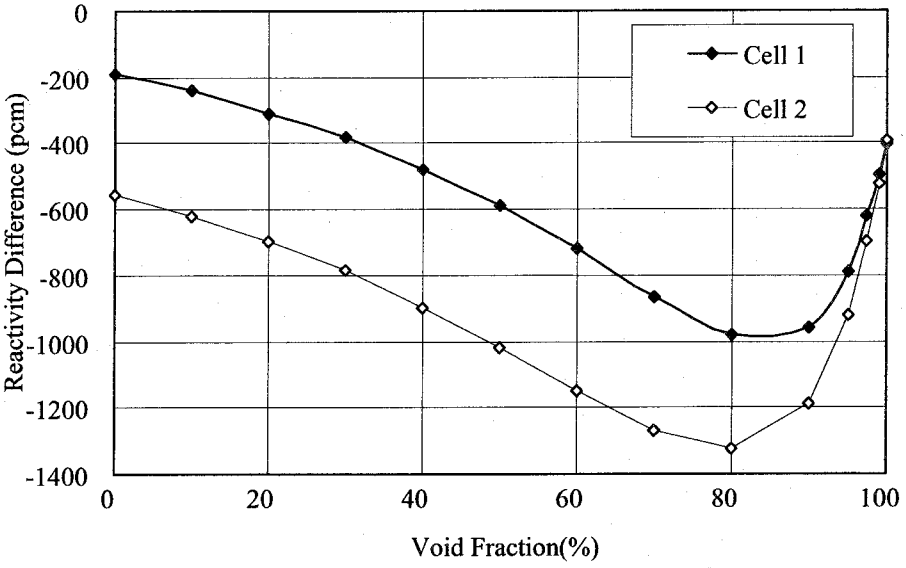


Figure 2.3 Void fraction dependence of $k_\infty$ value difference (A-S) between APOLLO-2/JEF2.2 (A) and SRAC/JENDL-3.2 (S).

The $k_\infty$ values for the 0% and 100% voided cells, the total void reactivity values (reactivity difference between 0% and 100% void), and their differences are shown in **Table 2.2**. For Cell 1, the $k_\infty$ discrepancy for the 100% voided cell is larger than that for the 0% void, whereas for Cell 2, an opposite trend is observed. The total void reactivity values are

calculated to be negative for both cells. However, the discrepancy in the total void reactivity between the APOLLO-2/JEF2.2 and SRAC/JENDL-3.2 results shows different trend for the two cells; it is negative for Cell 1 and positive for Cell 2.

Table 2.2 Comparison of $k_\infty$ values for 0% and 100% void and void reactivity

| | Cell 1 | | | Cell 2 | | |
|---|---|---|---|---|---|---|
| | APOLLO-2/ JEF2.2 | SRAC/ JENDL-3.2 | Difference* ($\Delta k/k$, pcm**) | APOLLO-2/ JEF2.2 | SRAC/ JENDL-3.2 | Difference ($\Delta k/k$, pcm) |
| $k_\infty$, 0% void | 1.10541 | 1.10773 | -189 | 1.13851 | 1.14572 | -552 |
| $k_\infty$,100% void | 1.09898 | 1.10387 | -403 | 1.13499 | 1.14009 | -394 |
| Void Reactivity (pcm) | -529 | -316 | -213 | -272 | -431 | +159 |

* [APOLLO-2/JEF2.2]-[SRAC/JENDL-3.2] ** 1 pcm = $1 \times 10^{-5}$, 1%=1000 pcm

To further investigate these discrepancies in $k_\infty$ values and void reactivities, the reactivity difference $\Delta\rho$ between the two different states $a$ and $b$ is decomposed into contributing nuclides $i$, energy groups $G$, and reactions using the following formula ;

$$\Delta\rho = \frac{1}{k_\infty}\sum_i\sum_G\left[\frac{\Delta P_i^G}{\overline{P}} - \frac{\Delta A_i^G}{\overline{A}}\right] = \sum_i\sum_G\frac{1}{k_\infty}\left[\frac{\Delta P_i^G}{\overline{P}} - \frac{(\Delta C_i^G + \Delta F_i^G - \Delta N_i^G)}{\overline{A}}\right] = \sum_i\sum_G \Delta\rho_i^G \,. \tag{2-1}$$

The production, capture, fission and $(n,2n)$ terms are defined as follows ;

$$\text{production term} = \frac{1}{k_\infty}\frac{\Delta P_i^G}{\overline{P}} = \frac{1}{k_\infty}\frac{\langle \nu\Sigma_{fi},\phi\rangle_b^{g\in G} - \langle \nu\Sigma_{fi},\phi\rangle_a^{g\in G}}{\overline{P}} \,, \tag{2-2}$$

$$\text{capture term} = -\frac{1}{k_\infty}\frac{\Delta C_i^G}{\overline{A}} = -\frac{1}{k_\infty}\frac{\langle \Sigma_{ci},\phi\rangle_b^{g\in G} - \langle \Sigma_{ci},\phi\rangle_a^{g\in G}}{\overline{A}} \,, \tag{2-3}$$

$$\text{fission term} = -\frac{1}{k_\infty}\frac{\Delta F_i^G}{\overline{A}} = -\frac{1}{k_\infty}\frac{\langle \Sigma_{fi},\phi\rangle_b^{g\in G} - \langle \Sigma_{fi},\phi\rangle_a^{g\in G}}{\overline{A}} \,, \tag{2-4}$$

$$(n,2n)\text{ term} = +\frac{1}{\overline{k_\infty}}\frac{\Delta N_i^G}{\overline{A}} = +\frac{1}{\overline{k_\infty}}\frac{\left\langle \Sigma_{(n,2n)i},\phi\right\rangle_b^{g\in G} - \left\langle \Sigma_{(n,2n)i},\phi\right\rangle_a^{g\in G}}{\overline{A}} \quad . \tag{2-5}$$

Here, the brackets ($\langle\ \rangle^{g\in G}$) denote the integration over energy range corresponding to the broad group $G$ and over the entire cell volume, and $\overline{R}$ denotes the average value of the physical quantity $R$ between the two states, *i.e.*,

$$\overline{k_\infty} = \frac{k_{\infty,a} + k_{\infty,b}}{2} \quad , \tag{2-6}$$

$$\overline{P} = \frac{\left\langle \nu\Sigma_f,\phi\right\rangle_a^{g\in all} + \left\langle \nu\Sigma_f,\phi\right\rangle_b^{g\in all}}{2} \quad , \tag{2-7}$$

$$\overline{A} = \frac{\left\langle (\Sigma_f + \Sigma_c - \Sigma_{(n,2n)}),\phi\right\rangle_a^{g\in all} + \left\langle (\Sigma_f + \Sigma_c - \Sigma_{(n,2n)}),\phi\right\rangle_b^{g\in all}}{2} \quad . \tag{2-8}$$

The two states $a$ and $b$ could be any two different states ( such as void fractions, code systems, libraries *etc.*). This formation is essentially based on that proposed by Okumura and Nishina in Ref.[10]; here, more detailed treatment of partial reaction terms has been made by the separate treatment of fission and production terms and the inclusion of $(n,2n)$ term.

### 2.4.2 BREAKDOWN OF REACTIVITY DIFFERENCE BETWEEN APOLLO-2/JEF2.2 AND SRAC/JENDL-3.2 INTO CONTRIBUTING COMPONENTS AT EACH VOID FRACTION

In this subsection, the two states $a$ and $b$ described above correspond to calculation results of APOLLO-2/JEF2.2 (A) and SRAC/JENDL-3.2 (S) , respectively. The differences (A-S) are analyzed in detail.

#### *2.4.2.A. Breakdown of Reactivity Based on One-group Collapsed Reaction Rates*

In order to investigate the global contribution of each individual isotopes to the

reactivity difference at each void fraction shown in Fig. 2.3, an analysis based on one-group collapsed cell averaged reaction rates has been performed.

**Figures 2.4** and **2.5** show the breakdown of the reactivity discrepancy between APOLLO-2/JEF2.2 and SRAC/JENDL-3.2 for Cell 1 and Cell 2, respectively. Here, only the one-group collapsed total components (summation of production, fission, capture and (*n,2n*) components) for each isotope are shown.

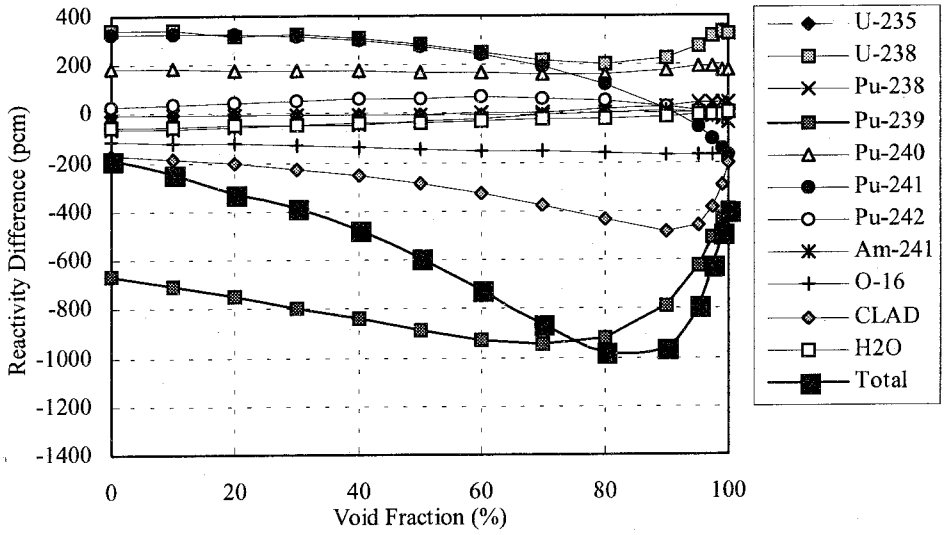


Figure 2.4 One-group breakdown of reactivity difference between APOLLO-2/JEF2.2 and SRAC/JENDL-3.2 for Cell 1. Only the total components are shown.

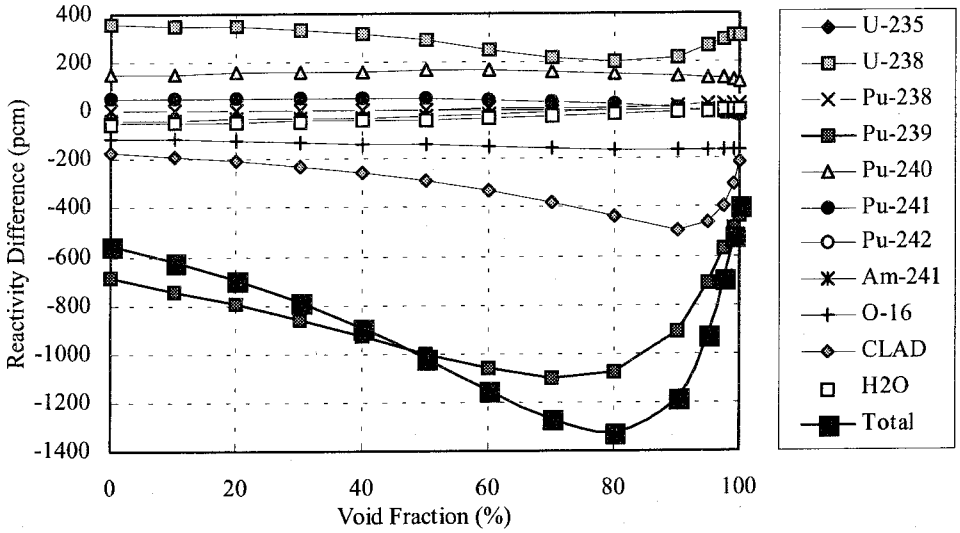


Figure 2.5 One-group breakdown of reactivity difference between APOLLO-2/JEF2.2 and SRAC/JENDL-3.2 for Cell 2. Only the total components are shown.

The reactivity discrepancy is a result of the cancellation of various negative and positive components, with some of them having larger magnitude than the total reactivity discrepancy. The large Pu-239 component, which shows a strong dependence on void fraction, is the most dominant cause of the reactivity discrepancy between the two codes.

The discrepancies caused by the fertile heavy nuclides, *i.e.* U-238, Pu-240 and Pu-242 are positive, showing that the energy-integrated capture rates obtained by APOLLO-2/JEF2.2 for these nuclides are smaller than those obtained by SRAC/JENDL-3.2. Among them, the U-238 component shows an apparent dependence on the void fraction, having a minimum value at approximately 80% void.

A clear difference between the two cells is found in the contribution of Pu-241. For Cell 1, the positive Pu-241 component, together with the U-238 component almost cancels with the negative Pu-239 component at 0% void and therefore acts to reduce the overall reactivity discrepancy. For Cell 2 with smaller Pu-241 content, such cancellation does not act as to reduce the overall reactivity discrepancy, so that the resulting reactivity discrepancy at 0% void becomes larger than that of Cell 1. Turning to 100% void, the contribution of Pu-241 turns to negative and therefore does not cancel with Pu-239 anymore in Cell 1. Thus the reactivity discrepancy at 100% void becomes larger than that at 0% void in Cell 1. For Cell 2, the reduction of the Pu-239 discrepancy dominates the overall reactivity discrepancy, and the reactivity discrepancy at 100% void becomes smaller than that at 0% void.

**Figures 2.6** and **2.7** show the contribution to the APOLLO-SRAC discrepancy (A-S) of the major heavy isotopes (U-238, Pu-239, 240 and 241) in their reaction types for Cell 1 and 2, respectively. The contribution of each individual isotope shows a characteristic dependence on void fraction, and the total component is a result of balance among the contributing reaction types. The difference between the two cells could be clearly seen in the void fraction dependence of each isotope; especially the total component of Pu-240 shows a

completely different profile. This is due to the different balance among the contributing reaction types, mainly by the difference in the capture term.

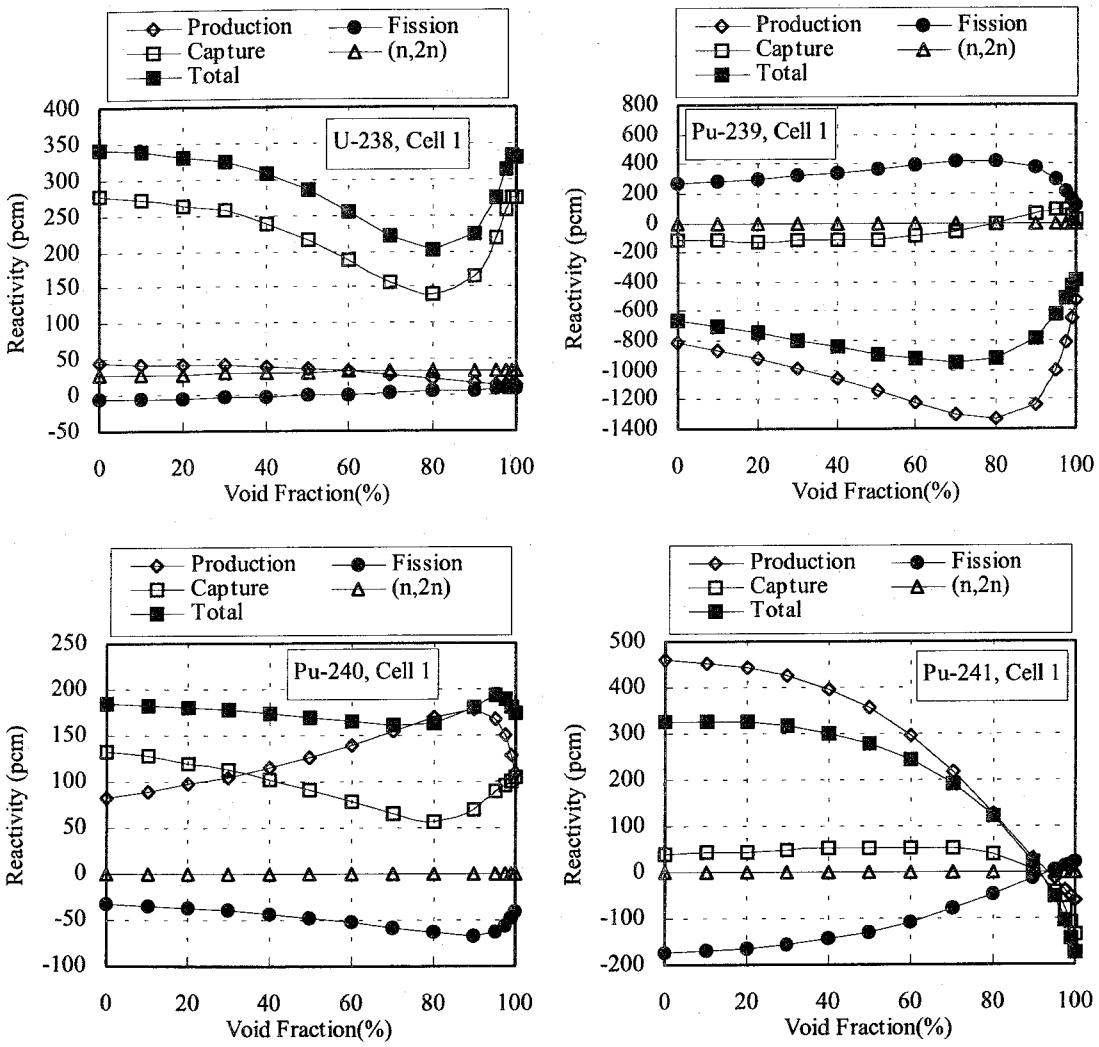


Figure 2.6 One-group breakdown of isotopic component of (A-S) discrepancy into reaction types for major heavy nuclides in Cell 1.

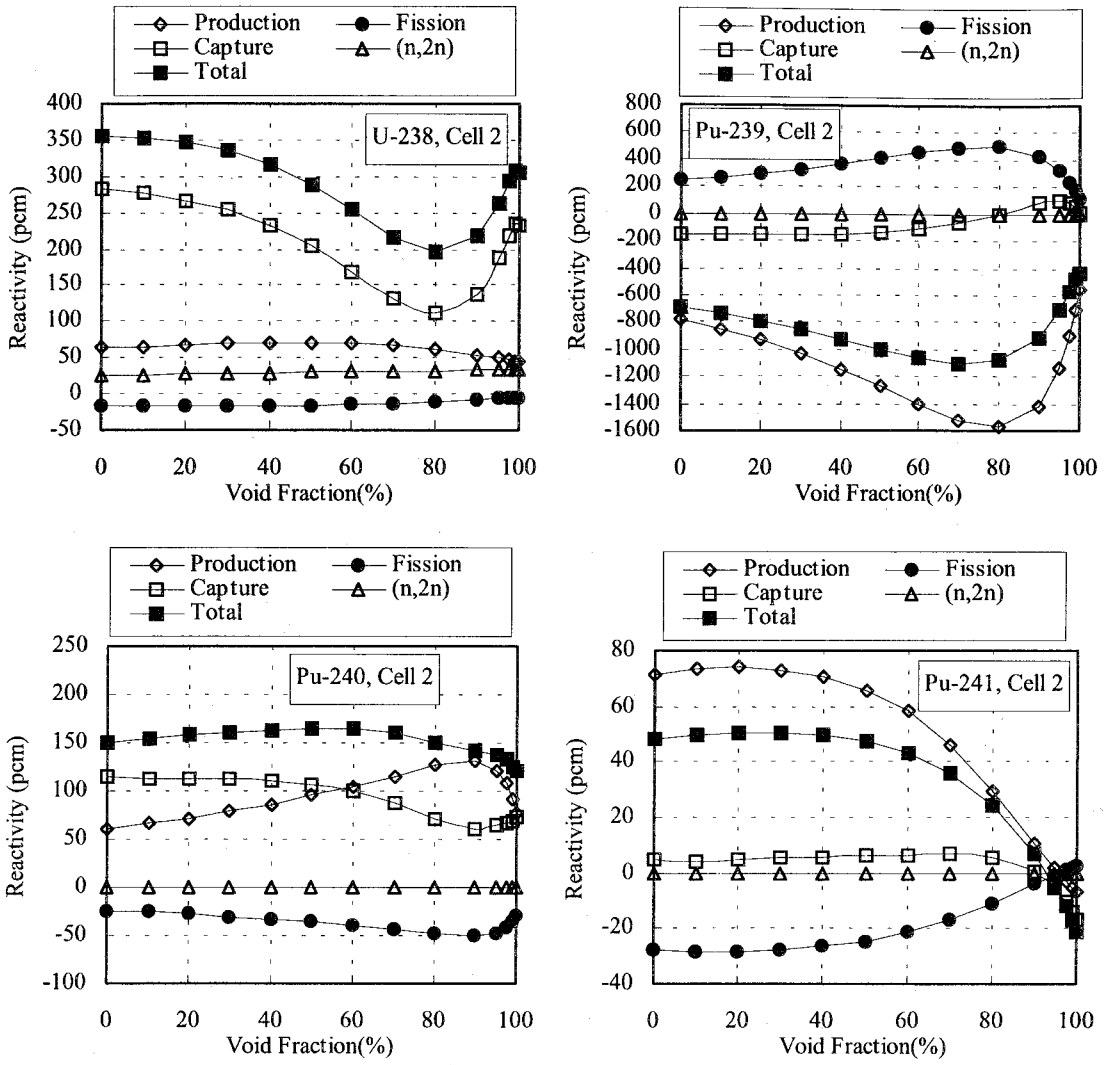


Figure 2.7 One-group breakdown of isotopic component of (A-S) discrepancy into reaction types for major heavy nuclides in Cell 2.

Turning to isotopes other than the heavy nuclides, the discrepancy due to the stainless steel cladding shows a considerable negative contribution, which also shows strong dependence on the void fraction. **Figure 2.8** shows the detailed contribution of the isotopes comprising stainless steel clad to the reactivity difference for Cell 1. The major contributors to the reactivity difference are Mn-55 and natural Fe, which show different dependence on the void fraction. The different shapes of the curves for the two isotopes indicate the different energy domain which dominates the reactivity difference caused by the two isotopes. The negative contribution of O-16 to the (A-S) discrepancy is also remarkable, especially in high

void fractions. Its contribution is approximately -120 pcm for reference 0% voided cells and gradually increases with void fraction, and reaches up to approximately -180 pcm for 100% voided cells. This effect is comparable to the contribution of some of the heavy isotopes.

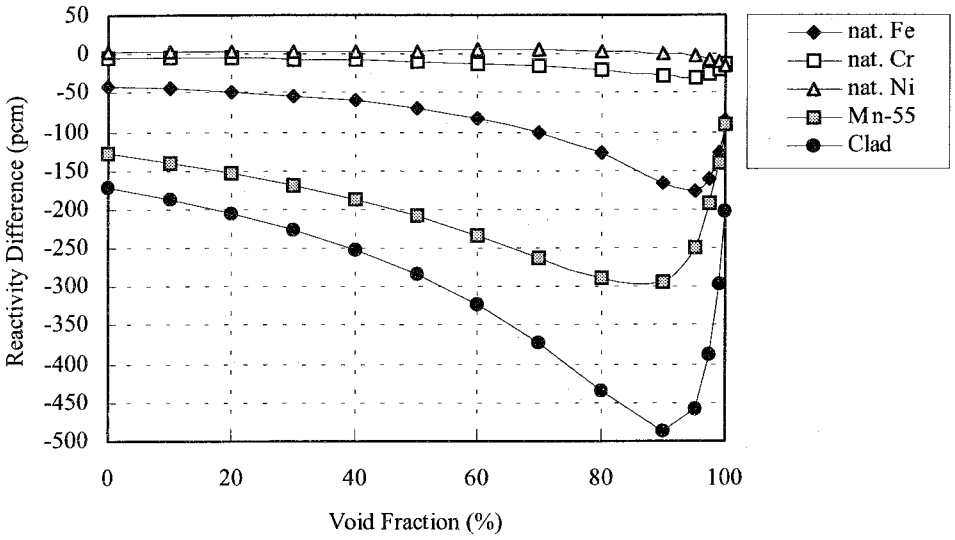


Figure 2.8 Contribution of stainless steel cladding to reactivity difference between APOLLO-2/JEF2.2 and SRAC/JENDL-3.2 for Cell 1.
Only the total components are shown.

### *2.4.2.B Analysis in Terms of Energy and Reaction Types Based on 15-group Collapsed Reaction Rates*

The cause of the various profile of the contribution of each isotopes and reaction types shown above indicates that they are composed of contributions from different energy domains, which change their importance according to the progression of voidage. As such phenomena could not be fully understood without the further analysis in terms of energy, a more detailed analysis based on 15-group collapsed reaction rates has been performed and will be discussed in this subsection.

**Table 2.3** shows the energy group structure of the 15-group employed in the analysis.

Due to the different energy group structure in the original fine-group library of the 172-group CEA93 library and the 107-group SRAC library, there are differences in some of the coarse groups. The largest difference is in the most upper energy considered in the two libraries ; CEA93 treats up to 19.6 MeV whereas SRAC library treats up to 10.0 MeV. However, due to the small fraction of neutron flux and hence the reaction rates within 10.0 MeV < E < 19.6 MeV, this difference in the uppermost energy which appears in the 1st group has proven to have very little effect to the total reactivity difference.

Table 2.3 Energy group structure of the 15-group

| Group | APOLLO-2/JEF2.2 | | | SRAC/JENDL-3.2 | | |
|---|---|---|---|---|---|---|
| | Upper Energy | Lower Energy | Lethargy Width | Upper Energy | Lower Energy | Lethargy Width |
| 1 | 1.964E+07 | 6.060E+06 | 1.18 | 1.000E+07 | 6.065E+06 | 0.50 |
| 2 | 6.060E+06 | 2.231E+06 | 1.00 | 6.065E+06 | 2.231E+06 | 1.00 |
| 3 | 2.231E+06 | 1.353E+06 | 0.50 | 2.231E+06 | 1.353E+06 | 0.50 |
| 4 | 1.353E+06 | 4.987E+05 | 1.00 | 1.353E+06 | 4.979E+05 | 1.00 |
| 5 | 4.987E+05 | 1.831E+05 | 1.00 | 4.979E+05 | 1.832E+05 | 1.00 |
| 6 | 1.831E+05 | 6.737E+04 | 1.00 | 1.832E+05 | 6.738E+04 | 1.00 |
| 7 | 6.737E+04 | 2.478E+04 | 1.00 | 6.738E+04 | 2.479E+04 | 1.00 |
| 8 | 2.478E+04 | 9.118E+03 | 1.00 | 2.479E+04 | 9.119E+03 | 1.00 |
| 9 | 9.118E+03 | 2.034E+03 | 1.50 | 9.119E+03 | 2.035E+03 | 1.50 |
| 10 | 2.034E+03 | 4.539E+02 | 1.50 | 2.035E+03 | 4.540E+02 | 1.50 |
| 11 | 4.539E+02 | 2.260E+01 | 3.00 | 4.540E+02 | 2.260E+01 | 3.00 |
| 12 | 2.260E+01 | 4.000E+00 | 1.73 | 2.260E+01 | 3.928E+00 | 1.75 |
| 13 | 4.000E+00 | 5.300E-01 | 2.02 | 3.928E+00 | 5.316E-01 | 2.00 |
| 14 | 5.300E-01 | 1.000E-01 | 1.67 | 5.316E-01 | 9.708E-02 | 1.70 |
| 15 | 1.000E-01 | 1.000E-04 | 6.91 | 9.708E-02 | 1.000E-04 | 6.88 |

As the voidage progresses, the neutron spectrum shifts towards higher energy, and the importance of each energy domain may change significantly. **Figure 2.9** shows the relative change of some of the cell averaged 15-group fluxes for Cell 1 calculated by SRAC/JENDL-3.2. Here, the flux for each indicated coarse group has been normalized to unity at 0% void to illustrate the relative change due to the progression of void. It should be noted that the neutron flux between 4 eV < E < 9 keV shows a non-monotonous change with progressing void. Especially for 10th (454 eV < E ≤ 2.03 keV), 11th (22.3 eV < E ≤ 454 eV)

and $12^{th}$ (4 eV < E ≤ 22.3 eV) groups, the neutron flux first increases with increasing void fraction, but then decreases with increasing void in higher void fraction range. The turning point from increase to decrease depends on the energy group. The void fraction value corresponding to the turning point becomes higher with increasing energy.

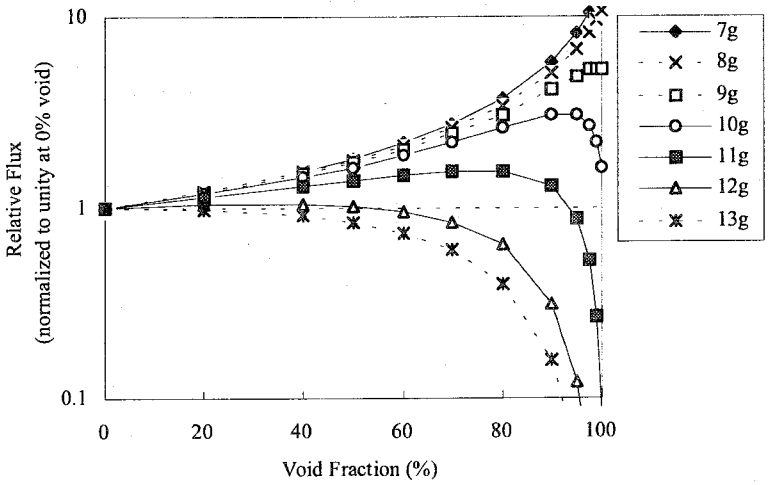


Figure 2.9 Void fraction dependence of cell-averaged flux of Cell 1 calculated by SRAC/JENDL-3.2.

This void fraction dependence of the neutron flux causes the void fraction dependence of each isotope, and due to the difference in the relative importance of each coarse group, the total void fraction dependence of each contributing isotope becomes also different. Furthermore, for fissionable isotopes, the fission term and the production term generally appear in opposite sign (unless the difference in ν-value is significant to change the sign of the production term), so that these two terms tend to cancel each other to a certain extent (the magnitude of the production term is generally larger than that of the fission term). These complicated balance among the energy-dependent, reaction type-dependent components lead to the unique behavior of each isotope as regards its contribution to the (A-S) discrepancy.

The contributions of the major isotopes to the reactivity difference are shown in **Fig. 2.10** and will be discussed in more detail. As the main characteristics of each component are similar between the two cells, the following discussion is mostly based on the results for Cell1.

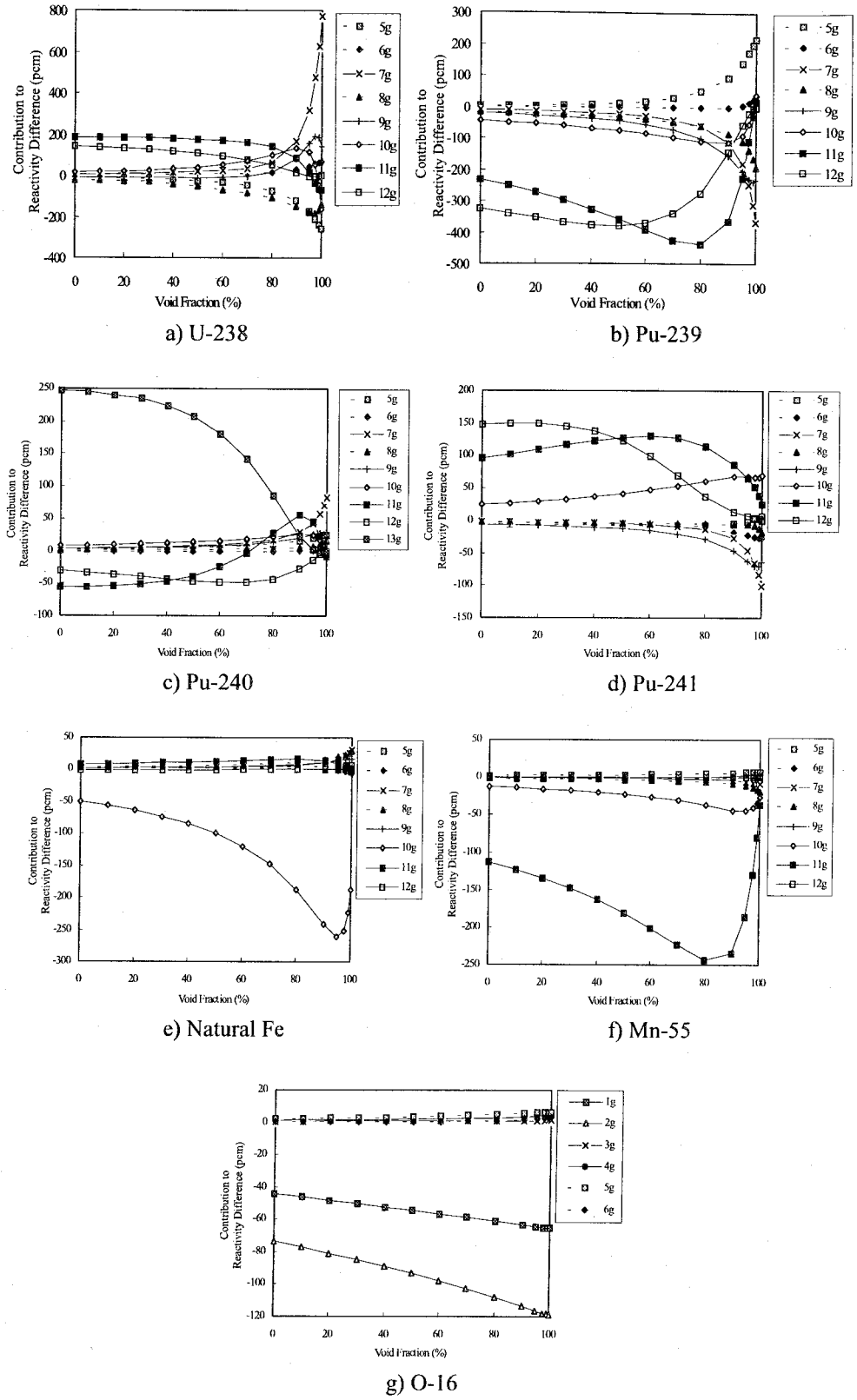


a) U-238

b) Pu-239

c) Pu-240

d) Pu-241

e) Natural Fe

f) Mn-55

g) O-16

Figure 2.10 Energy dependence of contribution of major nuclides to the reactivity difference between APOLLO-2/JEF2.2 and SRAC/JENDL-3.2 for Cell 1. Only the representative energy groups are shown.

- U-238

The void fraction dependence of the contribution of each group reflects the behavior of the cell-averaged flux described above. At low void fraction, the main discrepancy between the two code systems is caused by the resolved resonance range below 454 eV. The contribution of this energy range becomes negligible at high void fraction. Instead of this, the large positive contribution to the (A-S) discrepancy of the $7^{th}$ group (24.8 keV < E < 67.4 eV) component becomes significant at high void fraction over 90% void. This component cancels with the negative $5^{th}$ group and $8^{th}$ group components, which also increase their magnitudes with void fraction. The differences are mostly due to the capture rate difference, and as the capture cross sections in the unresolved through fast range are almost the same between the two code systems, it is suspected that these differences are mostly due to the secondary effect caused by the difference in the neutron flux.

- Pu-239

The most dominating components are the negative ones of the $11^{th}$ and $12^{th}$ groups, showing significant void fraction dependence which again reflects the flux behavior described above. At high void fraction, the $5^{th}$ group (positive component) and the $7^{th}$, $8^{th}$ and $9^{th}$ groups (negative component) show large contributions. Further analysis in terms of reaction types showed that the production term dominates the overall behavior for all groups. It has also been found that the fission term and the capture term do not always appear in the same sign. This means that for these groups, the reaction rate difference (and hence reactivity difference) is not only caused by the flux difference, but also by the difference of the cross section itself.

- Pu-240

The large positive contribution of 13$^{th}$ group showing approximately +250 pcm at 0% void is caused by the capture rate difference in the vicinity of resonance at 1 eV. This component fades away with increasing void fraction. The negative contributions of 11$^{th}$ and 12$^{th}$ groups also become small with increasing void fraction, so that the balance between these positive and negative components results in the more or less constant contribution of approximately +200 pcm throughout all the void fraction range.

- Pu-241

The positive contributions of 11$^{th}$ and 12$^{th}$ groups are significant at low void fraction. At high void fraction, the contribution of these groups becomes negligible and that of the negative 7$^{th}$ and 9$^{th}$ groups becomes the dominating component. This causes the total component to turn from positive to negative in accordance with the progression of void, which is a characteristic feature of Pu-241 component.

- Stainless Steel

The reactivity discrepancy due to two elements, natural Fe and Mn-55, reaches up to -460 pcm at around 90% void. The two elements show different contribution in terms of energy. For natural Fe, most of the reactivity difference is due to the negative 10$^{th}$ group, which contains the 1-keV resonance. This component reaches its maximum at 95% void. For Mn-55, most of the reactivity difference is due to the negative 11$^{th}$ group, containing the large resonance near 300 eV. Due to the voidage, the contribution of 11$^{th}$ group increases its importance to the reactivity difference up to approximately 80% void. Above 80% void, the contribution of this energy group rapidly decreases ; this directly reflects the neutron flux behavior shown in Fig. 2.9 previously. These contributions of these two elements show

strong dependence on the void fraction, which again correspond to the flux variation as described before.

This considerable contribution of the stainless steel materials to the discrepancy is found to be mainly due to the different treatment of the resonance cross sections of the cladding. In the APOLLO-2/JEF2.2 calculations, the resonance self-shielding of the isotopes comprised in the cladding was not taken into account. This treatment come from the unavailability of self-shielded data for these isotopes in the 172-group CEA93 library and therefore the resonance cross sections for the isotopes in the cladding become large compared to the SRAC/JENDL-3.2 calculations. Thus for both natural Fe and Mn-55, the capture rate difference between APOLLO-2/JEF2.2 and SRAC/JENDL-3.2 becomes positive, and this leads to negative contribution to the reactivity difference.

- O-16

The total reactivity difference is eventually determined by the contributions from the 1st and 2nd groups. These discrepancies could be attributed to the cross section difference in the fast energy range; such as (n,p) and (n,α) cross sections, which are currently included in the "capture" or absorption cross section in the cross section libraries used in both codes. These cross sections in JEF2.2 are larger than those in JENDL-3.2 above approximately 3 MeV. There is a large difference between the two libraries in the energy region of 100 eV< E < 1 MeV, but because of the small cross section value, the contribution of this energy region to the reactivity is relatively small.

### 2.4.3 BREAKDOWN OF TOTAL VOID REACTIVITY AND COMPARISON OF CONTRIBUTING COMPONENTS BETWEEN APOLLO-2/JEF2.2 AND SRAC/JENDL-3.2

In this subsection, the total void reactivity, defined as the reactivity difference between 0% void and 100% void, will be analyzed by decomposing into contributing components. In this case, the two states *a* and *b* in equations shown in Subsection 2.4.1 corresponds to 0% and 100% void, respectively. The results below are obtained in 15-groups.

**Tables 2.4** and **2.5** show the breakdown of total void reactivity value obtained by the two codes for Cell 1 and Cell 2, respectively. The difference between the results obtained by the two codes is also shown in the tables. Here, only the total component for each isotope is shown.

The void reactivity also is a result of cancellation between various positive and negative components, and the main contributors are U-238 (negative contribution), Pu-239 (positive), Pu-240 (positive), Pu-241 (negative) and Pu-242 (positive). The magnitude of the individual components is substantially large compared to the resulting total void reactivity. Especially for U-238 and Pu-240 components, their relative magnitudes reach up to more than several tens of the total void reactivity. Due to such complexity, the difference of void reactivity between APOLLO-2/JEF2.2 and SRAC/JENDL-3.2 becomes also a result of cancellation between the various components of different signs. Comparing the total (energy-integrated) components, APOLLO-2/JEF2.2 tends to give a larger contribution for each isotopes compared to SRAC/JENDL-3.2.

Table 2.4 Comparison of total void reactivity breakdown in 15-group for Cell 1

(in pcm)

| Group | Energy Range | | U-235 | U-238 | Pu-238 | Pu-239 | Pu-240 | Pu-241 | Pu-242 | Am-241 | O-16 | Nat. Fe | Nat. Cr | Nat. Ni | Mn-55 | H2O | Total |
|---|---|---|---|---|---|---|---|---|---|---|---|---|---|---|---|---|---|
| 1 | Eup-6.06MeV | A* | 1 | 339 | 2 | 56 | 21 | 10 | 5 | 1 | -51 | -9 | -2 | -10 | 0 | 57 | 421 |
| | | S* | 1 | 321 | 2 | 56 | 20 | 10 | 5 | 1 | -31 | -8 | -2 | -9 | 0 | 33 | 400 |
| | | A-S | 0 | 18 | 0 | -1 | 0 | 0 | 0 | 0 | -20 | -1 | 0 | -1 | 0 | 25 | 20 |
| 2 | 6.06MeV-2.23MeV | A | 13 | 2275 | 29 | 764 | 259 | 117 | 52 | 19 | -117 | -32 | -4 | -61 | 0 | 101 | 3416 |
| | | S | 13 | 2249 | 29 | 752 | 252 | 121 | 50 | 18 | -73 | -29 | -5 | -60 | 0 | 60 | 3378 |
| | | A-S | 0 | 27 | 1 | 12 | 7 | -3 | 2 | 1 | -45 | -3 | 1 | -1 | 0 | 41 | 38 |
| 3 | 2.23MeV-1.35MeV | A | 12 | 1526 | 28 | 769 | 236 | 119 | 50 | 18 | 0 | -5 | -2 | -9 | 0 | 0 | 2742 |
| | | S | 13 | 1574 | 27 | 760 | 236 | 129 | 50 | 17 | -1 | -8 | -2 | -10 | 0 | 1 | 2785 |
| | | A-S | -1 | -49 | 1 | 9 | 1 | -10 | 0 | 1 | 1 | 3 | 1 | 1 | 0 | 0 | -43 |
| 4 | 1.35MeV-499keV | A | 56 | -1747 | 116 | 3326 | 691 | 533 | 125 | 12 | 0 | -45 | -12 | -19 | -2 | 1 | 3035 |
| | | S | 55 | -1727 | 115 | 3223 | 655 | 551 | 122 | 18 | -4 | -68 | -15 | -23 | -2 | 1 | 2903 |
| | | A-S | 1 | -20 | 1 | 103 | 36 | -18 | 3 | -6 | 4 | 23 | 3 | 3 | 0 | -1 | 133 |
| 5 | 499keV-183keV | A | 85 | -3111 | 83 | 4194 | 26 | 878 | -4 | -38 | 0 | -118 | -24 | -48 | -5 | 1 | 1919 |
| | | S | 78 | -2851 | 75 | 3941 | 4 | 858 | -5 | -24 | -4 | -122 | -27 | -42 | -3 | 1 | 1880 |
| | | A-S | 7 | -260 | 8 | 253 | 23 | 20 | 1 | -14 | 4 | 4 | 3 | -6 | -1 | 0 | 39 |
| 6 | 183keV-67.4keV | A | 110 | -5184 | 48 | 4742 | -200 | 1245 | -47 | -73 | 0 | -225 | -52 | -78 | -13 | 1 | 274 |
| | | S | 104 | -5225 | 42 | 4662 | -200 | 1257 | -48 | -55 | -3 | -218 | -50 | -67 | -10 | 1 | 191 |
| | | A-S | 6 | 42 | 6 | 80 | 0 | -13 | 1 | -18 | 3 | -7 | -1 | -11 | -3 | 0 | 83 |
| 7 | 67.4keV-24.8keV | A | 102 | -8344 | 29 | 3704 | -332 | 1170 | -90 | -81 | 0 | -247 | -45 | -108 | -23 | 1 | -4263 |
| | | S | 102 | -9079 | 24 | 4021 | -409 | 1257 | -101 | -75 | -2 | -274 | -63 | -94 | -15 | 1 | -4706 |
| | | A-S | 1 | 735 | 5 | -317 | 77 | -87 | 11 | -6 | 2 | 27 | 18 | -15 | -9 | 0 | 443 |
| 8 | 24.8keV-9.12keV | A | 86 | -8460 | 11 | 2179 | -366 | 949 | -99 | -69 | 0 | -96 | -38 | -133 | -31 | 2 | -6063 |
| | | S | 82 | -8311 | 7 | 2328 | -379 | 955 | -102 | -66 | -1 | -121 | -35 | -137 | -14 | 2 | -5791 |
| | | A-S | 5 | -149 | 4 | -149 | 13 | -6 | 4 | -3 | 1 | 25 | -3 | 4 | -17 | 0 | -272 |
| 9 | 9.12keV-2.03keV | A | 76 | -6469 | 1 | 1265 | -374 | 847 | -96 | -61 | 0 | -77 | -120 | -24 | -22 | 4 | -5049 |
| | | S | 77 | -6598 | -3 | 1455 | -391 | 896 | -100 | -69 | 0 | -91 | -124 | -33 | -27 | 5 | -5003 |
| | | A-S | -1 | 129 | 4 | -190 | 17 | -50 | 4 | 8 | 0 | 14 | 5 | 9 | 5 | 0 | -45 |
| 10 | 2.03keV-454eV | A | 16 | -735 | 0 | 282 | -95 | 226 | -28 | -17 | 0 | -178 | -80 | -3 | -30 | 9 | -633 |
| | | S | 16 | -556 | -4 | 195 | -80 | 180 | -18 | -16 | 0 | -41 | -47 | -4 | -16 | 9 | -381 |
| | | A-S | 1 | -180 | 5 | 86 | -15 | 46 | -9 | -1 | 0 | -137 | -33 | 1 | -14 | 0 | -252 |
| 11 | 454eV-22.6eV | A | -132 | 6806 | 45 | -3232 | 1810 | -1899 | 210 | 144 | 0 | 91 | 35 | 24 | 181 | 42 | 4125 |
| | | S | -129 | 7035 | 41 | -3434 | 1757 | -1811 | 223 | 146 | 0 | 99 | 35 | 25 | 103 | 42 | 4131 |
| | | A-S | -3 | -228 | 4 | 202 | 53 | -89 | -12 | -3 | 0 | -8 | 0 | -2 | 78 | 0 | -6 |
| 12 | 22.6eV-4eV | A | -51 | 6067 | 52 | -3159 | 243 | -2923 | 13 | 132 | 0 | 109 | 42 | 29 | 18 | 47 | 619 |
| | | S | -52 | 6187 | 48 | -3444 | 212 | -2745 | 13 | 135 | 0 | 107 | 43 | 30 | 18 | 48 | 600 |
| | | A-S | 1 | -120 | 5 | 285 | 31 | -178 | 0 | -3 | 0 | 2 | -1 | -1 | 0 | -1 | 18 |
| 13 | 4eV-0.53eV | A | -49 | 403 | 51 | -1988 | 8725 | -526 | 1721 | 484 | 0 | 226 | 87 | 61 | 36 | 98 | 9330 |
| | | S | -49 | 397 | 43 | -1928 | 8941 | -489 | 1737 | 419 | 0 | 219 | 86 | 61 | 36 | 99 | 9573 |
| | | A-S | 0 | 5 | 8 | -60 | -216 | -37 | -16 | 65 | 0 | 7 | 1 | 0 | 0 | -2 | -244 |
| 14 | 0.53eV-0.1eV | A | -61 | 138 | 27 | -7352 | 747 | -1351 | 8 | 147 | 0 | 174 | 67 | 47 | 28 | 84 | -7298 |
| | | S | -61 | 140 | 28 | -7374 | 741 | -1303 | 8 | 138 | 0 | 172 | 68 | 48 | 28 | 87 | -7281 |
| | | A-S | 0 | -2 | -1 | 21 | 6 | -49 | 0 | 9 | 0 | 2 | -1 | -1 | -1 | -3 | -17 |
| 15 | 0.1eV- | A | -65 | 123 | 48 | -3118 | 384 | -873 | 6 | 41 | 0 | 152 | 59 | 41 | 24 | 75 | -3103 |
| | | S | -64 | 121 | 47 | -3039 | 377 | -829 | 6 | 40 | 0 | 149 | 59 | 41 | 24 | 76 | -2993 |
| | | A-S | -2 | 2 | 1 | -79 | 7 | -44 | 0 | 1 | 0 | 3 | 0 | 0 | 0 | -1 | -111 |
| | Total | A | 200 | -16372 | 570 | 2433 | 11776 | -1478 | 1828 | 658 | -169 | -280 | -87 | -290 | 162 | 521 | -529 |
| | | S | 185 | -16323 | 519 | 2177 | 11737 | -961 | 1839 | 627 | -117 | -234 | -79 | -273 | 124 | 464 | -316 |
| | | A-S | 15 | -49 | 51 | 256 | 39 | -517 | -12 | 31 | -52 | -46 | -8 | -18 | 38 | 57 | -214 |

*A: APOLLO-2/JEF2.2, S: SRAC/JENDL-3.2

Table 2.5 Comparison of total void reactivity breakdown in 15-group for Cell 2

(in pcm)

| Group | Energy Range | | U-235 | U-238 | Pu-238 | Pu-239 | Pu-240 | Pu-241 | Pu-242 | Am-241 | O-16 | Nat. Fe | Nat. Cr | Nat. Ni | Mn-55 | H2O | Total |
|---|---|---|---|---|---|---|---|---|---|---|---|---|---|---|---|---|---|
| 1 | Eup-6.06MeV | A* | 1 | 318 | 1 | 70 | 14 | 1 | 0 | 1 | -50 | -9 | -1 | -10 | 0 | 55 | 392 |
| | | S* | 1 | 297 | 1 | 70 | 14 | 1 | 0 | 1 | -30 | -8 | -1 | -9 | 0 | 31 | 369 |
| | | A-S | 0 | 20 | 0 | 0 | 0 | 0 | 0 | 0 | -20 | -1 | 0 | -1 | 0 | 24 | 23 |
| 2 | 6.06MeV-2.23MeV | A | 12 | 2121 | 16 | 962 | 181 | 15 | 4 | 8 | -115 | -32 | -3 | -60 | 0 | 99 | 3208 |
| | | S | 12 | 2078 | 16 | 940 | 175 | 15 | 4 | 8 | -71 | -28 | -5 | -59 | 0 | 59 | 3143 |
| | | A-S | 0 | 43 | 1 | 22 | 6 | 0 | 0 | 1 | -44 | -4 | 1 | -1 | 0 | 40 | 65 |
| 3 | 2.23MeV-1.35MeV | A | 11 | 1404 | 15 | 961 | 164 | 15 | 4 | 8 | 0 | -5 | -2 | -9 | 0 | 0 | 2566 |
| | | S | 12 | 1443 | 15 | 946 | 163 | 16 | 4 | 7 | -1 | -8 | -2 | -10 | 0 | 1 | 2584 |
| | | A-S | 0 | -39 | 1 | 15 | 1 | -1 | 0 | 0 | 1 | 3 | 1 | 1 | 0 | 0 | -18 |
| 4 | 1.35MeV-499keV | A | 51 | -1699 | 62 | 4107 | 473 | 64 | 10 | 5 | 0 | -43 | -11 | -19 | -1 | 1 | 2998 |
| | | S | 50 | -1678 | 61 | 3959 | 446 | 66 | 10 | 7 | -3 | -66 | -14 | -22 | -1 | 1 | 2816 |
| | | A-S | 1 | -22 | 1 | 148 | 27 | -2 | 0 | -3 | 3 | 22 | 3 | 3 | 0 | -1 | 182 |
| 5 | 499keV-183keV | A | 76 | -2999 | 44 | 5142 | 13 | 105 | 0 | -17 | 0 | -113 | -24 | -46 | -5 | 1 | 2177 |
| | | S | 70 | -2738 | 39 | 4796 | -3 | 102 | -1 | -11 | -4 | -116 | -26 | -40 | -3 | 1 | 2068 |
| | | A-S | 7 | -261 | 4 | 346 | 16 | 3 | 0 | -6 | 4 | 2 | 2 | -6 | -1 | 0 | 109 |
| 6 | 183keV-67.4keV | A | 99 | -4982 | 25 | 5784 | -147 | 149 | -4 | -33 | 0 | -216 | -50 | -75 | -13 | 1 | 538 |
| | | S | 92 | -5000 | 21 | 5638 | -147 | 149 | -4 | -25 | -3 | -204 | -48 | -64 | -9 | 1 | 399 |
| | | A-S | 7 | 18 | 3 | 145 | 0 | -1 | 0 | -8 | 3 | -12 | -2 | -11 | -3 | 0 | 139 |
| 7 | 67.4keV-24.8keV | A | 91 | -7988 | 14 | 4485 | -240 | 139 | -8 | -36 | 0 | -236 | -43 | -103 | -22 | 1 | -3946 |
| | | S | 89 | -8657 | 11 | 4826 | -295 | 148 | -8 | -33 | -2 | -256 | -60 | -89 | -14 | 1 | -4338 |
| | | A-S | 2 | 669 | 3 | -341 | 55 | -9 | 1 | -3 | 2 | 20 | 16 | -15 | -8 | 0 | 392 |
| 8 | 24.8keV-9.12keV | A | 76 | -8066 | 5 | 2596 | -263 | 112 | -8 | -31 | 0 | -91 | -36 | -127 | -29 | 2 | -5859 |
| | | S | 72 | -7915 | 2 | 2760 | -272 | 113 | -9 | -29 | -1 | -114 | -33 | -129 | -13 | 2 | -5566 |
| | | A-S | 5 | -151 | 2 | -165 | 9 | 0 | 0 | -2 | 1 | 23 | -3 | 3 | -16 | 0 | -294 |
| 9 | 9.12keV-2.03keV | A | 66 | -6130 | 0 | 1455 | -266 | 100 | -8 | -27 | 0 | -73 | -114 | -23 | -20 | 4 | -5036 |
| | | S | 66 | -6239 | -3 | 1665 | -278 | 105 | -8 | -30 | 0 | -86 | -118 | -31 | -25 | 4 | -4977 |
| | | A-S | 0 | 109 | 2 | -211 | 12 | -5 | 0 | 3 | 0 | 13 | 4 | 8 | 5 | 0 | -59 |
| 10 | 2.03keV-454eV | A | 13 | -637 | 0 | 296 | -66 | 26 | -2 | -7 | 0 | -164 | -75 | -3 | -28 | 8 | -638 |
| | | S | 13 | -461 | -2 | 192 | -54 | 20 | -2 | -7 | 0 | -31 | -43 | -3 | -14 | 8 | -384 |
| | | A-S | 0 | -175 | 2 | 105 | -12 | 6 | -1 | -1 | 0 | -133 | -33 | 1 | -14 | 0 | -254 |
| 11 | 454eV-22.6eV | A | -116 | 6575 | 26 | -3735 | 1393 | -231 | 20 | 64 | 0 | 88 | 34 | 23 | 177 | 41 | 4359 |
| | | S | -112 | 6785 | 25 | -3957 | 1332 | -218 | 22 | 66 | 0 | 95 | 34 | 24 | 100 | 41 | 4237 |
| | | A-S | -4 | -210 | 1 | 222 | 60 | -13 | -2 | -1 | 0 | -7 | 0 | -1 | 77 | 0 | 122 |
| 12 | 22.6eV-4eV | A | -44 | 6025 | 30 | -3562 | 184 | -380 | 1 | 62 | 0 | 109 | 42 | 29 | 18 | 47 | 2562 |
| | | S | -46 | 6138 | 28 | -3817 | 162 | -348 | 1 | 63 | 0 | 107 | 43 | 30 | 18 | 47 | 2427 |
| | | A-S | 1 | -113 | 2 | 255 | 22 | -31 | 0 | -1 | 0 | 3 | -1 | -1 | 0 | -1 | 136 |
| 13 | 4eV-0.53eV | A | -50 | 449 | 32 | -2801 | 8256 | -73 | 335 | 258 | 0 | 247 | 96 | 67 | 40 | 106 | 6961 |
| | | S | -50 | 443 | 32 | -2687 | 8427 | -67 | 285 | 221 | 0 | 239 | 94 | 67 | 39 | 107 | 7149 |
| | | A-S | 0 | 6 | 1 | -114 | -171 | -5 | 50 | 37 | 0 | 8 | 1 | 0 | 1 | -2 | -188 |
| 14 | 0.53eV-0.1eV | A | -54 | 131 | 15 | -8312 | 532 | -156 | 1 | 63 | 0 | 176 | 68 | 48 | 28 | 86 | -7374 |
| | | S | -53 | 132 | 15 | -8238 | 523 | -148 | 1 | 58 | 0 | 173 | 69 | 48 | 28 | 88 | -7306 |
| | | A-S | 0 | 0 | 0 | -74 | 9 | -8 | 0 | 5 | 0 | 3 | -1 | 0 | -1 | -2 | -69 |
| 15 | 0.1eV- | A | -60 | 120 | 27 | -3810 | 279 | -105 | 1 | 18 | 0 | 152 | 59 | 41 | 24 | 76 | -3177 |
| | | S | -58 | 117 | 26 | -3679 | 273 | -99 | 1 | 18 | 0 | 149 | 59 | 41 | 24 | 77 | -3052 |
| | | A-S | -2 | 3 | 1 | -131 | 7 | -6 | 0 | 1 | 0 | 3 | 0 | 1 | 0 | -1 | -126 |
| | Total | A | 172 | -15357 | 312 | 3636 | 10507 | -219 | 346 | 338 | -165 | -209 | -60 | -264 | 168 | 525 | -271 |
| | | S | 157 | -15256 | 287 | 3412 | 10468 | -146 | 296 | 314 | -113 | -153 | -50 | -245 | 129 | 469 | -431 |
| | | A-S | 15 | -101 | 25 | 224 | 40 | -74 | 49 | 24 | -52 | -56 | -10 | -19 | 39 | 57 | 160 |

*A: APOLLO-2/JEF2.2, S: SRAC/JENDL-3.2

Considering the absolute values of the void reactivity components, similar results were obtained by the two codes for the total contribution of the major fertile isotopes, namely for U-238, Pu-240 and Pu-242 components. Especially for U-238 and Pu-240 components with a significant magnitude exceeding 10000 pcm, the relative difference for these components between the two code systems is less than 1%. This reflects that the reactivity difference due to those isotopes is almost the same for 0% and 100% voided cells, as could be seen from the analysis of reactivity discrepancy given in Subsection 2.4.2. On the other hand, considerable discrepancies exist in the fissile Pu-239 and Pu-241 components, the latter showing the most significant difference of -517 pcm in Cell 1. This is approximately twice of the total discrepancy in the void reactivity. It should be noted that the positive discrepancy of Pu-239 and the negative discrepancy of Pu-241 components tend to cancel with each other in Cell 1. The total discrepancy for Cell 1 therefore becomes smaller than that for Cell 2, where the Pu-241 content is small and the cancellation does not occur. This clearly illustrates the impact of the isotopic composition of Pu to the void reactivity.

Turning to other isotopes, the structure materials in the stainless steel cladding also show relatively important contributions to the total void reactivity. Compared with the large contribution of the major heavy nuclide components, the magnitude of the cladding materials is small ; however, individual magnitude is still comparable to the total void reactivity. Among the isotopes comprising the stainless steel cladding, natural Fe, natural Cr and natural Ni serve as negative contributor, whereas Mn-55 serves as a positive contributor to the void reactivity, and APOLLO-2/JEF2.2 gives larger results compared to SRAC/JENDL-3.2 for all of them. Taking into account the absolute magnitude of each components, relatively large discrepancies are found for natural Fe and Mn-55. Relatively large discrepancies with respect to the total void reactivity are also observed for O-16 contained in the MOX pellet, and also in the $H_2O$ moderator.

The breakdown into contributing energy domains shows that, for each isotope, the energy-integrated reactivity effect is a result of competition between the positive and negative contributions from different energy domains. As was shown in Fig. 2.10, the neutron flux above the $10^{th}$ group (E > 454 eV) is increased when the cell is totally voided. Provided that the difference of the effective cross section in accordance with the progress of voidage is small, this behavior of flux means that compared to the unvoided cell, the reaction rate in the totally voided cell becomes larger above the $10^{th}$ group, whereas the reaction rate below the $11^{th}$ group becomes smaller. Thus for energy groups above the $10^{th}$ group, fission and capture terms become negative (note that these terms appear in the opposite sign as that of reaction rate difference), whereas production and (*n,2n*) terms become positive. For isotopes mainly acting as absorber (for example, the isotopes comprising stainless steel cladding), the total components for these isotopes therefore show a clear trend to be negative above the $10^{th}$ group and positive below the $11^{th}$ group. For the heavy isotopes, however, such trend could not seen in the total components (for example, see U-238) ; this is because the group-wise total reactivity effect is a result of the balance among the production, fission, capture and (*n,2n*) terms, which may appear in different magnitude and in different signs. The discrepancy between the individual isotopic components obtained by the two codes also is a result of balance among the reaction type-wise discrepancies. This clearly shows the importance and necessity of the detailed analysis in terms of energy and reaction types.

The contribution of the individual isotopes and the comparison between APOLLO-2/JEF2.2 and SRAC/JENDL-3.2 results are summarized below.

- U-238

The total component having a significant magnitude of approximately -16300 pcm could be clearly separated into three energy domains ; the positive contribution in the MeV

region, the large negative contribution in the keV region and the positive contribution in the resonance and thermal regions below 454 eV. The positive contribution in the MeV region comes from the large increase in fast fission, which becomes significant above the 3rd group. The small U-238 capture cross section and thus less negative capture term in this energy domain also act to enhance the positive contribution of the production term. In the 1st group, the (*n,2n*) term also shows a contribution of approximately 60 to 70 pcm. The capture rate increase above the 10th group (E > 454 eV) overrides the positive contribution from the fast and resonance regions, and results to the total capture term of approximately -21000 pcm.

Comparing the two codes, the fast fission effect is consistently obtained between the two codes. On the other hand, large discrepancy has been found at the 5th , 7th , 10th and 11th groups. It should be noted that, despite the small magnitude, the relative discrepancy at the 10th group is significant.

No clear difference between the two cells could be found. The smaller contribution of U-238 in Cell 2 clearly reflects the fact that the relative importance of U-238 as absorber in Cell 2 is smaller than that in Cell 1.

- Pu-239

The magnitude of the fission term is larger than that of the capture term for each energy group. On the other hand, the energy-integrated fission term becomes smaller than the capture term ; this comes from the balance between the negative terms above the 10th group and the positive terms below the 11th group. Comparing the two codes, large discrepancies with magnitude over 400 pcm are observed in the 5th, 7th, 9th and 12th groups.

- Pu-240

Good agreement of the energy-integrated components is achieved between the two

codes. However, the analysis in terms of energy revealed that this agreement is merely a result of cancellation between both the positive and negative discrepancies.

Contribution of the 13$^{th}$ group capture term, which contains the 1 eV resonance, is the most dominating component to the void reactivity. The difference of this component between the two codes is approximately -220 pcm, showing that the capture rate decrease due to voidage is estimated larger in SRAC/JENDL-3.2. As the neutron flux difference in this group is relatively small between the two codes, it could be concluded that the capture cross section of Pu-240 in the 13$^{th}$ group is larger in SRAC/JENDL-3.2 compared to APOLLO-2/JEF2.2.

- Pu-241

The largest discrepancy for the Cell 1 void coefficient components has been found between the two codes for Pu-241. The combination of fission and production terms below the 11$^{th}$ group (E < 454 eV) obtained by SRAC/JENDL-3.2 is larger in magnitude than that obtained by APOLLO-2/JEF2.2, which results to large discrepancy in this energy domain. The discrepancies in the 5$^{th}$, 7$^{th}$ and 9$^{th}$ groups also have considerable magnitude. Although the absolute magnitude is small, it should be noted that the capture terms for the 4$^{th}$, 5$^{th}$ and 6$^{th}$ groups show significant relative difference. This could be attributed to the large difference in the Pu-241 capture cross section in this energy domain between the nuclear data employed in JEF2.2 and JENDL-3.2.

- Pu-242

Contribution of the most dominating 13$^{th}$ group is in excellent agreement between the two codes for Cell 1. Above the 4$^{th}$ group, increase of the fast fission results in a positive reactivity effect. This is also in good agreement between the two code systems.

- Stainless Steel

The discrepancies for natural Fe and Mn-55 are mainly caused by the treatment of the main capture resonance as described previously, and appear in the $10^{th}$ and $11^{th}$ groups for the two isotopes respectively. The different resonance energy as well as the capture cross section in the keV range for these two isotopes lead to an opposite contribution to the void reactivity. As described before, the spectrum shift caused by the voidage decreases the capture rates for these isotopes below the $11^{th}$ group and increases the capture rates above the $10^{th}$ group. For natural Fe, the spectrum shift due to voidage results to the increase in the 1-keV resonance capture as well as the keV-region capture, which overrides the decrease in the thermal capture. This leads to the increase of the total capture rate and therefore serves as a negative contribution. On the contrary, the spectrum shift results to the large decrease in the 300-eV resonance capture for Mn-55, which leads to the decrease of the total capture rate and therefore serves as a positive contribution.

- O-16, $H_2O$

O-16 shows an important contribution at the $1^{st}$ and $2^{nd}$ groups; the increase of absorption rate due to the spectrum hardening serves as a negative component of more than -100 pcm. The effect of fast absorption is also notable in $H_2O$ moderator, where it acts as a positive effect until the absorption effect of the moderator no longer exists in the voided cell. Eventually all the difference between the two codes for O-16 and $H_2O$ components is caused at these two energy groups. This could be attributed to the cross section difference above 3 MeV; the absorption or "capture" cross sections which containing (n,p) and (n,$\alpha$) cross sections are larger in JEF2.2 than JENDL-3.2, so that for APOLLO-2/JEF2.2, the spectrum hardening due to the voidage leads to larger increase in the total absorption rate of oxygen

compared to SRAC/JENDL-3.2.

### 2.4.4 POSSIBLE CAUSES OF DISCREPANCIES FOUND BETWEEN THE TWO CODE SYSTEMS

From the discussions in the preceding section, several apparent causes of the discrepancies between the two code systems have been pointed out. These include the treatment of the major capture resonance of stainless steel materials, and the apparent difference between the cross section data used in the two code systems. However, some of the discrepancies still need further investigations, so the 15-group cell averaged flux and reaction rates are compared and the possible impact of its difference will be discussed below to identify the possible causes of the discrepancies, .

#### *2.4.4.A Comparison of Cell Averaged Neutron Flux and its Impact to the Observed Discrepancies*

The analysis of the breakdown results shows that, besides the energy groups containing the major resonance of individual isotopes, the relative discrepancy at a certain energy groups in the keV region shows a notable trend. For example, it has been found that for most of the isotopes, APOLLO-2/JEF2.2 tends to give larger reactivity effect in the $5^{th}$ group and smaller reactivity effect in the $7^{th}$ group, regardless of the reaction types. The similarity in the void fraction dependence of these groups to the reactivity difference has also been found. A notable trend could also be seen on the contribution of the $10^{th}$ energy group to the total void reactivity. Although the contribution of this energy group to the total void reactivity is relatively small, its relative error between the two code systems is significant. Compared to SRAC/JENDL-3.2, APOLLO-2/JEF2.2 tends to give larger magnitude for the $10^{th}$ group

component for all the heavy isotopes. These trends in the discrepancy between the two code systems indicate that, for these energy groups, the discrepancies are caused by the secondary effect arising from the discrepancy in the neutron flux.

**Figure 2.11** shows the comparison of cell-averaged 15-group neutron flux obtained by the two codes for Cell 1 at 0% and 100% void. The cell averaged spectrum shows good agreement at 0% void. On the other hand, significant discrepancies in the 5$^{th}$ and 7$^{th}$ groups could be observed at 100% void. For the 5$^{th}$ group, APOLLO-2/JEF2.2 gives larger neutron flux than SRAC/JENDL-3.2 by 5%, so that the reaction rate increase due to the voidage becomes more apparent in the APOLLO-2/JEF2.2 results. On the contrary, APOLLO-2/JEF2.2 gives smaller 7$^{th}$ group flux than SRAC/JENDL-3.2 by -7.2%, so that the reaction rate increase due to the voidage becomes less apparent. This corresponds to the behavior of the discrepancy of void reactivity components shown in Tables 2.4 and 2.5. The relative discrepancies found at the 9$^{th}$ and 10$^{th}$ group flux for the 100% voided cell are -3.0% and +6.7%, respectively. These discrepancies also serve to cause considerable discrepancy, especially large relative discrepancy to void reactivity components.

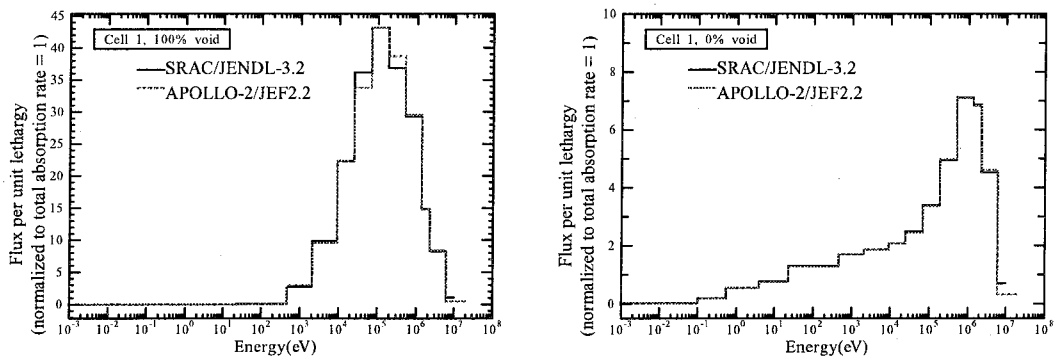


Figure 2.11 Comparison of cell-averaged 15-group flux of Cell 1 at 0% and 100% void.

The comparison of the 15-group cell averaged flux showed that, at least for the 5th, 7th, 9th and 10th groups, the discrepancy in the reactivity obtained by the two codes comes from the flux discrepancy and is less attributable to the cross section discrepancy. The cause of these discrepancies will be investigated through direct comparison of the fine-group (107 groups in SRAC/JENDL-3.2 and 172 groups in APOLLO-2/JEF2.2) cell averaged flux. **Figure 2.12** shows the normalized neutron spectra in the energy range above 1 keV for Cell 1 at 100% void obtained by SRAC/JENDL-3.2 and APOLLO-2/JEF2.2. Here, the neutron spectrum is shown by normalizing to the total absorption rate to be unity for each code system. Several differences can be found in the detailed structure of the spectrum, which are mainly attributable to the difference in the energy structure in the vicinity of the resonance of structure materials. Most significant difference can be observed in the vicinity of the oxygen resonance near 400 keV and the Fe resonance near 27 keV, which correspond to the 5th group (183 keV < E < 499 keV) and 7th group (24.8 keV < E < 67.4 keV) in the current 15-group

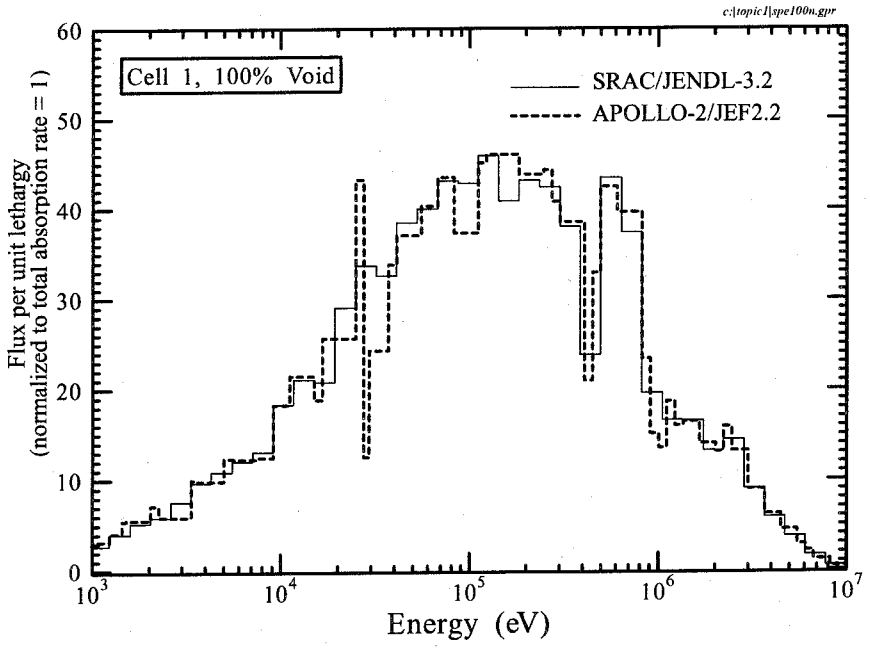


Figure 2.12 Comparison of cell-averaged neutron spectrum of Cell 1 at 100% void obtained by SRAC/JENDL-3.2 and APOLLO-2/JEF2.2. Energy range above 1 keV.

structure, respectively. In the vicinity of these resonances, the 172-group CEA93 library employs a more detailed energy group structure compared to the 107-group SRAC library in order to reproduce the cross section peaks of the resonances. For the 5$^{th}$ group (183 keV < E < 499 keV), the O-16 resonance around 400 keV is treated in a single energy group in the 107-group SRAC library, and the flux depression is larger compared to the APOLLO-2/JEF2.2 result. This leads to the smaller flux in the 5$^{th}$ group for SRAC/JENDL-3.2. For the 7$^{th}$ group (24.8 keV < E < 67.4 keV), the Fe scattering resonance at approximately 28 keV is treated in finer energy groups in the 172-group CEA93 library. This enables to reproduce the flux dip at the peak energy and the sharp flux peak in the next group due to the accumulation of scattered neutrons. The maximum lethargy loss due to the elastic scattering with Fe is approximately 0.0714 (calculated for Fe-56), and in the 107-group structure of SRAC with the lethargy width of $\Delta u$=0.25 in this energy range, neutrons scattered by this Fe resonance will stay in the same energy group. This is shown by the very small flux change around 300 keV calculated by SRAC/JENDL-3.2. Because of this difference in the energy structure and hence the representation of the cross section, APOLLO-2/JEF2.2 gives stronger flux depression in the vicinity of Fe resonance which could be clearly observed in the energy range just above the resonance.

As the secondary effect caused by these differences in the flux, the reaction rate of the heavy nuclides calculated by SRAC/JENDL-3.2 becomes smaller than that by APOLLO-2/JEF2.2 in the 5$^{th}$ group and larger in the 7$^{th}$ group. As the voidage progresses, the importance of these two groups increases, which leads to a considerable contribution to the total reactivity difference.

**Figure 2.13** shows the fine-group neutron spectrum in the energy range corresponding to the 10$^{th}$ group. The higher neutron flux for APOLLO-2/JEF2.2 is caused by a small flux "peak" at about 2 keV (52$^{nd}$ group of the 172-group CEA93 library), which provides larger

slowing-down source for the energy groups below 2 keV. Through examination of cross section curves, it has been found that this shape of the spectrum comes from the Mn-55 scattering resonance. Just between the 2.4 keV and 1.1 keV resonances of Mn-55, the 52nd group of CEA93 library has a small cross section value, so that the neutron flux in this energy group becomes larger than the neighboring groups. Neutrons scattered at the 2.4 keV resonance also accumulate in the 52nd group, which results to a small peak in the neutron flux.

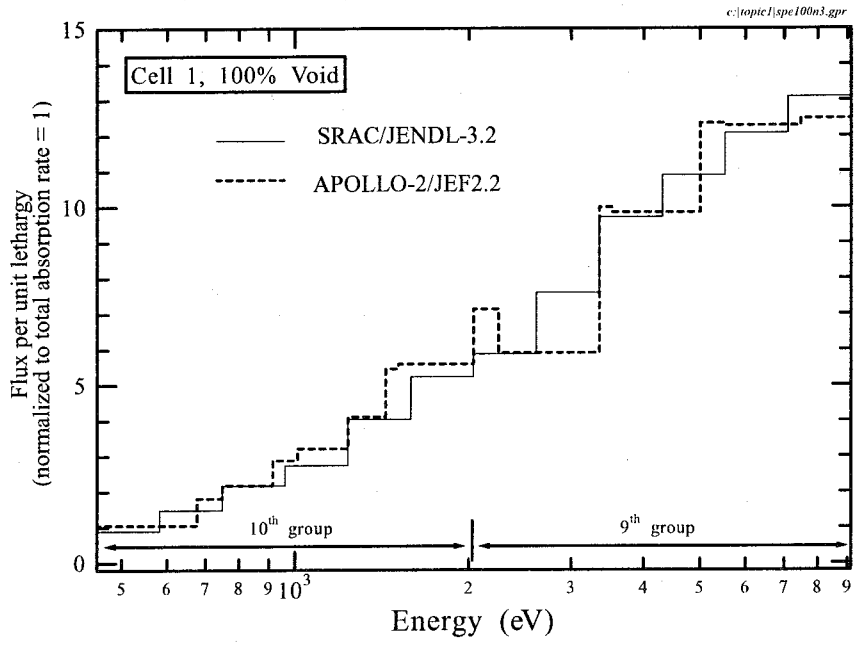


Figure 2.13 Comparison of cell-averaged neutron spectrum of Cell 1 at 100% void obtained by SRAC/JENDL-3.2 and APOLLO-2/JEF2.2. Energy range is 454 ev < E < 9 keV.

### *2.4.4.B Analysis of Reaction Rate Difference of Major Isotopes*

As shown in the preceding subsections, discrepancies for several energy groups could be attributed to the difference in the flux itself. The reaction rate difference $\Delta R$ of major isotopes are decomposed into two components, namely the flux term $\bar{\Sigma}\Delta\phi$ and the cross

section term $\bar{\phi}\Delta\Sigma$ as follows ;

$$\Delta R = \bar{\Sigma}\Delta\phi + \bar{\phi}\Delta\Sigma, \tag{2-9}$$

where

$$\bar{\Sigma} = \frac{\Sigma_{APOLLO-2} + \Sigma_{SRAC}}{2}, \quad \bar{\phi} = \frac{\phi_{APOLLO-2} + \phi_{SRAC}}{2}, \tag{2-10}$$

and

$$\Delta\Sigma = \Sigma_{APOLLO-2} - \Sigma_{SRAC}, \quad \Delta\phi = \phi_{APOLLO-2} - \phi_{SRAC}. \tag{2-11}$$

The cross section difference and the flux difference are correlated and this cross term should be also taken into account for the precise discussion, but in this analysis we assume that the two terms could be treated to be separable.

Through the examination of the results, the following comments on cross section and neutron flux difference are derived.

- For the 0% voided cell, APOLLO-2/JEF2.2 generally gives smaller effective cross section for the giant resonance of heavy nuclides in the resolved resonance region compared to SRAC/JENDL-3.2. This was found in the 10, 11 and 12$^{th}$ groups for the U-238 capture, the 12$^{th}$ group for the Pu-239 fission, the 13$^{th}$ group for the Pu-240 capture and the 11$^{th}$ group for the Pu-242 capture.

- The different treatment of resonance self-shielding is thought to be the cause of different sign appearing in cross section terms for the 0% and 100% voided cells. This could be best seen in the 11$^{th}$ group for the U-238, the 13$^{th}$ group for the Pu-239, the 11$^{th}$ and 12$^{th}$ groups for the Pu-240 and the 11$^{th}$ group for the Pu-242.

- The major differences in the natural Fe and Mn-55 capture rates are arising from the significant differences of resonance capture cross sections, which could be seen at the $10^{th}$ group for natural Fe, the $11^{th}$ group for Mn-55. This comes from the different treatment of those resonance cross sections in the two code systems.

- Differences in the U-238 capture above the $3^{rd}$ group, the Pu-239 fission above the $4^{th}$ group, the Pu-241 capture above the $7^{th}$ group and the natural Fe and Mn-55 capture above the keV region are attributable to the difference in the cross section data itself.

The analysis of the reaction rate discrepancy presented here, however, is in a preliminary stage, and more precise treatment of the correlation between the cross section difference and the flux difference is required for further understanding. Thus, sensitivity studies of the MOX lattices are desired to be performed as the future topic of the study.

## 2.5 CONCLUSION

In this chapter, studies related to the analysis of void coefficient in MOX fueled tight-pitch lattice light water reactor cells have been summarized. The discrepancy of the $k_\infty$ and void reactivity values obtained by the French APOLLO-2/JEF2.2 and the Japanese SRAC/JENDL-3.2 have been analyzed based on detailed decomposition of reactivity difference into contributing nuclide, reaction type and energy group.

The discrepancy of $k_\infty$ values is mainly caused by the Pu-239 component, which shows a strong dependence on the void fraction. The void fraction dependence of Pu-241 strongly affects the overall reactivity discrepancy. The reactivity discrepancy therefore is sensitive to the Pu isotopic composition. Considerable discrepancy due to stainless steel clad and oxygen has been observed.

The discrepancy of void reactivity is also caused by the Pu-239 and Pu-241 components. The differences between APOLLO-2/JEF2.2 and SRAC/JENDL-3.2 for the Pu-239 and Pu-241 components have opposite signs and act as to cancel each other; the overall discrepancy in the void reactivity therefore is sensitive to the isotopic composition of the Pu. Apart from the heavy nuclides, the different treatments of resonance self-shielding for the structure materials in the stainless steel cladding also act as a cause of the discrepancies.

The discrepancies related to the structure materials and oxygen are significant, sometimes having the magnitude comparable to those of the heavy isotopes. The cross section difference for oxygen is considerable and has a certain impact on cell parameters at high void fraction. For structure materials, it has been found that, not only the resonance self-shielding but also the energy group structure in the keV region is important, since the structural material resonances play an important role in forming the neutron spectrum.

The present method for the reaction rate-based decomposition of reactivity components

has shown to be successfully applied for detailed analysis of reactivity difference, where the reactivity difference is caused by a balance of both negative and positive components. However, as the present study is mostly based on intercomparison between reaction rates obtained by the two code systems, the discrepancies arising from the cross section libraries and discrepancies arising from the calculation method employed in both code systems are not completely separated. Results of sensitivity analysis are expected to provide important information, and remain as a subject to be performed in the future in conjunction with the extension of this study.

## References for Chapter 2


[1] EDLUND, M. C.: *Ann. Nucl. Energy* **2**, 801 (1975).

[2] EDLUND, M. C.: *Trans. Am. Nucl. Soc.*, **24**, 508 (1976).

[3] OLDEKOP, W., BERGER, H.-D. and ZEGGEL, W.: *Nucl. Technol.*, **59**, 212 (1982).

[4] PENNDORF, K., SCHULT, F. and BUNEMANN, D.: *Nucl. Technol.*, **59**, 256 (1982).

[5] RONEN, Y., COJOCARU, M., REGEV, D. *et al.*: *Ann. Nucl. Energy*, **5**, 221 (1978).

[6] RONEN, Y., COJOCARU, M. and RADKOWSKY, A.: *Trans. Am. Nucl. Soc.*, **34**, 784 (1980).

[7] CHAWLA, R., GMÜR, K. *et al.*: *Nucl. Technol.*, **67**, 360 (1984).

[8] RONEN, Y., LEIBSON, M. J. and RADKOWSKY, A.: *Nucl. Technol.*, **80**, 225 (1988).

[9] CHAWLA, R.: *Atomkernenergie* **37**, 303 (1981).

[10] OKUMURA, K. and NISHINA, K.: *Nucl. Sci. Eng.*, **102**, 381 (1989).

[11] CHAWLA, R.: NEACRP-A-726(1985).

[12] BERGER, H. D., BÖHME, R. and CHAWLA, R.: *Proc. Int'l. Topical Mtg. on Advances in Reactor Physics, Mathematics and Computation*, Paris, France, 1987, Vol. **1**, 107 (1987).

[13] PELLONI, S., CHAWLA, R. and STEPHANEK, J.: *Proc. Int'l. Topical Mtg. on Advances in Reactor Physics, Mathematics and Computation*, Paris, France, 1987, Vol. **1**, 119 (1987).

[14] SEILER, R., CHAWLA, R. *et al.*: *Nucl. Technol.*, **80**, 311(1988).

[15] PELLONI, S., STEPHANEK, J. and VONTOBEL, P.: *Nucl .Sci. Eng.*, **103**, 247 (1989).

[16] AXMANN, J. K., KLÜVER, B. *et al.*: *Nucl. Eng. Design* **118**, 61 (1990) .

[17] CHAWLA, R., BÖHME, R. *et al.*: *Kerntechnik* **57**, 14 (1992).

[18] AKIE, H., ISHIGURO, Y. and TAKANO, H.: NEACRP-L-309; JAERI-M 88-200

(1988).

[19] BERNNAT, W., ISHIGURO, Y. *et al.*: *Proc. Int, Conf. on the Physics of Reactors : Operation, Design and Computation PHYSOR90*, Marseille, France, April 23-27, 1990, Vol. **1**, p. I-54 (1990).

[20] BROGLI, R., MOLDASCHL, H. and RUMMEL, I.: *Nucl. Eng. Design*, **147**, 1 (1993).

[21] BÖHME, R., BERGER, H.-D. *et al.*: *Nucl. Eng. Design*, **168**, 271 (1997) .

[22] LEHMANN, S., HETZELT, L. and AXMANN, J. K.: *Kerntechnik* **62**, 15 (1997) .

[23] CATHALAU, S., BENSLIMANE, A. *et al.*: *Nucl. Sci. Eng.*, **121**, 326 (1995).

[24] TSUCHIHASHI, K., ISHIGURO, Y. *et al.*: JAERI-1302, Japan Atomic Energy Research Institute (1986).

[25] SANCHEZ, R., MONDOT, J. *et al.*: *Proc. ANS Int. Topical Mtg. Advances in Reactor Physics, Mathematics and Computations*, Paris, France, April 27-30, 1987, Vol. **3**, p.1563 (1987).

[26] MORI, T. and NAKAGAWA, M.: JAERI-Data/Code 94-007, Japan Atomic Energy Research Institute (1994).

[27] JEONG, C-J., OKUMURA, K. *et al.*: *J. Nucl. Sci. Technol.*, **27**[6], 515 (1990).

[28] ISHIGURO, Y.: JAERI-M-5527, Japan Atomic Energy Research Institute (1974).

[29] SANCHEZ, R., COSTE, M. *et al.*: *Proc. Int, Conf. on the Physics of Reactors : Operation, Design and Computation PHYSOR90*, Marseille, France, April 23-27, 1990, Vol. **3**, p. PII-149,(1990).

[30] CATHALAU, S., CABRILLAT, J. C. *et al.*: *Proc. Int. Conf. on the Physics of Reactors PHYSOR96*, Mito, Japan, Sept. 16-20, 1996, Vol. **H**, p.84 (1996).

[31] MATSUURA, H., UEJI, M. *et al.*: *Proc. Int. Conf. on Future Nuclear Systems GLOBAL97*, Yokohama, Japan, p.395 (1997).

[32] UMANO, T., MARUYAMA, H. *et al.*: JAERI-Conf 99-002, 78 (1999).

[33] CATHALAU, S., FOUGERAS, P. *et al.*: *Proc. Int'l. Conf. Physics of Nuclear Science and Technology*, Long Island, New York, USA, October 5-8, 1998, Vol. **1**, 393 (1998).

# Chapter 3

# Verification of $^{232}$Th Nuclear Data through Analysis of Critical Experiments in Thermal-Neutron Systems Using the Kyoto University Critical Assembly

## 3.1 INTRODUCTION

From the early days of nuclear energy development, there has been a continuous interest in utilization of $^{232}$Th as a fertile material to produce $^{233}$U, which is a fissile material with excellent nuclear properties to be used as an energy source. The reason is mainly due to the attractive aspects of the thorium-based fuel cycle, which include the following ;

- thorium is far more abundant than uranium; it is estimated to be around triple of the uranium resource,
- thermal breeding is feasible due to the large $\eta$-value of $^{233}$U,
- the production of transuranium elements is essentially lower than that in the uranium-plutonium cycle,
- the high energy gamma-ray emission from the thorium-uranium fuel, mainly from daughter nuclides of $^{232}$U, is considered to be beneficial from the viewpoint of the non-proliferation of nuclear materials.

Among these distinguishing aspects of the thorium-based fuel cycle, the increasing concerns about the non-proliferation of nuclear materials and the strong demand for eliminating long-lived radiotoxic isotopes in the nuclear fuel cycle have recently acted as

strong motivations to pay attention and to reexamine the use of thorium-based fuel cycles. The renewed international interest on thorium-based fuel cycles has led to various new activities, including the proposal of Radkowsky Thorium Reactor[1]-[3], effective burning of weapons-grade plutonium[4]-[6], enhancement of proliferation resistance of the fuel cycle[7]-[9], incineration of transuranium elements by combining thorium-based fuel cycles with accelerator driven systems[10]-[12] and application of the thorium-based fuel to various reactor concepts[13]-[19]. An excellent comprehensive review of the activities and the perspectives of thorium fuel cycle is given in Ref. [20]. It should be noted that the increasing attention has been focused on thermal-neutron systems as a feasible system for thorium utilization in the recent activities.

These activities are mainly performed through neutronics calculations, and the results of design studies on the thorium-based fuel cycles could certainly be affected by the scheme of calculation, including both the nuclear data and neutronics design code. However, investigation on the sensitivity of the calculation scheme to the nuclear characteristics of thorium-based fuel cycle has not been performed intensively. The possible ambiguities in the calculation scheme today is considered to be coming from the evaluated cross section itself. This is mainly attributable to the recent development in computing resources, which have enabled to perform detailed Monte Carlo calculations with easily available computing resources and have acted to eliminate ambiguities caused by approximations in modeling, which are inevitable in deterministic methods. It should be noted that, compared to the uranium-plutonium fuel cycle, less attention has been paid to the nuclear data related to the thorium-based fuel cycle, and their ambiguities are rather large to be utilized for detailed design calculations[21]. Even the most essential $^{232}$Th cross sections in major evaluated libraries still have rather large discrepancies, as will be shown later in this chapter. Therefore, to conduct further the feasibility studies on neutronic performance in consideration

of the various candidates of the reactor concepts using thorium-based fuel cycle, it is considered to be necessary to assess the current $^{232}$Th cross sections and to clarify how the difference in $^{232}$Th cross section data may affect the nuclear characteristics of thorium-based fuel cycle. An example of such assessment has been performed for the fast spectrum thorium-uranium systems[22], but there are no apparent activities for the thermal thorium-uranium systems.

In order to perform this assessment, the integral experiment data of thorium-based thermal systems performed at the Kyoto University Critical Assembly (KUCA) in Kyoto University Research Reactor Institute have been chosen to be analyzed in the present study. In the KUCA, an experimental study on the thorium-uranium fuel cycle was initiated in 1977 [23]. In this study, critical experiments using a solid moderator core of the KUCA containing thorium metal plates have been performed [24]-[28] as well as the basic study on fusion-fission hybrid reactors containing thorium by using a Cockcroft-Walton type accelerator in the KUCA and thorium piles [29]-[32]. As these experiments were dedicated for the integral test of nuclear data and the numerical calculation scheme of thorium-loaded thermal systems, their analyses are considered to be useful for the assessment of $^{232}$Th cross sections intended in the present study. The experiments are still under progress in order to extend our database on thorium-based fuel systems. It should be noted that only a limited activity[33] could be found for recent experimental studies on nuclear characteristics of thorium-based fuel systems.

Analyses of the thorium-loaded experiments at the KUCA have been performed in the past [24],[26]; they employed older evaluated cross section libraries such as ENDF/B-IV and calculation scheme which included geometrical approximations for core modeling as well as the multigroup treatment of the cross sections. As stated before, recent development of continuous energy Monte Carlo codes and the expansion of computational resources enabled us to perform the criticality analysis of the experiments with a minimal approximation on the

core geometry, so that the nuclear data itself can be more directly assessed. In the present study, detailed Monte Carlo analysis of the critical experiments has been executed to assess the $^{232}$Th cross section more directly among the recently evaluated cross section libraries, namely JENDL-3.2 [34], ENDF/B-VI [35] and JEF2.2 [36] and to point out the impact of discrepancy among the evaluated $^{232}$Th cross sections to nuclear characteristics in the thorium-based fuel cycle.

## 3.2 DIFFERENCE BETWEEN THORIUM CROSS SECTIONS IN EVALUATED LIBRARIES AND ITS IMPACT TO NUCLEAR CHARACTERISTICS OF THERMAL THORIUM-URANIUM SYSTEM

The $^{232}$Th cross sections in the evaluated libraries JENDL-3.2, ENDF/B-VI and JEF2.2 are compared, and the major difference among the cross sections and its impact to nuclear characteristics of thorium-uranium system will be described in this section. As our current interest is focused on thermal systems, discussion on fission cross section will be omitted.

**Figure 3.1** shows the comparison of $^{232}$Th capture cross sections taken from the three libraries described above. The major difference exists in the unresolved resonance range ; compared to the other libraries, JENDL-3.2 gives smaller capture cross sections in the range of approximately 100 eV to 5 keV. There also exist notable differences at the valleys of the resonances. Especially, the difference observed below the first resonance at about 25 eV to 1/v thermal cross section range is considered to have a large impact in thermal neutron systems.

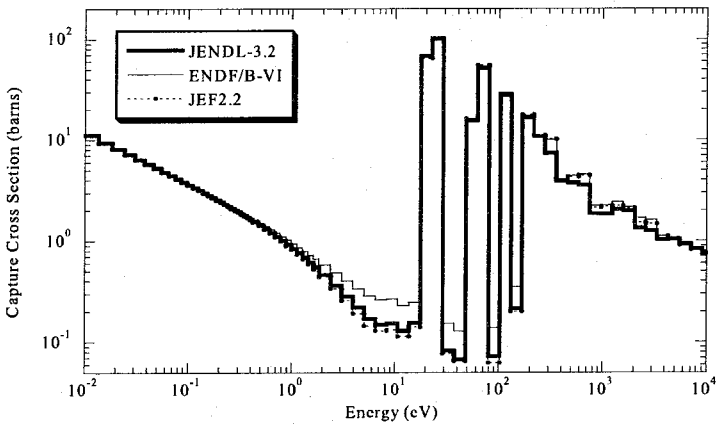


Figure 3.1 $^{232}$Th capture cross sections taken from JENDL-3.2, ENDF/B-VI and JEF2.2.

At higher energy region, difference of total cross section becomes apparent as shown in **Fig. 3.2**. A notable discrepancy exists between JEF2.2 and the other two libraries. This is attributable to the difference in elastic and inelastic scattering cross sections as shown in **Fig. 3.3**.

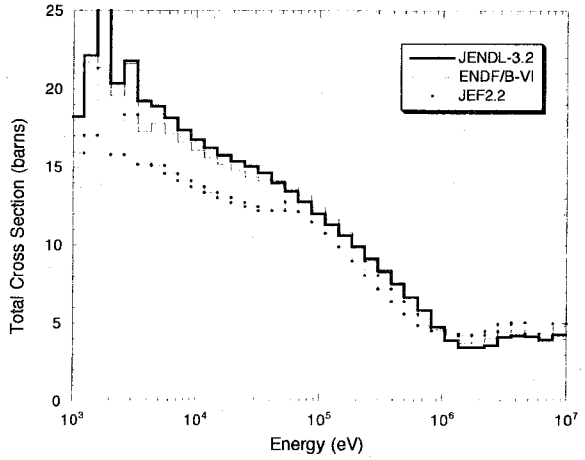


Figure 3.2 $^{232}$Th total cross sections taken from JENDL-3.2, ENDF/B-VI and JEF2.2 (E >103 eV).

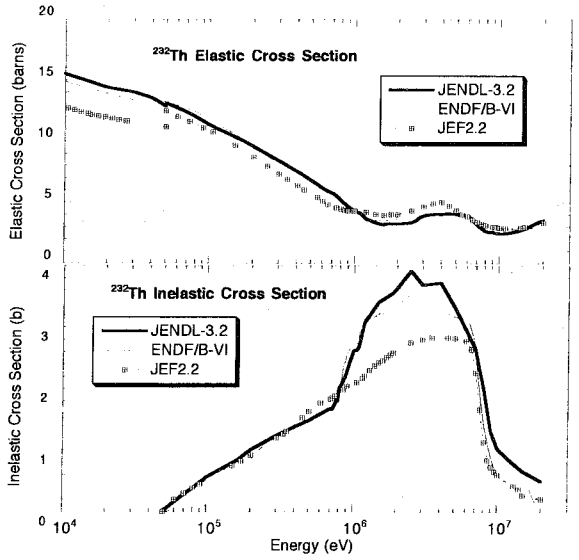


Figure 3.3 $^{232}$Th elastic and inelastic scattering cross sections taken from JENDL-3.2, ENDF/B-VI and JEF2.2.

These discrepancies in the evaluated $^{232}$Th cross sections can lead to difference in the nuclear characteristics of the thorium-uranium fueled system. To demonstrate this, infinite pin cell calculations for a $ThO_2$-$UO_2$ cell have been performed. **Table 3.1** shows the specification of the $ThO_2$-$UO_2$ pin cell, which was taken from the cell model used in Ref. [18], except that the cladding material was changed to natural zirconium for simplicity in this study.

Table 3.1 Specifications of the $ThO_2$-$UO_2$ pin cell

| Material | Isotope | Number Density ($10^{24}$atoms/cm$^3$) |
|---|---|---|
| Fuel pellet: $ThO_2$-$UO_2$<br>Outer diameter: 0.823 cm<br>Temperature: 1611 K | $^{232}$Th<br>$^{235}$U<br>$^{238}$U<br>$^{16}$O | 1.61665E-2*<br>1.14010E-3<br>4.64713E-3<br>4.39075E-2 |
| Clad: Natural Zirconium<br>Clad Outer Diameter: 0.9424 cm<br>Fuel-Clad gap: none<br>Temperature: 750 K | natural Zr | 4.16248E-2 |
| Moderator: $H_2O$<br>Pin pitch: 1.27 cm<br>Temperature: 605 K | H in $H_2O$<br>$^{16}$O | 4.30769E-2<br>2.15384E-2 |

* Read as $1.61665\times 10^{-2}$

Cell calculations were performed using the SRAC code system [37] in 107 energy groups. Calculations have been performed using $^{232}$Th cross sections taken from JENDL-3.2 or ENDF/B-VI, together with all other cross sections taken from JENDL-3.2. **Table 3.2** shows the comparison of $k_\infty$ values obtained by using the two $^{232}$Th data libraries. The difference in the $^{232}$Th nuclear data alone leads to significant difference in reactivity of $-1.09\%\Delta k/k$. This reactivity difference can be further decomposed into contributing components using the following formula [38];

$$\Delta\rho \cong \frac{1}{k_\infty}\sum_i\sum_g\left(\frac{\Delta P_i^g}{\overline{P}}-\frac{\Delta C_i^g}{\overline{A}}-\frac{\Delta F_i^g}{\overline{A}}+\frac{\Delta N_i^g}{\overline{A}}\right)=\sum_i\sum_g\Delta\rho_i^g, \qquad (3\text{-}1)$$

where $\rho$ is the reactivity, indices $i$ and $g$ correspond to the nuclide and the energy group, respectively, and $P_i^g$, $C_i^g$, $F_i^g$ and $N_i^g$ are the space-integrated production, capture, fission and $(n,2n)$ reaction rates, respectively. $\Delta$ denotes the difference between each term obtained using $^{232}$Th cross section from ENDF/B-VI and JENDL-3.2. $\overline{k_\infty}$, $\overline{P}$ and $\overline{A}$ denotes the averaged $k_\infty$ value, production and absorption rates obtained using $^{232}$Th cross section from ENDF/B-VI and JENDL-3.2, respectively.

Table 3.2 Comparison of $k_\infty$ for the $ThO_2$-$UO_2$ pin cell

| Case | $k_\infty$ |
|---|---|
| All nuclides from JENDL-3.2 | 1.22710 |
| $^{232}$Th from ENDF/B-VI.5 + other nuclides from JENDL-3.2 | 1.21084 |
| Reactivity Difference ($\%\Delta k/k$) | -1.09 |

The result of the decomposition is shown in **Fig. 3.4**, where only the total contribution of the nuclide $i$ for the group $g$, $\Delta\rho_i^g = \frac{1}{\overline{k_\infty}}\left(\frac{\Delta P_i^g}{\overline{P}} - \frac{\Delta C_i^g}{\overline{A}} - \frac{\Delta F_i^g}{\overline{A}} + \frac{\Delta N_i^g}{\overline{A}}\right)$, is shown for simplicity. A significant contribution of $^{232}$Th could be seen in the resonance region, which is directly attributable to the capture cross section difference shown in Fig. 3.1. The negative contribution of $^{235}$U in the thermal region is a secondary effect due to the spectrum difference caused by the $^{232}$Th contribution in the resonance region ; the increase in $^{232}$Th capture rate in the resonance region leads to the decrease in resonance escape probability and thus the decrease of thermal neutrons, which then leads to the decrease of $^{235}$U thermal fission rate.

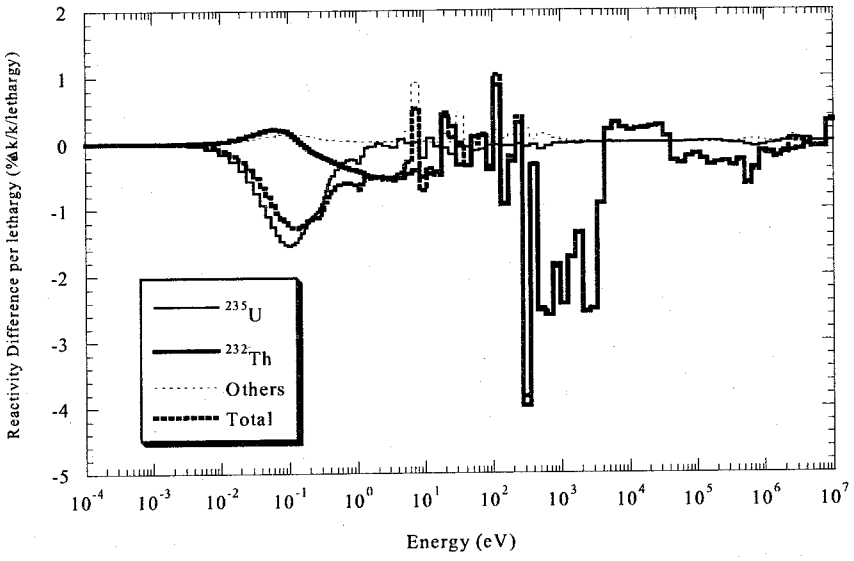


Figure 3.4 Breakdown of reactivity difference due to the use of different $^{232}$Th cross sections in $ThO_2$-$UO_2$ Cell.

This simple example demonstrates that the difference in the current $^{232}$Th evaluations is rather significant and that the use of different $^{232}$Th cross section data can lead to significant difference in nuclear characteristics of thorium-loaded systems. Therefore, it is desirable to perform an assessment of the evaluated $^{232}$Th cross sections in order to qualify the reliability and the prediction accuracy of nuclear characteristics in thorium-based thermal systems. This assessment will be performed through analysis of critical experiments in thorium-loaded thermal systems performed at the KUCA as will be described in the preceding section.

## 3.3 CRITICAL EXPERIMENTS ON THORIUM-URANIUM FUEL CYCLE AT THE KUCA

The KUCA is a multi-core type critical assembly constructed in 1974 for the reactor physics study and the education. The critical experiments on the thorium-uranium fuel cycle have been performed by using one of the solid moderated core, B-core [39]. A schematic view of the critical assembly is shown in **Fig. 3.5**. The materials used in the solid moderated cores are in the form of plates with nominal cross section of 5.08cm (2 inches) square. The main fuel material is 93%-enriched uranium-aluminum alloy (EU) plate with 0.15875cm (1/16 inch) in thickness, which can be combined with moderator plates such as polyethylene and graphite of various thickness. Thorium and natural uranium metal plates are also usable as experimental material plates, which have been used in the critical experiments treated in this study. The material plates are piled up in aluminum square

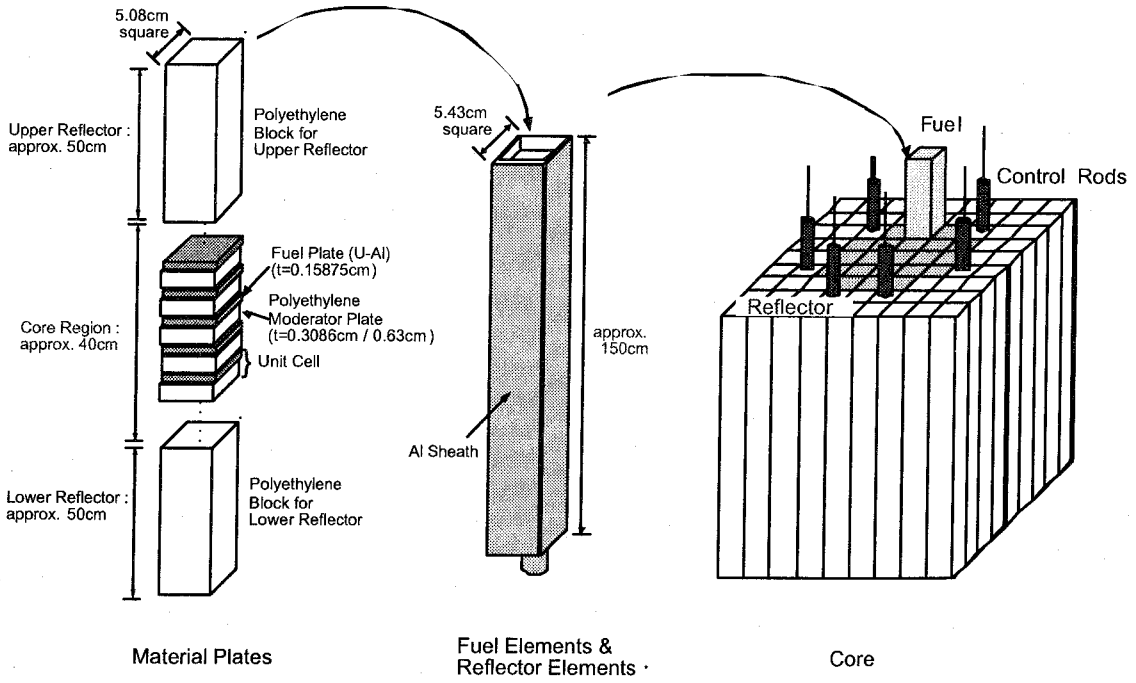


Figure 3.5 Schematic view of KUCA solid moderated core.

sheaths of 1.5 m in length, and these sheaths are then arranged onto the grid plate to construct the critical assembly.

In this study, the results of the zone-type thorium-uranium core experiments were used for the assessment of $^{232}$Th cross sections. The configurations of the zone-type cores are shown in **Fig. 3.6**. The critical cores consist of the central test zone containing thorium and graphite with various volume ratios and the driver fuel surrounding the test region. The test zone elements, shown in **Fig. 3.7**, comprise of thorium-graphite regions with various combination of thorium metal plates of 0.3175 cm (1/8") in thickness and graphite plates of 0.635 cm (1/4"), 1.27 cm (1/2") or 5.08 cm (2"), sandwiched by the upper and lower graphite reflectors. The axial heights of the thorium-graphite region, upper and lower graphite reflectors are approximately 55 cm, 33 cm and 58 cm, respectively. In addition to the experiments using thorium, experiments have been performed by substituting the thorium plates in the thorium-graphite regions with three natural uranium (NU) plates of 0.315 cm (*i.e.* 0.105 cm each×3) in total thickness. These experiments were performed by systematically varying the ratio of thorium to graphite (C/Th) or uranium to graphite (C/NU) in the test zone as shown in **Table 3.3**. Six cores with thorium test zones (Th-zone cores), four cores with natural-uranium test zones (NU-zone cores) and one reference graphite test zone core were constructed. The test zone elements are loaded in the central 3 by 3 test zone, and are

Table 3.3 Configurations of the test zone elements

| Th Test Zone Elements | | | NU Test Zone Elements | | |
|---|---|---|---|---|---|
| ID | C/Th* | Structure | ID | C/NU* | Structure |
| Th I | 96 | [1/8"Th+4"C]×5 cells | NU I | 65 | [3.15mmNU+4"C]×5 cells |
| Th II' | 48 | [1/8"Th+2"C]×10 cells | NU III | 16 | [3.15mmNU+1"C]×20 cells |
| Th III | 24 | [1/8"Th+1"C]×20 cells | NU IV | 8 | [3.15mmNU+1/2"C]×36 cells |
| Th IV' | 12 | [1/8"Th+1/2"C]×35 cells | NU V | 4 | [3.15mmNU+1/4"C]×58 cells |
| Th V | 6 | [1/8"Th+1/4"C]×58 cells | | | |
| Th Lump | 0 | Th Lump (1/8"Th×175) | | | |

*Atom number ratio

surrounded by driver fuels containing EU and polyethylene plates. The same driver fuels with $H/^{235}U$ ratio of approximately 316 were used throughout the series of the experiments. The driver fuel was then surrounded by polyethylene reflector elements. The calculated neutron spectra at the center of the test zones show remarkable variance depending on the C/Th ratio as shown in **Fig. 3.8**.

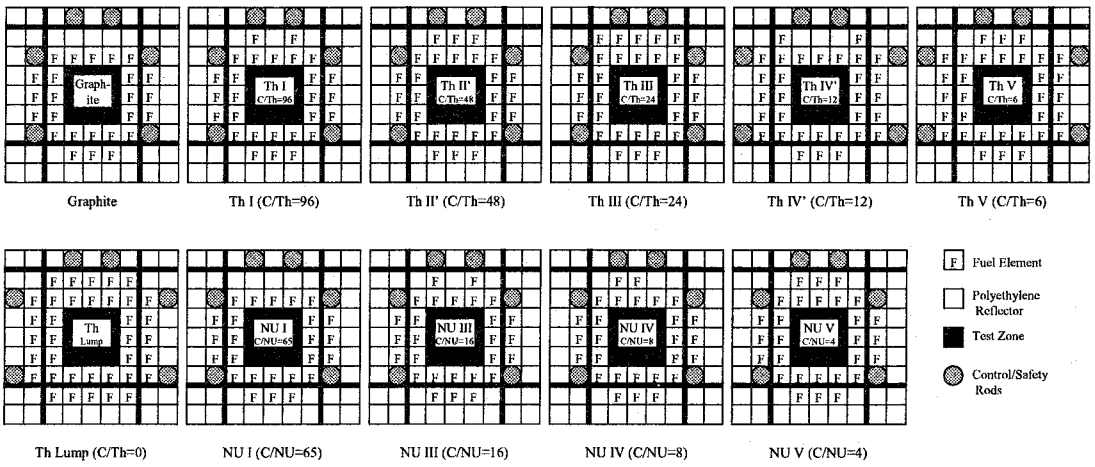


Figure 3.6 Core configurations of Th- and NU-zone type critical experiments.

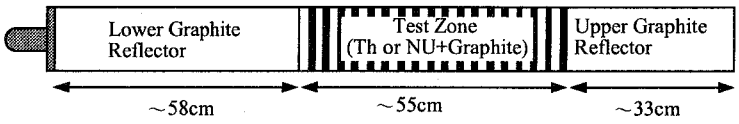


Figure 3.7 Test zone element.

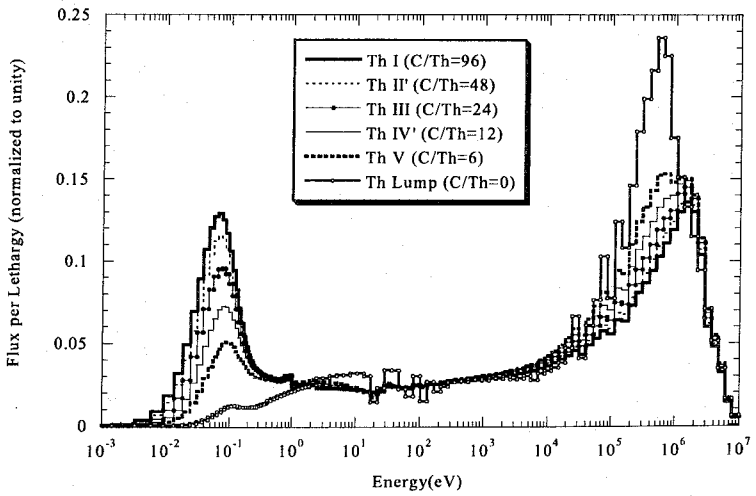


Figure 3.8 Calculated spectrum at the center of Th-zone critical core.

## 3.4 ANALYSIS, RESULTS AND DISCUSSION

### 3.4.1 CRITICALITY ANALYSES USING MVP

The criticality analyses have been performed by using the continuous energy Monte Carlo code MVP[40] together with the JENDL-3.2 nuclear data library. The detailed configuration of the core was treated explicitly to avoid any possible ambiguities caused by approximations in the core modeling. In the MVP calculations, 3,000,000 neutron histories were traced to suppress the statistical error in $k_{eff}$ values to less than 0.1% ($2\sigma$), while the typical experimental error for the $k_{eff}$ values was estimated to be approximately $3\times10^{-4}$ (0.03%).

**Figure 3.9** shows the C/E value of $k_{eff}$ for the Th-zone and NU-zone cores. The C/E values suffer from a certain pedestal of around 0.7% ; this overestimation is consistent with the reported feature of JENDL-3.2 results for $^{235}U$ thermal systems [39], [41]. This is caused by the $^{235}U$ cross sections in the driver region and is mainly attributable to the inadequate evaluation of $^{235}U$ capture cross sections in the resonance region, and the use of the

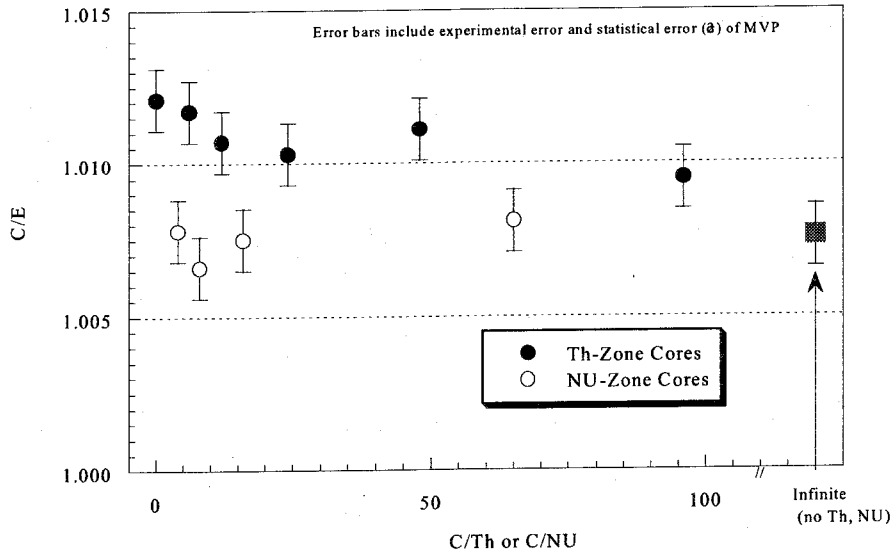


Figure 3.9 C/E value of $k_{eff}$ for the Th- and NU-zone cores using JENDL-3.2.

forthcoming JENDL-3.3 is expected to solve this problem. Through comparison between the C/E trends for the Th-zone and NU-zone cores, it is apparent that the C/E values for cores containing thorium are systematically larger than those for cores containing natural uranium. Furthermore, the C/E values for cores containing thorium increase with decreasing C/Th ratio, in other words, with increasing fraction of thorium in the test zone, whereas the C/E values for cores containing natural uranium remain almost constant regardless of the change in C/NU ratio.

In order to examine the impact of different $^{232}$Th cross section evaluations to the criticality, the Monte Carlo calculations were performed for Th-zone cores by using MVP using $^{232}$Th cross sections from JENDL-3.2, ENDF/B-VI or JEF2.2. Note that in the calculations, only the $^{232}$Th cross sections were taken from JENDL-3.2, ENDF/B-VI or JEF2.2, whereas the cross sections for all other nuclides were taken from JENDL-3.2. **Figure 3.10** shows the thus obtained C/E values of $k_{eff}$ for the six Th-zone cores. The use of $^{232}$Th cross sections from ENDF/B-VI and JEF2.2 leads to lower C/E compared with JENDL-3.2, especially for cores with the smaller C/Th ratio. Unlike the case for JENDL-3.2, the C/E values decrease with C/Th ratio for C/Th < 50 when $^{232}$Th cross sections from

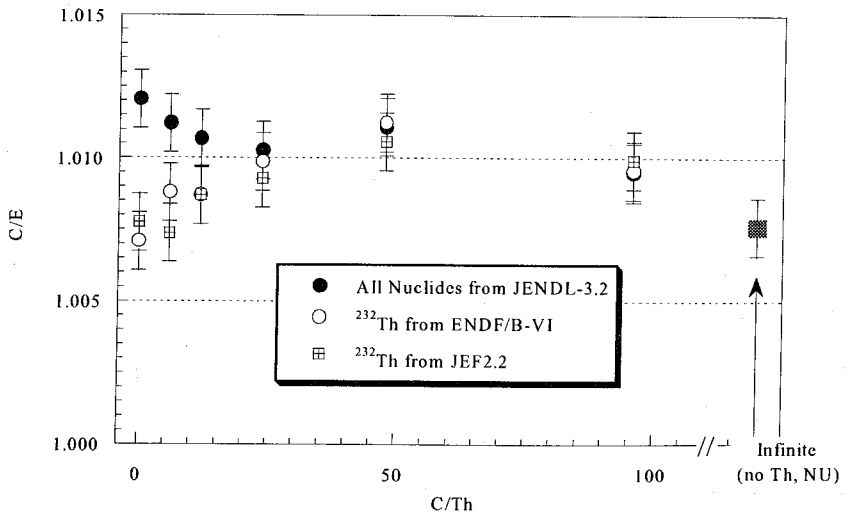


Figure 3.10 Comparison among C/E values of $k_{eff}$ for the Th-zone cores obtained using $^{232}$Th cross sections from JENDL-3.2, ENDF/B-VI and JEF2.2.

ENDF/B-VI and JEF2.2 are used. This leads to the increasing discrepancy among the C/E values obtained using $^{232}$Th cross sections from JENDL-3.2 and other libraries as shown in **Fig. 3.11**, where the differences are shown in the measure of reactivity difference. It could be seen that ENDF/B-VI and JEF2.2 show very similar trends, and the reactivity difference from JENDL-3.2 becomes approximately up to -0.5% $\Delta k/k$ for the Th-Lump core.

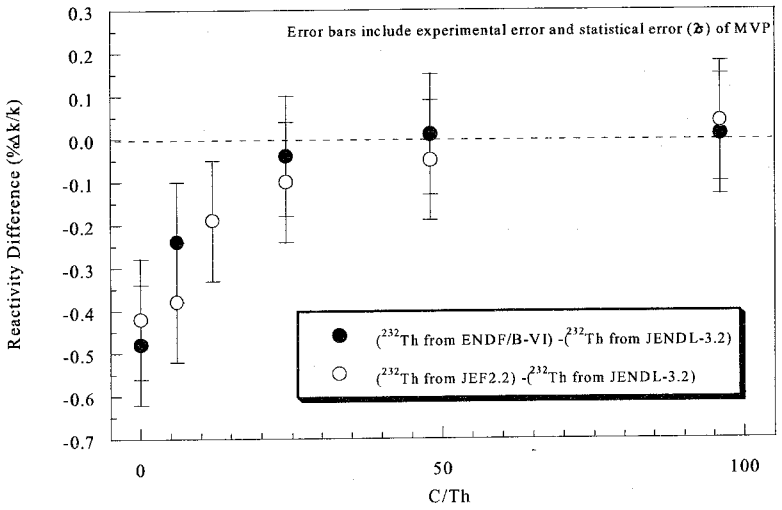


Figure 3.11 Reactivity difference of Th-zone cores obtained by using $^{232}$Th cross sections from JENDL-3.2 and other libraries.

From these results, it could be concluded that none of the current $^{232}$Th evaluations can satisfactorily predict the criticality of the zone-type core constructed in the KUCA. Furthermore, the different $^{232}$Th evaluated data may lead to considerable difference in the criticality predictions of thorium-based thermal systems, especially under hard-spectrum conditions.

In the remaining part of this chapter, detailed comparison between the criticality calculation results using $^{232}$Th cross sections from different evaluated libraries will be performed in order to draw some information on the aforementioned ambiguities in the $^{232}$Th cross sections.

### 3.4.2 INVESTIGATION ON IMPACT OF $^{232}$Th CROSS SECTION DIFFERENCE TO CRITICALITY USING SRAC/CITATION

The impact of different $^{232}$Th cross section evaluations to the criticality has been further investigated through the aid of perturbation calculations using the CITATION module in the SRAC code system (hereafter denoted as SRAC/CITATION) based on simplified two-dimensional cylindrical core models of the Th-zone cores shown in Fig.3.6. In the SRAC/CITATION calculations, only the $^{232}$Th cross sections were taken from JENDL-3.2, ENDF/B-VI or JEF2.2, whereas the cross sections for all other nuclides were taken from JENDL-3.2. The core calculation using JENDL-3.2 for all the nuclides was taken as the reference case and the change in the $^{232}$Th cross section in the test zone from JENDL-3.2 to other libraries was treated as perturbation. Hereafter, the perturbation cases are denoted as follows ;

- Case A: $^{232}$Th cross section in the test zone was changed from JENDL-3.2 to ENDF/B-VI,
- Case B: $^{232}$Th cross section in the test zone was changed from JENDL-3.2 to JEF2.2.

These perturbation calculations were performed using the built-in first-order perturbation capability of SRAC/CITATION. Although the SRAC/CITATION scheme is based on diffusion theory and thus is considered to be less accurate than the MVP calculation, the deterministic scheme employed could yield more detailed information on the reactivity difference caused by the difference in the $^{232}$Th cross sections. **Figure 3.12** shows the reactivity caused by the perturbation of Cases A and B . The reactivity change shows a similar trend to that obtained by MVP ; it depends on the C/Th ratio of the test zone and the curve is almost identical between the both Cases A and B. It should be noted that the

validity of the SRAC/CITATION perturbation scheme was confirmed by the satisfactory agreement with the directly calculated reactivity difference by MVP.

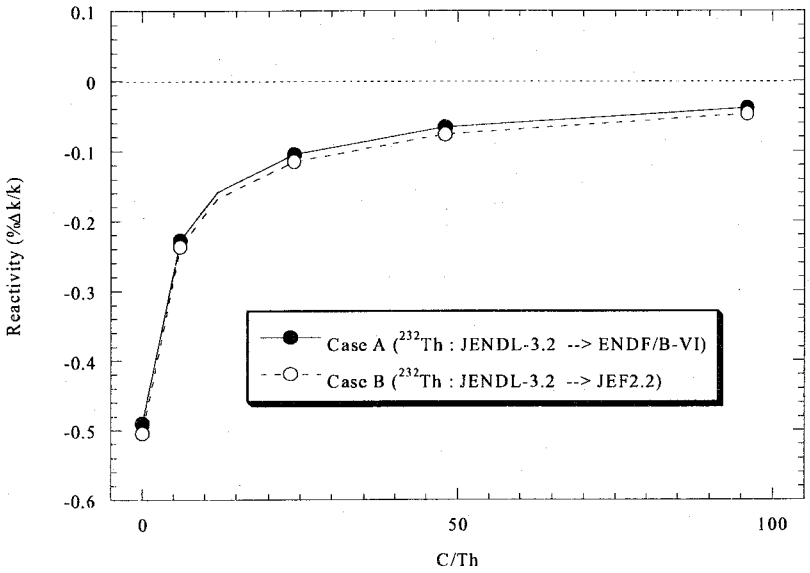


Figure 3.12 Reactivity difference obtained by perturbation calculations.

**Figures 3.13** and **3.14** show the energy breakdown of the reactivity difference for ENDF/B-VI and JEF2.2, respectively. Even though the overall reactivity difference was quite similar as shown in Fig. 3.11 or 3.12, it was found that the energy dependence of the reactivity difference is completely different between the two cases. For the Case A, a large portion of the reactivity difference arises from the resonance region and the epithermal region of E > 1 eV. On the other hand, large contribution could be found at the fast region and also at the thermal region for the Case B. This energy dependence was analyzed through the comparison of reactivity components. **Figures 3.15** and **3.16** show the energy dependence of the reactivity components in the Th-V core (C/Th=6) for the two cases, respectively.

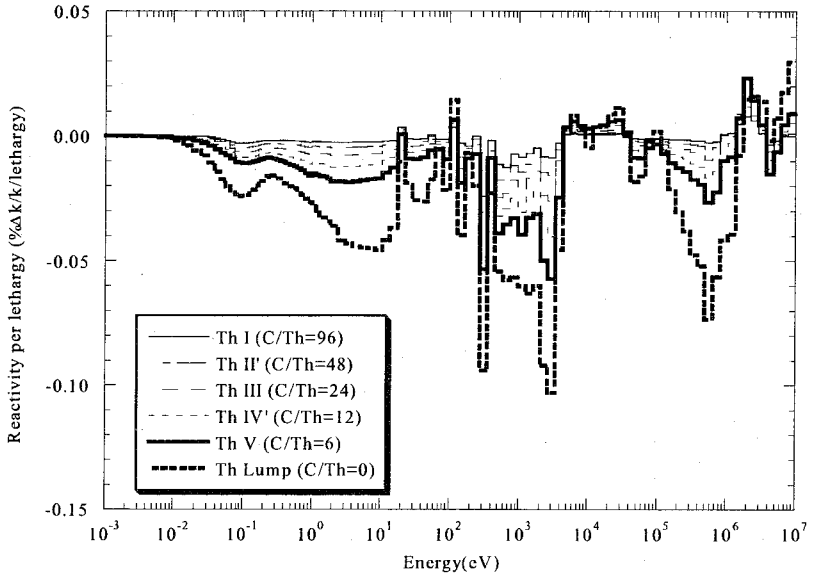


Figure 3.13 Energy dependence of reactivity difference caused by the use of different $^{232}$Th cross sections, Case A.

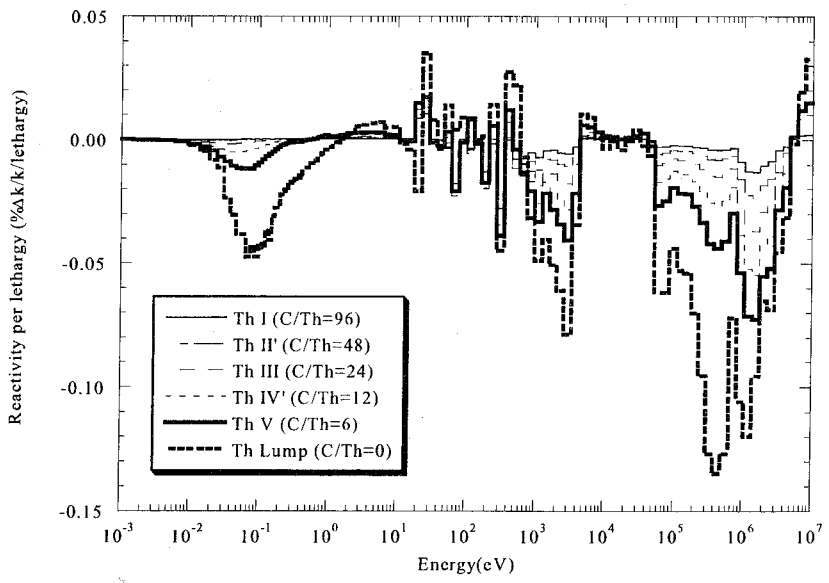


Figure 3.14 Energy dependence of reactivity difference caused by the use of different $^{232}$Th cross sections, Case B.

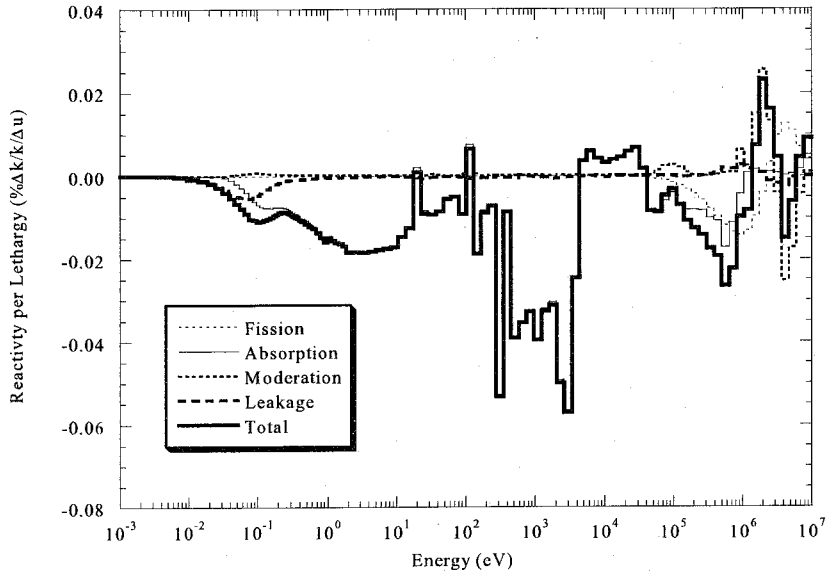


Figure 3.15 Energy dependence of reactivity component for Th-V Core, Case A.

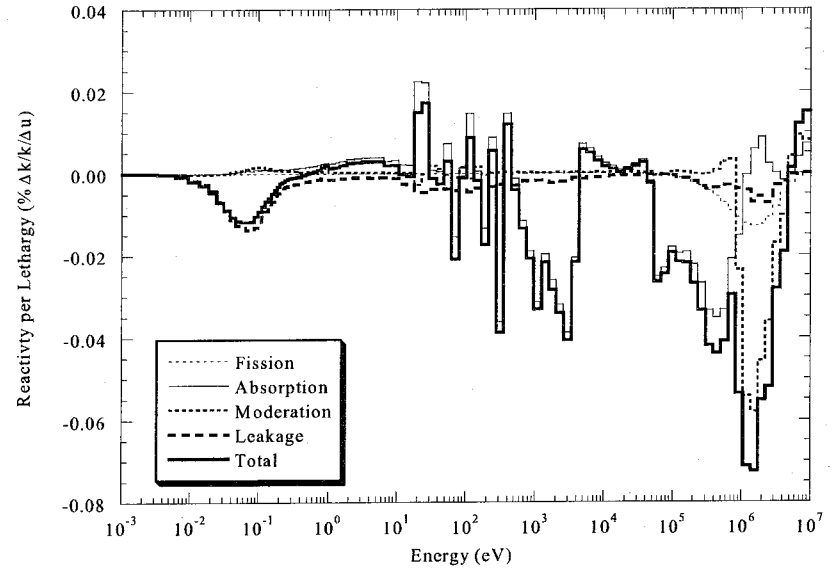


Figure 3.16 Energy dependence of reactivity component for Th-V Core, Case B.

For Case A, the dominant difference appears in the absorption component in the resonance range. The smaller capture cross sections in JENDL-3.2, especially in the unresolved resonance range of approximately 100 eV to 5 keV, leads to the negative absorption components. The discrepancy observed in thermal cross sections of JENDL-3.2 and ENDF/B-VI also has a significant impact. On the contrary, the dominant difference appears for the absorption component above 1 keV and the moderation component above 1 MeV for Case B. These components are directly attributable to the difference in resonance capture cross sections and to that in scattering cross sections between JENDL-3.2 and JEF2.2. In the thermal range, a small negative contribution of the leakage component appears in the both cases. This leakage component at the thermal region is due to the spectrum change, which is a secondary effect caused by the cross section differences in the resonance and fast regions.

The results of the perturbation calculations clearly reflect the difference between the $^{232}$Th cross section evaluations. The current disagreement among the evaluations can lead to rather large discrepancy in the nuclear characteristics of thorium-loaded thermal systems. In order to improve further the reliability and the prediction accuracy of the neutronics design for the thorium-based fuel cycle, it is desirable to reduce the uncertainty in the capture and scattering cross sections mentioned above. From this point of view, experimental studies including sample reactivity worth measurement in thorium-loaded cores at the KUCA are currently being performed in order to extend the experimental database for thermal systems containing thorium. It is expected that the analyses of those experiments would provide invaluable information on the uncertainty of the cross sections mentioned in the present study.

## 3.5 CONCLUSION

In this chapter, an assessment of $^{232}$Th nuclear data has been performed through the analysis of thorium-loaded critical experiments in thermal neutron systems by using the Kyoto University Critical Assembly (KUCA). The impact of the difference among the nuclear data libraries of $^{232}$Th was examined through neutronics calculations.

Through the analysis, it was found that JENDL-3.2 overestimates the $k_{eff}$ values of thorium-loaded KUCA cores by about 0.9% to 1.2%. Although approximately 0.7% of the overestimation is due to the $^{235}$U cross section used in the driver region, the overestimation for thorium-loaded cores is apparently larger than those for cores free from thorium by about 0.2% to 0.5%. This overestimation depends on neutron spectrum and becomes larger with hardening spectrum in the core. The use of $^{232}$Th cross sections from ENDF/B-VI and JEF2.2 also leads to the overestimation of the $k_{eff}$ values. Compared to JENDL-3.2, $^{232}$Th cross sections from ENDF/B-VI and JEF2.2 give smaller $k_{eff}$ values for hard spectrum cores, leading to the reactivity difference up to -0.5%. It became clear that none of the current $^{232}$Th evaluated cross sections can accurately simulate the criticality of the zone-type cores constructed in the series of KUCA experiments.

It was shown that the different $^{232}$Th evaluations may lead to considerable difference in criticality predictions for thorium-loaded thermal reactors. The difference is mainly attributable to the difference in the capture cross sections at the thermal region, the lower resonance and unresolved resonance regions, where JENDL-3.2 gives smaller cross section compared to ENDF/B-VI. The contribution of scattering cross section difference in the fast region could be also considerable in systems with hard spectrum, and further improvement in the aforementioned cross section evaluations is necessary to improve the reliability and the prediction accuracy of nuclear characteristics of thermal systems containing thorium.

## References for Chapter 3


[1] GALPERIN, A. and RADKOWSKY, A.: *Proc. Ninth International Conf. on Emerging Nuclear Energy Systems (ICENES'98)*, Tel-Aviv, Israel, June 28-July 2, 1998, Vol. **2**, 637 (1998).

[2] MOROZOV, A.G., GALPERIN, A. and TODOSOW, M.: *Nucl. Energy International*, Vol.**44**, No. **534**, 13 (1999).

[3] RADKOWSKY, A.: *Nucl. Energy International*, Vol.**44**, No. **534**, 14 (1999).

[4] GALPERIN, A.: *Ann. Nucl. Energy*, **22**, 507 (1995).

[5] GALPERIN, A. and Raizes, G.: *Nucl. Technol.*, **117**, 125 (1997).

[6] ARKHIPOV, V., RUTTEN, H.J. and GALPERIN, A.: *Proc. Ninth International Conf. on Emerging Nuclear Energy Systems (ICENES'98)*, Tel-Aviv, Israel, June 28-July2, 1998, Vol.**2**, 647 (1998).

[7] GALPERIN, A., REICHERT, P. and RADKOWSKY, A.: *Science and Global Security*, **6**, 265 (1997).

[8] PEREIRA, C. and LEITE, E.M.: *Ann. Nucl. Energy*, **25**, 937 (1998).

[9] GENNADY, K. *et al.*: *Proc. International Conf. on the Physics of Nuclear Science and Technology*, Long Island, New York, USA, Oct. 5-8, 1998, Vol. **1**, 331 (1998).

[10] SALVATORES, M. *et al.*: *Nucl. Sci. Eng.*, **126**, 333 (1997).

[11] BACHER, P.: *Nucl. Eng. Design*, **187**, 185 (1999).

[12] DAVID, S. *et al.*: *Nucl. Instrum. Methods in Physical Res. A* **443**, 510 (2000).

[13] SEFIDVASH, F. : *Nucl. Eng. Design*, **167**, 203 (1996) .

[14] TOMMASI, J., PUILL, A. and LEE, Y.-K.: *Proc. International Conf. on Future Nuclear Systems (Global'97)*, Oct.5-10, 1997, Yokohama, Japan, Vol.**1**, 308 (1997).

[15] JAGANNATHAN, V. *et al.*: *Proc. International Conf. on the Physics of Nuclear Science and Technology*, Long Island, New York, USA, Oct. 5-8, 1998, vol. **1**, 323 (1998).

[16] KIM, M.-H. and LIM, J.-Y.: *Proc. International Conf. on Mathematics and Computation, Reactor Physics and Environmental Analysis in Nuclear Applications*, Madrid, Spain, Sep. 27-30, 1999, 1674 (1999).

[17] KLOOSTERMAN, J. L. and DAMEN, P. M. G.: *J. Nucl. Mat.*, **274**, 112 (1999).

[18] CANER, M. and DUGAN, E. T.: *Ann. Nucl. Energy*, **27**, 759 (2000).

[19] RUTTEN, H.J. and HAAS, K.A.: *Nucl. Eng. Design*, **195**, 353 (2000).

[20] LUNG, M. and GREMM, O.: *Nucl. Eng. Design.*, **180**, 133 (1998).

[21] KUZMINOV, B.D. and MANOKHIN, V.N.: *Proc. International Conf. on Nuclear Data for Science and Technology*, Trieste, Italy, May 19-24, 1997, Vol. **2**, 1167 (1997).

[22] PELLONI, S., YOUINOU, G. and WYDLER, P.: *Proc. International Conf. on Nuclear Data for Science and Technology*, Trieste, Italy, May 19-24,1997, Vol. **2**, 1172 (1997).

[23] KIMURA, I.: *Progress in Nucl. Energy*, **29** (Supplement), 445 (1995).

[24] KOBAYASHI, K. *et al.*: *Nucl. Sci. Eng.*, **71**, 143 (1979).

[25] OKAYA, S., KOBAYASHI, K. and KANDA, K.: *Annu. Rep. Res. Reactor Inst. Kyoto Univ.*, **20**, 48 (1987).

[26] KIKUCHI, H. *et al.*, *Annu. Rep. Res. Reactor Inst. Kyoto Univ.*, **21**, 34 (1988).

[27] KOBAYASHI, K. *et al.*: *Proc. Indo-Japan Seminar on Thorium Utilization*, Dec. 10-13, 1990, Bombay, India, 248 (1991).

[28] IWASAKI, T. *et al.*, *Proc. International Conf. on the Physics of Reactors PHYSOR96*, Mito, Ibaraki, Japan, Sept. 16-20, 1996, Vol. **2**, E-266 (1996).

[29] HAYASHI, S.A. *et al.*: *JAERI-M* 91-032, 237, Japan Atomic Energy Research Institute (1991).

[30] ICHIHARA, C. *et al.*: *JAERI-M* 91-032, 415, Japan Atomic Energy Research Institute (1991).

[31] ICHIHARA, C. *et al.*: *JAERI-M* 91-062, 255, Japan Atomic Energy Research Institute (1991).

[32] KIMURA, I. *et al.*: *Proc. Indo-Japan Seminar on Thorium Utilization*, Dec. 10-13,

1990, Bombay, India, 255 (1991).

[33] GOLUBEV, V. I. *et al.*: *Proc. International Conf. on the Physics of Reactors PHYSOR96*, Mito, Ibaraki, Japan, Sept. 16-20, 1996, Vol. **2**, E-276 (1996).

[34] NAKAGAWA, T. *et al.*: *J. Nucl. Sci. Technol.*, **32**, 1259 (1995).

[35] ROSE, P. F. (comp. and ed.): BNL-NCS-17541 (4th Ed.) (1991).

[36] NORDBORG, C. and SALVATORES, M.: *Proc. International Conf. on Nuclear Data for Science and Technology*, Gatlinburg, Tennessee, USA, May 9-13, 1994, Vol. **2**, 680 (1994).

[37] OKUMURA, K., KANEKO, K. and TSUCHIHASHI, K.: *JAERI-Data/Code* 96-015, Japan Atomic Energy Research Institute (1996) (in Japanese).

[38] UNESAKI, H., SHIROYA, S., KANDA, K., CATHALAU, S. *et al.*: *Nucl. Sci. Eng.*, **135**, 1 (2000).

[39] UNESAKI, H. and SHIROYA, S.: *Proc. International Conf. on the Physics of Nuclear Science and Technology*, Oct. 5-8, 1998, Long Island, New York, Vol. **2**, 1587 (1998).

[40] MORI, T. and NAKAGAWA, M.: *JAERI-Data/Code* 94-007, Japan Atomic Energy Research Institute (1995) (in Japanese).

[41] HASEGAWA, A.: *JAERI-Conf* 97-005, 27, Japan Atomic Energy Research Institute (1997).

# Chapter 4

# Verification of $^{237}$Np and $^{241}$Am Fission Cross Sections Based on Fission Rate Ratio Measurements at the Kyoto University Critical Assembly

## 4.1 INTRODUCTION

The elimination of the minor actinides (MAs) is one of the dominating aspects for the utilization of nuclear power as the energy resource extending into the future. Studies on the methods to cope with the MAs generated in the fuel cycle have been intensively carried out in the recent years[1]. These include studies on incineration of MAs by using nuclear reactors or accelerator-driven subcritical systems by means of nuclear transmutation. Among them, the concept of incineration of MAs in light water reactors has recently being intensively studied[2]-[5] as a realistic option to confine MAs in the nuclear fuel cycle and to avoid the accumulation of long-lived MAs in high level wastes. Among the MAs produced in power reactors, neptunium-237 ($^{237}$Np) and americium-241 ($^{241}$Am) are the most burdensome isotopes because of their significant production rates, long half-lifes and hazard indeces. Therefore, the main objective of MA incineration system by using light water reactors is currently being set to the effective incineration of $^{237}$Np and $^{241}$Am.

The incineration properties of MAs are directly goverened by the reaction rate of MAs in the transmutation system. Therefore, in the research and development of the transmutation system, it is indispensable to assess the nuclear data of MAs for attaining the

reliability in the estimation of the nuclear characteristics of the core containing MA.

The incineration of MAs could be performed either through capture or direct fission process. In the capture process, the target MA nuclide is transmutated into other nuclide through neutron capture followed by the $\alpha$ or $\beta$ decay, until the transmutated nuclide undergoes fission. On the other hand, the target MA nuclide is directly incinerated in the direct fission process. The transmutation and incineration process of MAs in the actual system is based on the complex combination of these two processes, so that the knowledge of both the capture and fission cross sections of MA nuclide is indispensable for the accurate evaluation of the transmutation properties.

However, the lack of integral experiment data of MA reaction rates makes it difficult to evaluate the reliability of the nuclear data of MA, which directly affects the calculated incineration properties of the MA incineration systems. Most of the recent activities related to MA incineration studies are either cross section measurements or application studies on the conceptual design of the incineration system. Activities on integral measurements of MA reaction rate are restricted to fast neutron systems, and no activity has been reported in thermal neutron systems, especially in nuclear reactors. Therefore, in order to assess and verify the nuclear data of MA for incineration system using thermal reactors, it is strongly desired to accumulate the integral experimental data which could be used for the verification of MA nuclear data and to improve the reliability of the designed characteristics of the MA incineration systems.

From these points of view, a series of integral experiments for the measurement of MA reaction rates in thermal neutron system has been performed at Kyoto University Critical Assembly (KUCA) in order to obtain experimental data to be used for the assessment of the nuclear data of MAs. Experiments for both capture and fission reaction rate measurement have been performed in the series; the experiments have been hitherto performed for $^{237}$Np

capture[6], $^{237}$Np fission[7] and $^{241}$Am fission rate measurements[8]. It should be noted that this series of KUCA experiments is the first activity ever reported on integral evaluation of MA nuclear data in thermal neutron systems. The results of the two fission rate measurements and validation of the fission cross sections will be described in this chapter.

## 4.2 CURRENT STATUS OF $^{237}$Np AND $^{241}$Am FISSION CROSS SECTIONS

In this section, the current status of the fission cross sections of $^{237}$Np and $^{241}$Am is reviewed.

### 4.2.1 CURRENT STATUS OF $^{237}$Np FISSION CROSS SECTION

The fission cross sections of $^{237}$Np have been measured and reported by several authors[9]-[14]. These reports, however, show marked discrepancy among the measured cross sections, especially in the resonance region. Consequently, the fission cross sections of $^{237}$Np contained in representative evaluated nuclear data libraries show large discrepancy. The fission cross sections of $^{237}$Np($n,f$) taken from JENDL-3.2[15], ENDF/B-VI[16] (rev.5) and JEF2.2 [17] are shown in **Fig. 4.1**. The cross sections are shown in the 107 group structure utilized in the neutronics code system SRAC[18]. The most notable difference could be found at the resonance region, where JENDL-3.2 is larger than ENDF/B-VI.5 and JEF2.2 by a

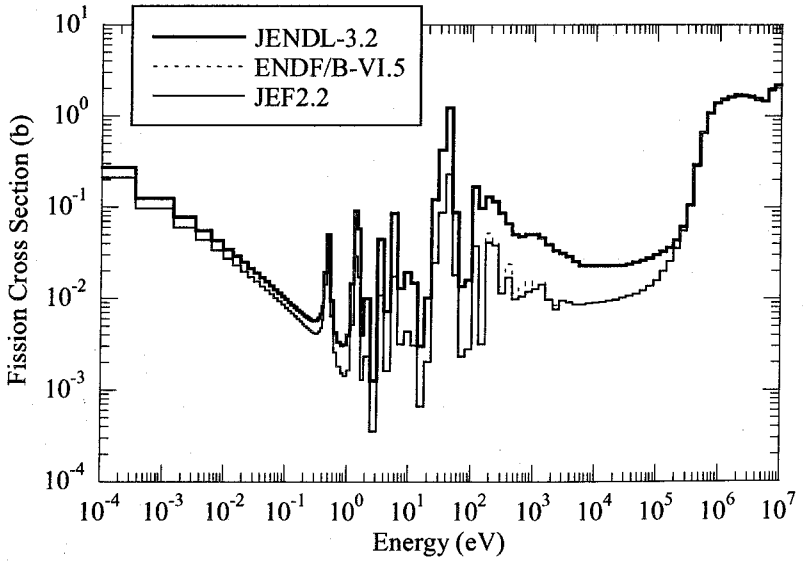


Figure 4.1 Fission cross sections of $^{237}$Np.

factor of 3 to 5. For the threshold fission in the fast energy range, the differences in the evaluated cross sections are not as significant as those in the resonance region, but there still exists the discrepancy of 3 to 5%. Furthermore, recent measurement at the keV range[19] revealed that the fission cross sections of $^{237}$Np at this range might not be adequately described in the aforementioned nuclear libraries.

### 4.2.2 CURRENT STATUS OF $^{241}$Am FISSION CROSS SECTION

The most recent measurement of the fission cross sections of $^{241}$Am has been performed between 0.1 eV and 10 keV by using the Kyoto University Lead Slowing-down Spectrometer (KULS) installed at the 46 MeV electron linac facility at Kyoto University Research Reactor Institute[20]. The results show a general agreement with the evaluated cross section data contained in JENDL-3.2 and ENDF/B-VI. However, some discrepancies are found between the measurements and evaluated cross sections in the resonance and thermal energy ranges.

The $^{241}$Am fission cross sections in the evaluated libraries show notable

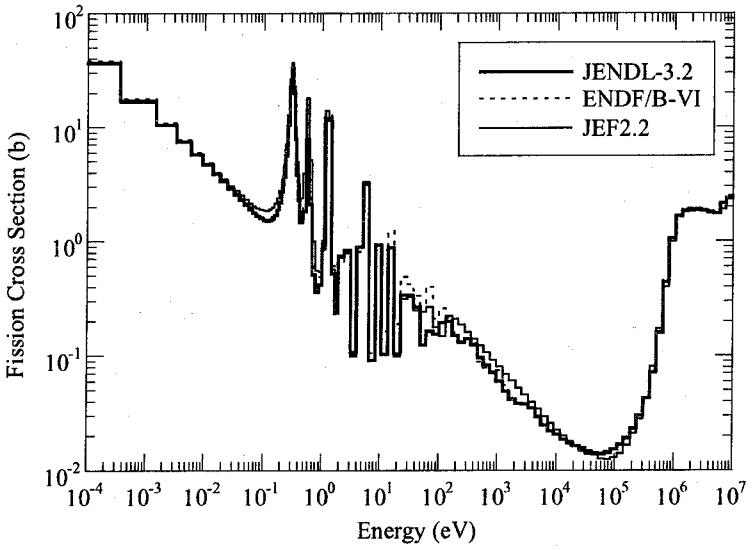


Figure 4.2 Fission cross sections of $^{241}$Am.

discrepancies as shown in **Fig. 4.2**, where the $^{241}$Am fission cross sections taken from JENDL-3.2, ENDF/B-VI and JEF2.2 libraries are shown in the 107 group structure utilized in the SRAC code system. Considerable differences could be found in various energy regions; especially for thermal systems, the difference at the low-energy resonance and thermal energy regions may have significant impact on nuclear characteristics.

The observed discrepancies among the measured and evaluated data, and also those among the different evaluated data, may directly influence the transmutation performance in the transmutation system and lead to uncertainty in the incineration properties of MAs. Therefore, it is desirable to examine the evaluated data through systematic comparison with the results of integral experiments. Although extensive research on transmutation and incineration of americium and neptunium has been performed [21]-[26], integral experiments directly aimed for the assessment of the cross section data itself were rather scarce[27]-[30] and were performed in fast neutron systems. The present series of integral experiments for the fission rate measurement at the KUCA and their analysis would be of great importance for providing experimental database in thermal neutron systems.

## 4.3 EXPERIMENTAL

### 4.3.1 EXPERIMENTAL NEUTRON FIELDS AVAILABLE IN THE KUCA

Experiments were performed using polyethylene moderated and reflected, highly-enriched uranium cores constructed at a solid moderated core (B-core) in the KUCA[31]. In order to systematically vary the neutron spectrum of the experimental neutron field, the $H/^{235}U$ ratio of the core has been systematically varied by changing the combination of the polyethylene moderator plates (5.08 cm square, 0.63 cm or 0.3086 cm in thickness) and 93% enriched uranium-aluminum fuel plates (5.08 cm square, 0.15875 cm in thickness) in a unit cell. Five cores were employed in this series of experiments; those cores were designated as EEE1, EE1, E1, E2 and E3 cores, respectively. **Table 4.1** shows the specification of the experimental cores. **Figure 4.3** shows the neutron spectra calculated by TWOTRAN at the core center (*i.e.* the position of the fission chamber in the void element) of the five cores. The detail of the fission chamber location and the calculation procedure will be described afterwards. In order to qualitatively describe the neutron fields, spectrum indices defined as the fraction of the neutron flux in the energy region below 1 eV relative to the total neutron flux have been calculated from the spectrum shown in Fig.4.3 and are also shown in Table 4.1. The core configurations of the experimental cores are shown in **Fig. 4.4**. The fuel elements consist of active core region of about 40 cm in height and the upper and lower polyethylene reflector regions of about 50 cm thick. The fuel elements are assembled on the grid plate and surrounded by the polyethylene reflector and control/safety rods. A special void element was located at the core center, where the fission chamber was loaded as will be described afterwards. Note that only the polyethylene reflector elements in the neighbor of the core are shown in Fig.4.4, whereas in the actual core configuration the thickness of the

polyethylene reflector regions is more than 30 cm in the horizontal direction.

Table 4.1 Specifications of the experimental cores

| Core | Unit Cell Structure* | $H/^{235}U$ | Spectrum Index** |
|---|---|---|---|
| EEE1 | EU+EU+EU+1/8P | 34 | 0.065 |
| EE1 | EU+EU+1/8P | 52 | 0.088 |
| E1 | EU+1/8P | 103 | 0.141 |
| E2 | 1/8P+EU+1/8P | 207 | 0.220 |
| E3 | 1/4P+EU+1/8P | 316 | 0.287 |

* EU: 93% Enriched Uranium-Aluminum (0.15875 cm), 1/8P: Polyethylene (0.3086 cm), 1/4P: Polyethylene (0.63 cm)
** Calculated fraction of the neutron flux in the energy region below 1 eV relative to the total neutron flux at the fission chamber position

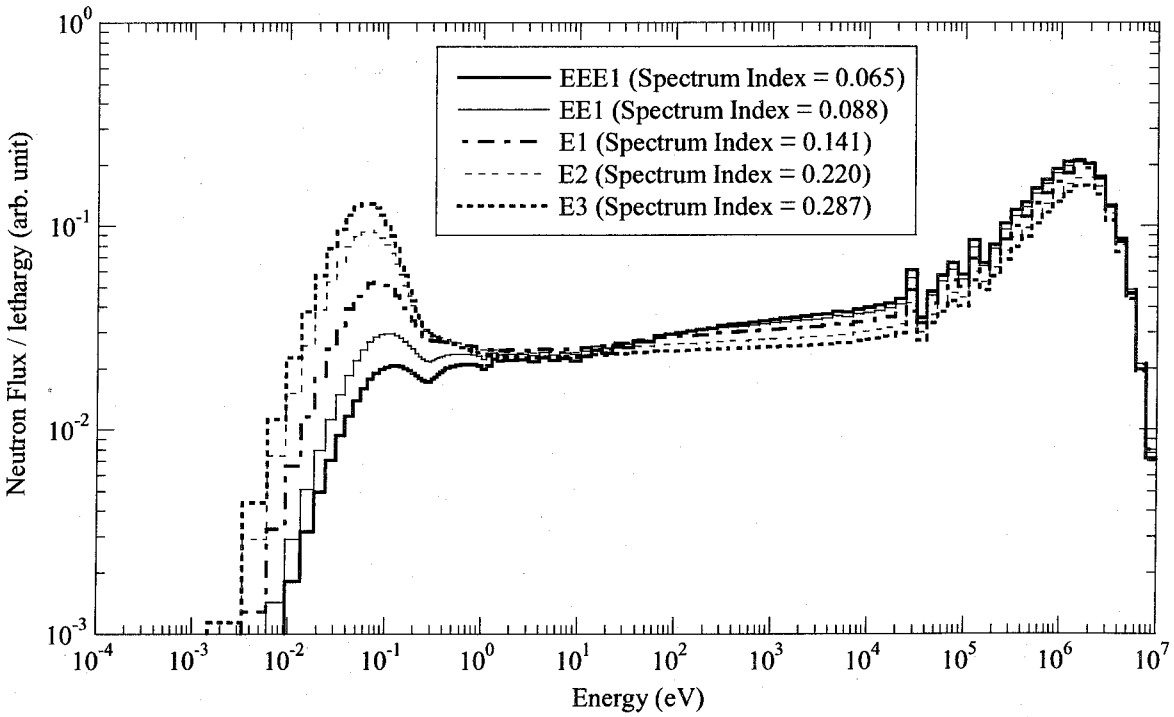


Figure 4.3 Calculated neutron spectra for the experimental cores.

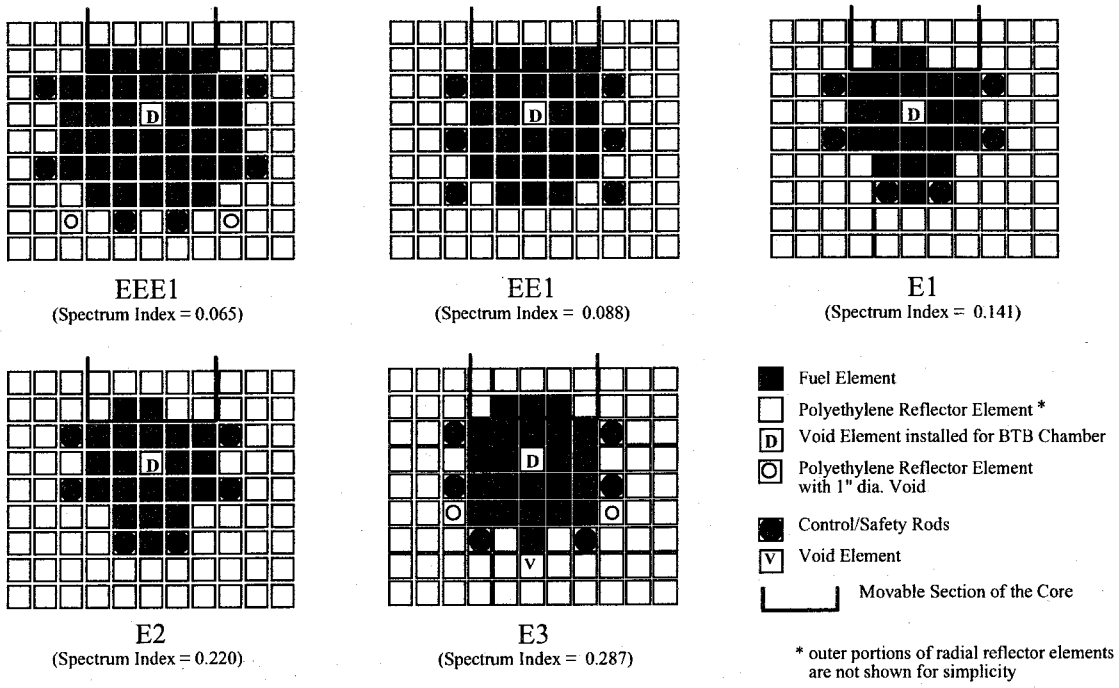


Figure 4.4 Configuration of the experimental cores.

### 4.3.2 $^{237}$Np, $^{241}$Am AND $^{235}$U SAMPLES

In the measurement, the fission rates of $^{237}$Np and $^{241}$Am were measured as the fission rate ratio relative to $^{235}$U by using a special fission chamber (back-to-back type double fission chamber)[32]; this fission chamber will be called hereafter as "BTB chamber", and its detailed description will be given in Subsection 4.3.3. The samples are electrodeposited on a stainless steel backing plate of 28 mm in diameter and 0.2 mm in thickness. The radioactive diameter of the deposit is 20 mm. The specifications of the $^{237}$Np, $^{241}$Am and $^{235}$U samples are as follows;

*a) $^{237}$Np sample*

The Np sample used in this study is identical to that described by Yamanaka *et al.*[14] in their study on the fission cross section measurement, where the detailed description of the

sample preparation is given. The number of $^{237}$Np atoms, together with the observed impurities in the deposit is shown in **Table 4.2**.

*b) $^{241}$Am sample*

The $^{241}$Am sample used in this study is identical to that used in the fission cross section measurement by Yamamoto *et al.*[20], where the detailed description of the sample preparation is given. The number of $^{241}$Am atoms in the deposit is shown in **Table 4.2**. No trace of significant impurities has been observed.

*c) $^{235}$U sample*

The U sample (99.91% enriched) is essentially the same to that described in Ref.[4] and [20] except for the number of $^{235}$U atoms in the deposit.

The number of $^{235}$U atoms in the U sample was determined by 1) the alpha-ray spectrometry with a Si surface barrier detector conducted in a vacuum chamber and 2) the relative fission rate measurement using the BTB chamber with another U sample as reference, whose number of atoms was previously determined[33]. The errors for the number of atoms were determined by 1) taking account of counting statistics in the activity measurement and the uncertainty in the geometrical detection efficiency for the alpha-ray spectrometry

Table 4.2 Number of target nuclides and impurities in the samples

| Sample | Np | | Am | | U | |
|---|---|---|---|---|---|---|
| Target Nuclide | $^{237}$Np | $(1.99\pm0.02)\times10^{17}$ | $^{241}$Am | $(1.73\pm0.02)\times10^{16}$ | $^{235}$U | $(1.49\pm0.02)\times10^{16}$ |
| Impurities | $^{238}$Pu | approx. 0.3ppm | not detected | | $^{234}$U | approx. 470ppm |
| | $^{239}$Pu | approx. 1.1ppm | | | $^{236}$U | approx. 160ppm* |
| | | | | | $^{238}$U | approx. 400ppm* |

* taken from mill sheet data

measurement and by 2) taking account of counting statistics of the fission counts, the difference in the efficiency of the two chambers and the uncertainty in the reference U sample for the relative fission rate measurement. The final number of $^{235}U$ atoms has been determined as the weighted average of the two measured results since the two results have agreed within the experimental error. The impurities in the deposit were also determined through the alpha-ray spectroscopy.

### 4.3.3 BTB CHAMBER

The fission rate ratio measurements have been performed using the BTB chamber. The BTB chamber has been hitherto widely used for the measurement of fission cross sections of various heavy nuclides at KULS.[14][20][32][34] The structure of the BTB chamber is shown in **Fig. 4.5**. The BTB chamber consists of two identical parallel plate-type fission chambers. The fissionable materials, electrodeposited onto backing plates as described previously, are loaded in the two chambers, so that the backing plates of the samples face each other and thus is called the back-to-back type. The BTB chamber is mostly made of aluminum and is filled with gas of (97% argon + 3% nitrogen) at a pressure of 1 atm. Fission events in two chambers of the BTB chamber were independently accumulated as electric pulses which were generated through the ionization process of filling gas induced by fission fragments.

The BTB chamber was inserted into a void core element and was settled at the height of core mid plane by using aluminum tubes set in the void element. The void element containing the BTB chamber was loaded in the core center as already shown in Fig. 4.4.

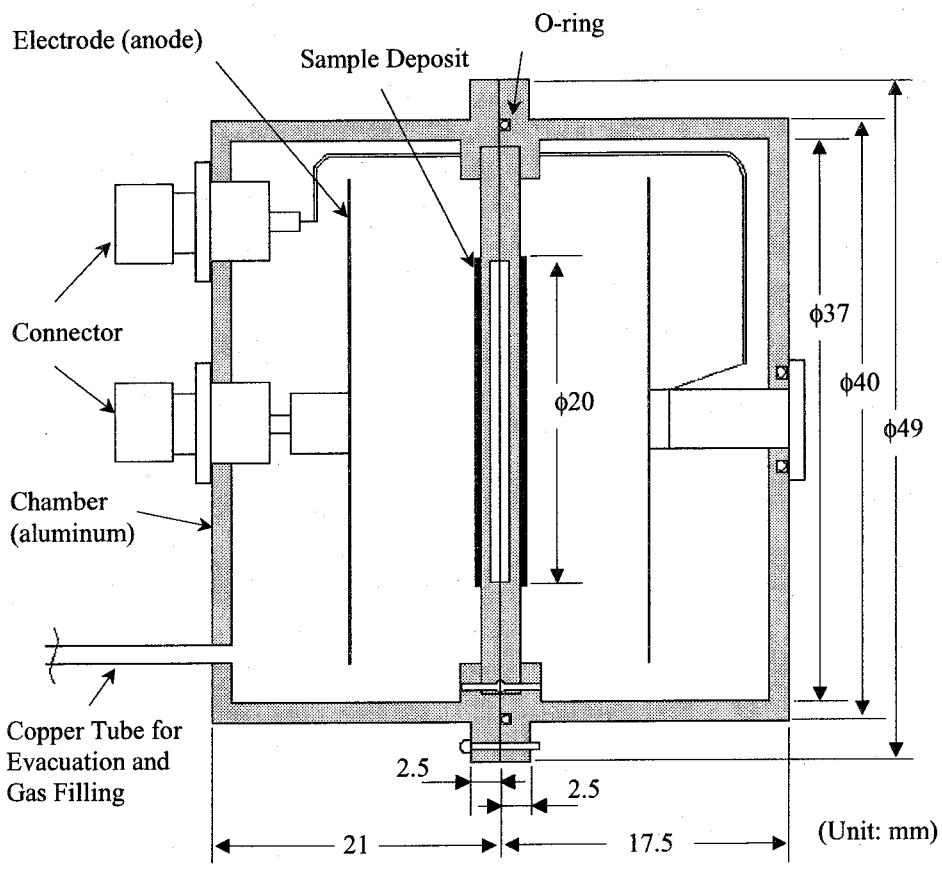


Figure 4.5 BTB chamber.

### 4.3.4 ELECTRONICS FOR DATA COLLECTING

Two identical electronic circuits were used for the MA and U chambers as shown in **Fig. 4.6**. The fission pulse spectra were stored in a personal computer (PC)-driven multichannel analyzer (MCA) system, while the scaler data from single channel analyzers (SCAs) were used for monitoring purpose. **Figure 4.7** shows a typical pulse height spectrum from the BTB chamber. The fission pulse could be clearly distinguished from the noise and the $\alpha$ pulses by a simple discrimination using SCA. The discrimination level was set at the minimum count region between the ($\alpha$+noise) and the fission components. This discrimination level was artificially shifted within the minimum count region so as to check

the influence to the deduced fission count ratio. The change in the fission count ratio caused by shifting the discrimination level was taken into account as one of the experimental uncertainties.

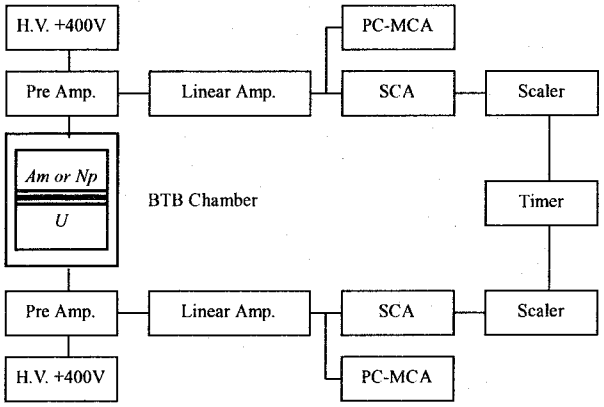


H.V.: High voltage power supply
Pre Amp.: Preamplifier
Linear Amp.: Linear amplifier
SCA: Single channel analyzer
PC-MCA: PC-driven multi-channel analyzer

Figure 4.6 Electronic circuit.

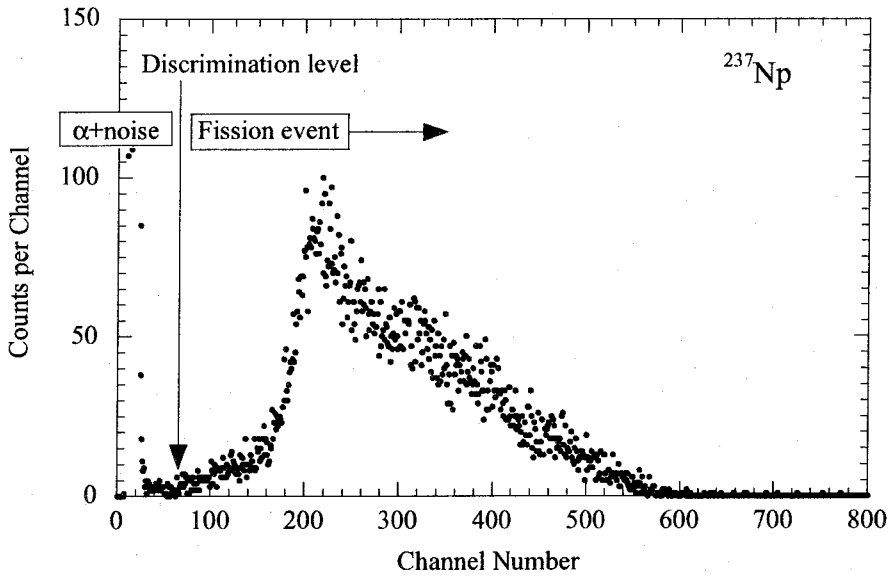


Figure 4.7 Typical pulse height distribution from the BTB chamber.

### 4.3.5 FISSION RATE RATIO MEASUREMENT

During the fission rate ratio measurements, the reactor power was set to be about 2 to 5 W to obtain the sufficient count rates of the fission events. The maximum fission event count rates for Np, Am and U chambers were about 40, 10 and 600 cps, respectively. These count rates were low enough so that the count loss effect due to the detector deadtime could be ignored. The irradiation time were adjusted so that the accumulated fission events for the MA samples, which are much smaller than that for $^{235}$U, exceeded 10000 counts. The measurements of 500 to 2000 seconds have been repeated for five times for each core configuration.

The fission count data from both chambers are then used to obtain the fission rate ratio, normalized to the number of atoms, by the following equation ;

$$\text{MA}/^{235}\text{U} \quad \text{fission rate ratio} = \quad (C_{MA} / C_U) \times (N_U / N_{MA}), \qquad (4\text{-}1)$$

where

$C_{MA}$ : integrated fission counts of the Np or Am chamber,

$C_U$ : integrated fission counts of the U chamber,

$N_U$ : number of $^{235}$U atoms in the U deposit,

$N_{MA}$ : number of $^{237}$Np or $^{241}$Am atoms in the Np or Am deposit.

### 4.3.6 EVALUATION OF EXPERIMENTAL UNCERTAINTIES

The following experimental uncertainties have been considered in the present measurement.

*a) statistical error for fission event measurements*

The statistical error for the fission event measurement was obtained as a standard deviation of the accumulated fission event counts. This statistical error was evaluated to be about 1.0 to 1.7% for MA samples and about 0.2 to 0.5% for $^{235}$U sample.

*b) uncertainties in number of atoms in the sample deposit*

As shown in Table 4.2, the uncertainties in number of atoms in the sample deposit were evaluated to be about 1.0 to 1.3%.

*c) uncertainties of the determination of discrimination level*

As described in Subsection 4.3.4, the discrimination level between the ($\alpha$+noise) and the fission components as shown in Fig. 4.7 was artificially shifted within the minimum count region so as to check the influence to the deduced fission count ratio. The change in the fission count ratio caused by shifting the discrimination level was found to be 0.2 to 1.6%.

*d) sample position in BTB chamber*

The systematic differences between the MA and U sample positions in the BTB chamber were examined by interchanging the two samples in the BTB chamber in the Np fission rate measurements. Five measurement runs were performed for each sample position. The difference in the fission count ratio before and after interchanging the sample was ranged from 0.1 to 0.7%, which ensures the good symmetry of the two chambers in BTB and of the irradiation field. As for the final experimental value, the average value of the fission count ratio obtained by interchanging the positions of the two samples was adopted. For the Am fission rate measurements, the above method has not been performed in order to avoid the contamination of the BTB chamber by $^{241}$Am. Therefore, the difference in fission rate ratio reported by Yamamoto *et al.*[20] have been taken into account as experimental uncertainty. This value is reported to be 1.1%, which is slightly

larger but is considered to be sufficiently comparable to the value directly obtained for $^{237}Np/^{235}U$ fission rate ratio.

*e) effect of impurities*

It has been certified through neutronics calculation that the impurities contained in the samples have negligible effect of less than 0.01% to the measured fission rate ratio and therefore could be neglected in the present measurement.

*f) self-shielding effect of fission fragments*

The range of the fission fragment is reported to be about 8.3 mg/cm$^2$ in $UO_2$ [19], 8 to 11 mg/cm$^2$ in $^{235}U$ metallic foil and 3 to 4 mg/cm$^2$ in Al[35]. Assuming that the fission fragment range does not differ significantly for U and MA deposit and considering the thickness of the deposits (approximately $2\times10^{-3}$ mg/cm$^2$), the self-shielding of the fission fragments in the deposit could be neglected in the present measurement.

*g) effect of photo-fission*

The effect of the background counts caused by photo fission reactions was reported to be very small [20] and therefore could be neglected in the present measurement.

Based on the quantitative evaluations described above, the experimental uncertainties due to a) statistical error, b) number of atoms, c) discrimination level and d) sample position in BTB chamber, were considered to be significant and have been taken into account as summarized in **Table 4.3**. The obtained $^{237}Np/^{235}U$ and $^{241}Am/^{235}U$ fission rate ratios are summarized in **Tables 4.4** and **4.5**, respectively.

Table 4.3 Experimental uncertainties

| | Uncertainty (%) | |
|---|---|---|
| | $^{237}Np/^{235}U$ | $^{241}Am/^{235}U$ |
| Statistical Error for $^{237}Np$ or $^{241}Am$ | 0.7 to 0.8 | 0.6 to 1.4 |
| Statistical Error for $^{235}U$ | 0.2 to 0.5 | 0.1 to 0.2 |
| Number of Atoms for $^{237}Np$ or $^{241}Am$ | 1.0 | 1.0 |
| Number of Atoms for $^{235}U$ | 1.3 | 1.3 |
| Discrimination for $^{237}Np$ or $^{241}Am$ | 0.5 to 1.0 | 0.5 to 0.9 |
| Discrimination for $^{235}U$ | 0.2 to 0.9 | 0.2 to 1.6 |
| Sample Position in BTB Chamber | 0.1 to 0.7 | 1.1 |
| Total Uncertainty | 2.0 to 2.3 | 2.1 to 2.3 |

Table 4.4 Experimental results for the $^{237}Np/^{235}U$ fission rate ratio

| Core | Spectrum Index | $^{241}Am/^{235}U$ Fission Rate Ratio |
|---|---|---|
| EEE1 | 0.065 | 0.0298 (2.2 %)* |
| EE1 | 0.088 | 0.0212(2.3 %) |
| E1 | 0.141 | 0.0119 (2.3 %) |
| E2 | 0.220 | 0.00646 (2.1 %) |
| E3 | 0.287 | 0.00439 (2.0 %) |

* Relative error in % ($1\sigma$)

Table 4.5 Experimental results for the $^{241}Am/^{235}U$ fission rate ratio

| Core | Spectrum Index | $^{241}Am/^{235}U$ Fission Rate Ratio |
|---|---|---|
| EEE1 | 0.065 | 0.0522 (2.2 %)* |
| EE1 | 0.088 | 0.0411 (2.3 %) |
| E1 | 0.141 | 0.0268 (2.1 %) |
| E2 | 0.220 | 0.0183 (2.1 %) |
| E3 | 0.287 | 0.0144 (2.2 %) |

* Relative error in % ($1\sigma$)

## 4.4 ANALYSIS

### 4.4.1 FISSION RATE CALCULATIONS BY MVP CODE

The fission rate ratio calculations were performed by using the continuous energy Monte Carlo code MVP[36] (ver.2.0). Neutron spectra were obtained through eigenvalue calculations performed based on JENDL-3.2, whereas the fission rate ratios were obtained based on the $^{235}U$ cross sections from JENDL-3.2 and MA cross sections from JENDL-3.2, ENDF/B-VI or JEF2.2. In the analysis, the as-built configurations of the experimental cores, including the plate arrangement in the fuel region, structure of the control rod elements and the heterogeneity of the gap between the fuel elements (due to the aluminum support blade structure), were treated explicitly in order to avoid any possible ambiguities due to the geometrical approximations. However, due to their very small volumes, it was practically impossible to treat the as-build electrodeposited samples in the BTB fission chamber as tally regions in the whole core calculations by MVP. Therefore, the fission rate ratios were obtained as an averaged value over the inner part of the BTB chamber without taking the samples into account. In this calculation model, the detailed structure of the BTB fission chamber excluding the sample plates was considered, so the perturbation of neutron spectra caused by the aluminum structure of the BTB fission chamber itself was taken into account. A typical MVP run with 9,000,000 neutrons (30,000 particles $\times$ 300 batches, with 3 reject batches) gave fission rates with statistical error of approximately 1%.

The MVP calculation was used for the evaluation of integrated fission rate, which could be directly compared to the experimental results. Together with this, energy dependent fission rates were calculated by using the deterministic transport theory code TWOTRAN implemented in the SRAC code system. The energy-dependent fission rates

were used for the analysis of the fission rate ratio differences between the libraries used. The correction factors for the neutron spectrum perturbation caused by the presence of the sample plates, especially due to the presence of the stainless backing plate of the electrodeposited samples, were obtained using an supplementary calculation using the SRAC code system. The detail of this procedure will be given below.

### 4.4.2 DETERMINISTIC ANALYSIS USING SRAC CODE SYSTEM

The SRAC code system was used for the calculation of energy-dependent neutron spectrum and fission rate, as well as the correction factors for neutron spectrum perturbation caused by the presence of the sample plates. After the cell homogenization using the PIJ routine together with the PEACO routine for calculating effective cross section, the energy-dependent neutron flux was obtained by the transport core calculation module TWOTRAN using a two-dimensional RZ model with 107 energy groups and the $S_{16}P_1$ approximation. The representative models of calculation for cell homogenization (PIJ routine) and the core calculation (TWOTRAN) are shown in **Figs. 4.8** and **4.9**, respectively. In the TWOTRAN calculations, the BTB chamber was treated to be located at the center of the two-dimensional cylindrical core, whereas in the actual experiment the BTB chamber was not always loaded at the core center. However, the difference in the neutron spectrum due to this difference in the loading position was found to be small from the results of the TWOTRAN calculation and thus was ignored in the present analysis. Energy-dependent fission rates were obtained by multiplying the calculated neutron spectra at the BTB chamber position and the infinitely diluted fission cross sections of $^{237}$Np, $^{241}$Am and $^{235}$U.

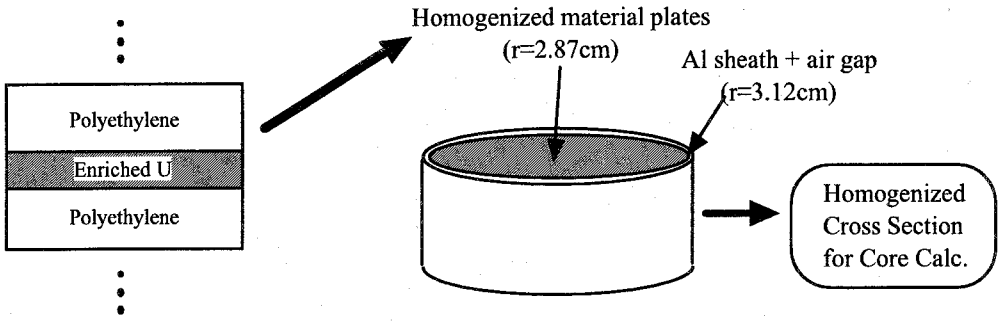


Step 1) Homogenization of material plates (1-D slab)

Step 2) Homogenization of Al sheath and homogenized material plates (1-D cylinder)

Figure 4.8 Calculation model for cell homogenization by PIJ.

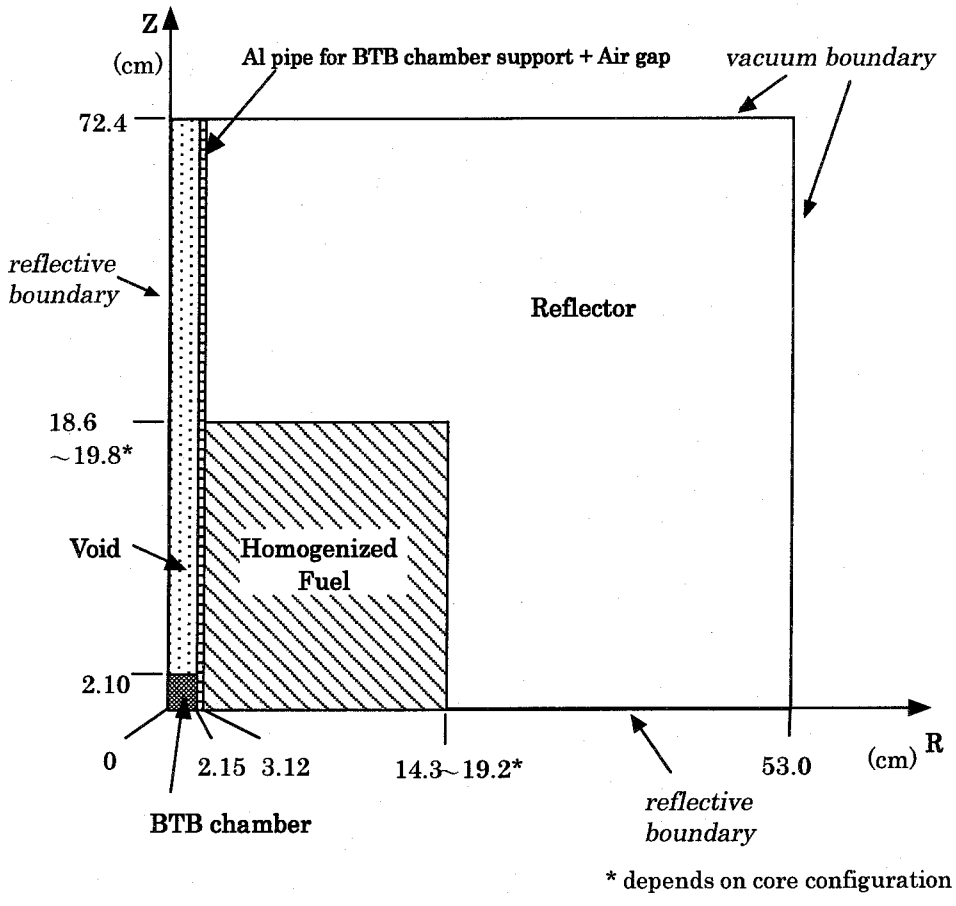


Figure 4.9 Calculation model for core calculation by TWOTRAN.

### 4.4.3 CALCULATION OF THE CORRECTION FACTORS

The self-shielding and flux depression of the samples and other equipments were investigated as the possible correction factors. Among them, it was found that the correction for the flux depression caused by the stainless steel backing plate of electrodeposited samples was most significant. All other effects were found to be very small and therefore were ignored in the present analysis.

(1) *Self-shielding effects of the MA and U samples*

The self-shielding correction for the MA and U samples has been estimated using the analytical expression[37]. It has been confirmed that the overall self-shielding correction for the MA and U samples was less than 0.2% and therefore has been ignored in the current analysis.

(2) *Flux depression caused by the BTB chamber structure*

Calculation of the correction factors for the neutron spectrum perturbation as descibed above has been performed using a simplified 1-dimensional slab model treating the Np or Am deposit, stainless steel backing plate and U deposit regions by using the ANISN code implemented in the SRAC code system. The neutron spectrum at the BTB position obtained by the TWOTRAN calculation was fed as an external source. The correction factors for the neutron spectrum perturbation was obtained as the ratio of fission rate ratio with the stainless steel backing plate to that without the stainless steel backing plate. Thus obtained correction factors are shown in **Table 4.6**. The correction factors ranging from 1.022 to 1.032 for $^{237}Np/^{235}U$ and 1.013 to 1.017 for $^{241}Am/^{235}U$ were found to be necessary. The procedure for obtaining the correction factors was validated by a complementary MVP calculation. In this MVP calculation, the neutron spectrum obtained by TWOTRAN was fed as an external source to the stand-alone BTB chamber, where the detailed structure of

the chamber was treated explicitly. The obtained $^{237}Np/^{235}U$ fission rate ratio was compared to that obtained by the similar MVP calculation with Np and U regions alone (*i.e.* without the stainless steel backing plate). The calculation was performed only for the E3 core which gives the largest correction factor. The obtained correction factor was $1.039 \pm 0.026$. Although the statistical error is large, this correction factor agreed well with the correction factor of 1.032 obtained by the deterministic calculation, which supports the validity of the correction factors shown in Table 4.6.

Table 4.6 Correction factors for flux depression caused by the stainless backing plate of the samples

| Core | Spectrum Index | Correction Factor, $^{237}Np/^{235}U$ | Correction Factor, $^{241}Am/^{235}U$ |
|---|---|---|---|
| EEE1 | 0.065 | 1.022 | 1.016 |
| EE1 | 0.088 | 1.024 | 1.017 |
| E1 | 0.141 | 1.028 | 1.016 |
| E2 | 0.220 | 1.031 | 1.015 |
| E3 | 0.287 | 1.032 | 1.013 |

### 4.4.4 CALCULATION OF FISSION RATE RATIOS

Using the obtained correction factors, the calculated fission rate ratios were derived by using the following formula;

$$R^{MVP}_{BTB-SP} = R^{MVP}_{BTB-NoSP} \times \frac{R^{MVP}_{BTB-SP}}{R^{MVP}_{BTB-NoSP}} \approx R^{MVP}_{BTB-NoSP} \times \frac{R^{ANISN}_{BTB-SP}}{R^{ANISN}_{BTB-NoSP}} = R^{MVP}_{BTB-NoSP} \times f_{SP} \quad , \tag{4-2}$$

where

$R^{MVP}_{BTB-SP}$ : derived value of the calculated fission rate ratio, corresponding to the MVP results taking the sample plates into account,

$R^{MVP}_{BTB-NoSP}$ : fission rate ratio obtained by the MVP calculation without taking the sample plates into account,

$R^{ANISN}_{BTB-SP}$ : fission rate ratio obtained by the one-dimensional ANISN calculation taking the sample plates into account,

$R^{ANISN}_{BTB-NoSP}$ : fission rate ratio obtained by the one-dimensional ANISN calculation without taking the sample plates into account, and

$f_{SP} \equiv \frac{R^{ANISN}_{BTB-SP}}{R^{ANISN}_{BTB-NoSP}}$ : correction factor for the spectrum perturbation caused by the sample plates, obtained by the one-dimensional ANISN calculation.

Several complementary calculations were performed to check the sensitivity of calculation models and nuclear data used for the spectrum calculation to the calculated fission rate ratios. Through the calculations, it was verified that the incorrectness of calculated neutron spectra, due to any systematic error in the core calculation model itself, is unlikely to be occurring in the present analysis. It was also verified that the difference in the heavy nuclide data used for the neutron spectrum calculation does not have significant impact on the calculated fission rate ratios.

## 4.5 RESULTS AND DISCUSSION

### 4.5.1 $^{237}Np/^{235}U$ FISSION RATE RATIOS

The calculated-to-experimental ratio (C/E) for the $^{237}Np/^{235}U$ fission rate ratios was obtained as summarized in **Table 4.7** and shown in **Fig. 4.10**. Among the three libraries used for $^{237}Np$, JENDL-3.2 gives the best estimate with C/E ranging from 0.93 to 0.98 and an average value of $0.95 \pm 0.03$. ENDF/B-VI and JEF2.2 are almost identical and give smaller C/E values of about 4 to 5% compared to JENDL-3.2 for all cores. There was no apparent dependence of the C/E value to the spectrum index for all cases. The averaged C/E value for ENDF/B-VI is about 0.90, which is comparable to the recently reported values for dosimetry set irradiation results[38][39]. It should be noted that the prediction accuracy of C/E=0.95 is somewhat inferior when compared to that of the $^{237}Np$ capture rate ratio relative to $^{197}Au$ measured at the KUCA and the heavy water facility of the Kyoto University Research Reactor (KUR), where the average C/E was found to be about 0.99[2].

Table 4.7 C/E values of $^{237}Np/^{235}U$ fission rate ratios*

| Core | Spectrum Index | $^{237}Np$ taken from JENDL-3.2 | $^{237}Np$ taken from ENDF/B-VI | $^{237}Np$ taken from JEF2.2 |
|---|---|---|---|---|
| EEE1 | 0.065 | $0.973 \pm 2.6\%$** | $0.931 \pm 2.6\%$ | $0.920 \pm 2.6\%$ |
| EE1 | 0.088 | $0.975 \pm 2.6\%$ | $0.934 \pm 2.6\%$ | $0.924 \pm 2.6\%$ |
| E1 | 0.141 | $0.935 \pm 2.5\%$ | $0.893 \pm 2.5\%$ | $0.882 \pm 2.5\%$ |
| E2 | 0.220 | $0.925 \pm 2.3\%$ | $0.880 \pm 2.3\%$ | $0.869 \pm 2.3\%$ |
| E3 | 0.287 | $0.941 \pm 2.2\%$ | $0.899 \pm 2.2\%$ | $0.889 \pm 2.2\%$ |

* $^{235}U$ from JENDL-3.2 used for all cases
** Relative error

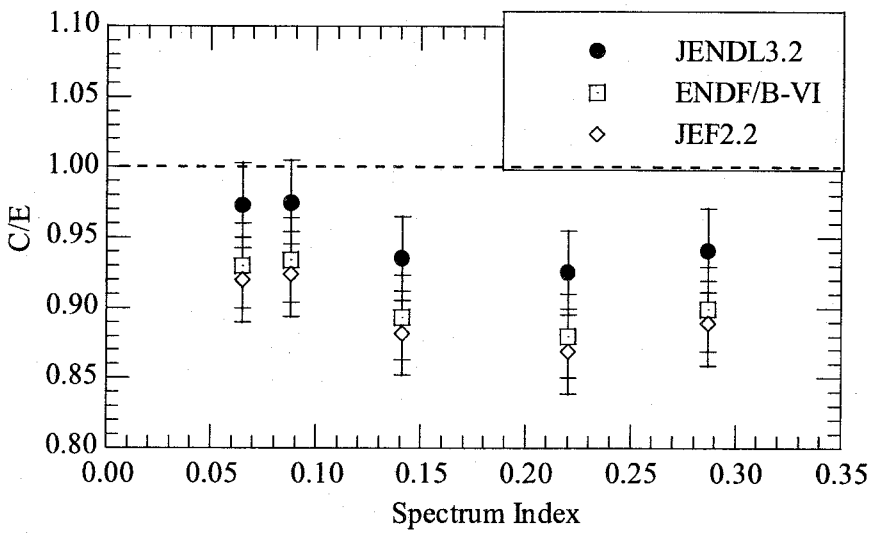


Figure 4.10 C/E values of $^{237}Np/^{235}U$ fission rate ratios.

Examination of the calculated individual fission rates showed that the difference in $^{235}U$ fission rate is very small between the libraries used. Consequently, the difference between the C/E values of the $^{237}Np/^{235}U$ fission rate ratio is considered to be directly attributable to the difference between the fission cross sections of $^{237}Np$. Thus the differences between the C/E values using various libraries were further investigated through comparison of the energy-wise fission rates of $^{237}Np$. This comparison was performed by using the neutron spectra obtained by TWOTRAN implemented in the SRAC code system on the basis of a two-dimensional RZ model with 107 energy groups. Here, the cross sections for $^{235}U$ and other structure or moderator materials were adopted from JENDL-3.2 in the spectrum calculation. The validity of this TWOTRAN calculation was verified by the agreement of the C/E values obtained by TWOTRAN and MVP; the average values of C/E are $0.93 \pm 0.01$ for the TWOTRAN results and $0.95 \pm 0.03$ for the MVP results, and they agree within the statistical error of the MVP results.

**Figure 4.11** shows the differences between the energy-dependent $^{237}Np$ fission rates

obtained based on the $^{237}Np$ fission cross sections from ENDF/B-VI and JENDL-3.2 in 107 energy groups. The main difference is arising from the cross section difference around 1MeV and at the vicinity of main resonance at 39.9 eV. In order to examine those differences of the fission rate in detail, the whole energy domain is subdivided into four representative energy domains as shown in **Table 4.8**, and the contribution of each energy domain is shown as the fraction of fission rate difference in each energy domain to the total fission rate difference. It could be seen that the main contribution comes from the energy domain of unresolved resonance to resolved resonance, which includes the major resonance at 39.9 eV. It should also be noted that the difference in the energy domain of fast fission is also significant.

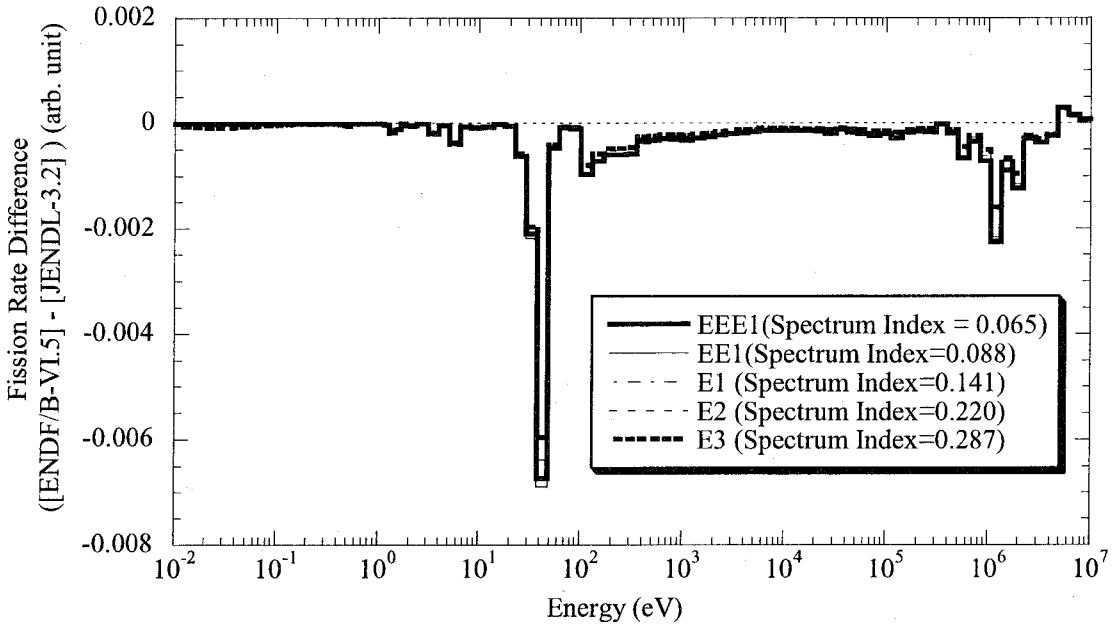


Figure 4.11 $^{237}Np$ fission rate difference between ENDF/B-VI and JENDL-3.2.

Table 4.8 Contribution of representative energy domains to difference between total $^{237}$Np fission rates obtained by using JENDL-3.2 and ENDF/B-VI

| Energy domain | Energy Range(eV) | Contribution to Total $^{237}$Np Fission Rate Difference |
|---|---|---|
| Fast Fission | $5\times10^5 < E < 1\times10^7$ | 20% to 24% |
| Unresolved resonance to resolved resonance | $60 < E < 5\times10^5$ | 33% to 36% |
| Vicinity of main resonance at 39.9 eV | $11 < E < 60$ | 36% to 38% |
| Rest of resolved resonance to thermal region | $E < 11$ | 4% to 9% |

These results indicate that the accuracy of $^{237}$Np fission cross section in both the fast and resonance regions affects the $^{237}$Np transmutation rate, and in order to further improve its prediction accuracy, further evaluation and validation of cross sections for both the fast fission and resonance cross sections would be inevitable. Taking into account the aforementioned C/E values, it can be concluded that the fission cross sections in JENDL-3.2 are superior to those in other libraries and can be used for the prediction of the Np transmutation rate in the thermal system with a prediction precision of $^{237}$Np fission rate within 10%.

### 4.5.2 $^{241}$Am/$^{235}$U FISSION RATE RATIOS

The C/E values of $^{241}$Am/$^{235}$U fission rate ratios were obtained as summarized in **Table 4.9** and shown in **Fig. 4.12**. The C/E values are generally smaller than unity by -13% to -1%. The C/E values obtained by JENDL-3.2 ranged from 0.86 to 0.90, with an average value of 0.88 and were the smallest among the three libraries examined. The C/E values based on $^{241}$Am fission cross sections from ENDF/B-VI were generally larger than

JENDL-3.2 results by about 2%, independent of the spectrum index. On the contrary, C/E values based on $^{241}$Am fission cross sections from JEF2.2 were larger than those based on the former two libraries, and ranged from 0.94 to 0.99, giving the C/E results most close to unity. This led to considerable differences of 7 to 9% between JENDL-3.2 and JEF2.2 results. There was no apparent dependence of the C/E value on the spectrum index for all cases.

Table 4.9 C/E values for the $^{241}$Am/$^{235}$U fission rate ratios*

| Core | Spectrum Index | $^{241}$Am taken from JENDL-3.2 | $^{241}$Am taken from ENDF/B-VI | $^{241}$Am taken from JEF2.2 |
|---|---|---|---|---|
| EEE1 | 0.065 | 0.866± 2.7%** | 0.891± 2.7% | 0.935± 2.7% |
| EE1 | 0.088 | 0.899± 2.6% | 0.923± 2.6% | 0.981± 2.7% |
| E1 | 0.141 | 0.898± 2.4% | 0.923± 2.4% | 0.993± 2.4% |
| E2 | 0.220 | 0.859± 2.4% | 0.884± 2.4% | 0.956± 2.4% |
| E3 | 0.287 | 0.864± 2.3% | 0.890± 2.3% | 0.960± 2.3% |

* $^{235}$U from JENDL-3.2 used for all cases
** Relative error

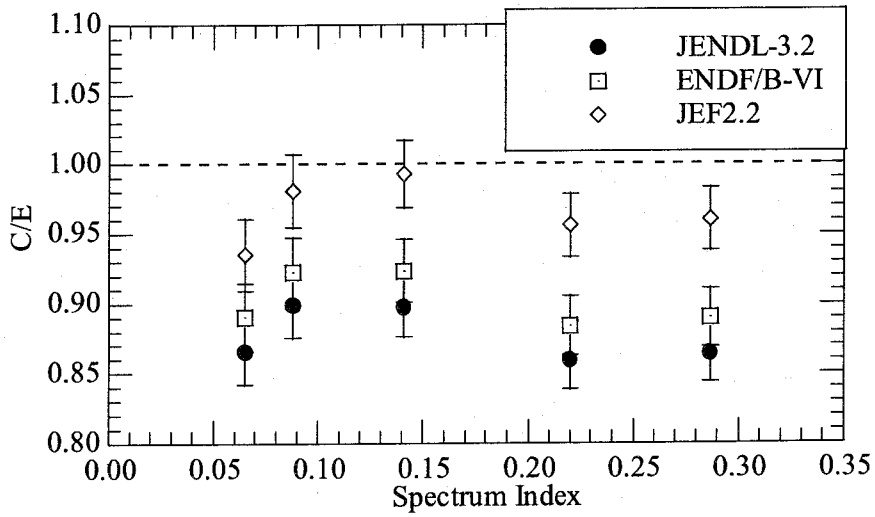


Figure 4.12 C/E values for the $^{241}$Am/$^{235}$U fission rate ratios.

Similarily to the analysis of $^{237}$Np fission rate, the differences among the C/E values based on various libraries were further investigated through comparison of the energy-wise fission rates of $^{241}$Am obtained by TWOTRAN implemented in the SRAC code system using a two-dimensional RZ model with 107 energy groups. **Figure 4.13** shows the $^{241}$Am fission rate difference between JEF2.2 and JENDL-3.2. The large difference between JENDL-3.2 and JEF2.2 arises mainly from the significant cross section difference at the low-energy resonances, especially at the vicinity of resonance at 0.576 eV. Contribution of thermal cross section difference became also apparent for well-thermalized cores, which led to the increasing discrepancy of C/E values with spectrum index.

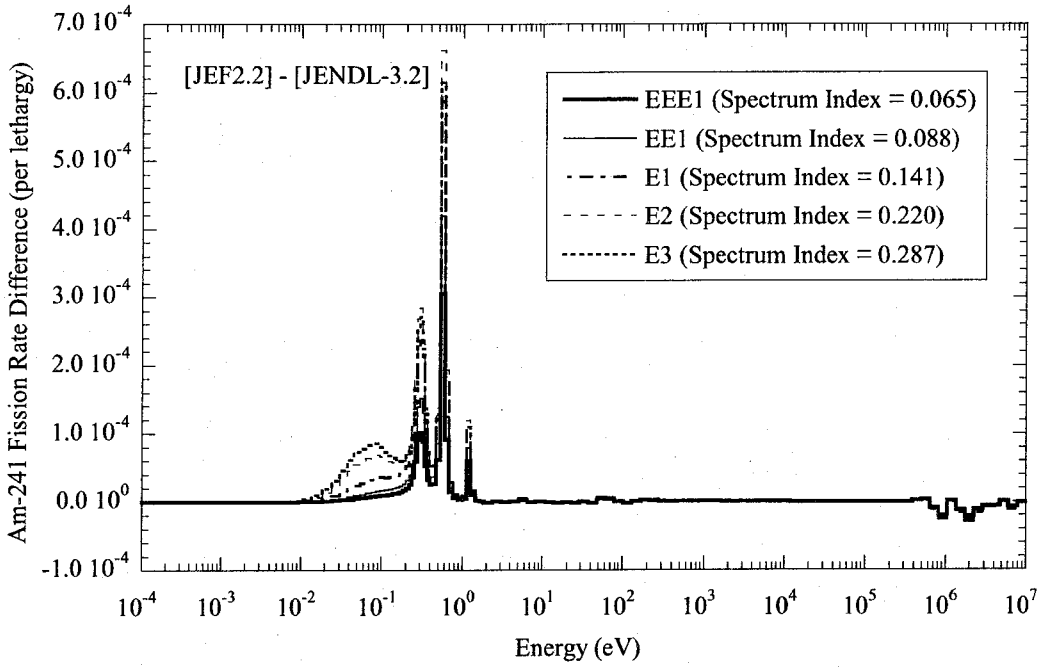


Figure 4.13 $^{241}$Am fission rate difference between JEF2.2 and JENDL-3.2.

In order to have a more clear sight on this issue, the difference of the integrated $^{241}$Am fission rate between JEF2.2 and JENDL-3.2 in representative energy domains is shown in **Fig. 4.14** . A large portion of the reaction rate difference comes from the first two resonances, which are contained in the energy domains of 0.88 eV to 0.41 eV and 0.41 eV to 0.12 eV,

respectively. The contribution of thermal component below 0.12 eV increases significantly with spectrum index, *i.e.* the softening of the spectrum. These trends are in clear contrast when compared with the results for ENDF/B-VI shown in **Fig. 4.15**, where the magnitudes of each components are much more lower than those for JEF2.2.

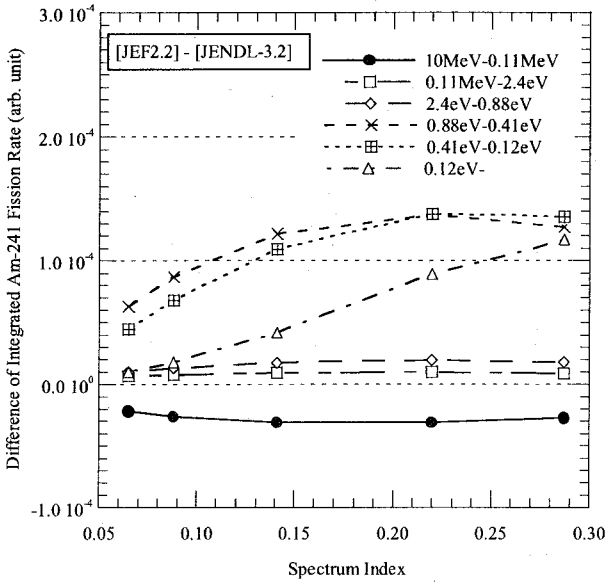


Figure 4.14 Difference of integrated $^{241}$Am fission rate between JEF2.2 and JENDL-3.2 in representative energy domains.

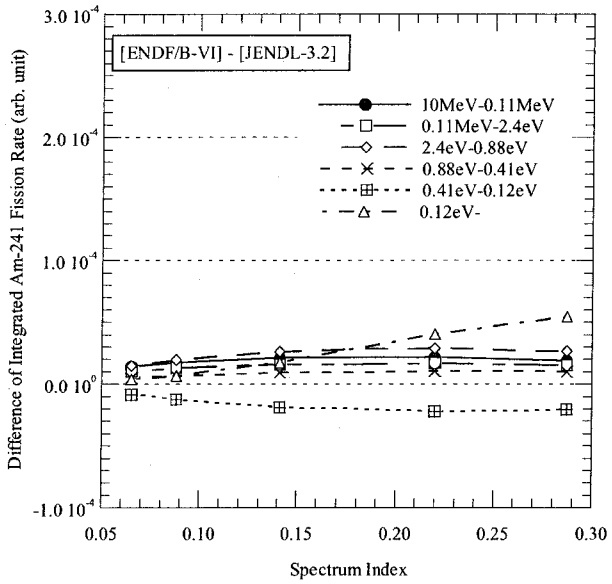


Fig. 4.15 Difference of integrated $^{241}$Am fission rate between ENDF/B-VI and JENDL-3.2 in representative energy domains.

One possible cause of the reaction rate discrepancies at the thermal region is the difference in thermal fission cross section. The fission cross section at 0.0253 eV is 3.018 b in JENDL-3.2, which is lower than those in ENDF/B-VI (3.15 b) and JEF2.2 (3.16 b). This value of JENDL-3.2 has been commented to be underestimating by Yamamoto *et al.*[20], who gave an experimental value of 3.15±0.097 b, and the increase of this thermal fission cross section will slightly improve the overall C/E value based on JENDL-3.2, especially for well-thermalized systems. However, despite the similar thermal fission cross section values, there exist a significant difference between ENDF/B-VI and JEF2.2.

According to the headers of $^{241}$Am cross section data in each library, it is noteworthy that resonance parameters given by Derrien and Lucas[40] are used in all libraries for the resolved resonances[41]. However, several differences could be found for the treatment of resolved resonance as summarized in **Table 4.10**. The major difference is the treatment of the negative energy resonances, which are used in order to obtain a good representation in the thermal energy range ; five negative energy resonances are used in JENDL-3.2 and ENDF/B-VI, whereas one negative energy resonance is used in JEF2.2. This difference resulted in the cross section difference at the vicinity of the cross section dip between the

Table 4.10 Description of resolved resonance parameters for $^{241}$Am in JENDL-3.2, ENDF/B-VI and JEF2.2

| Library | JENDL-3.2 | ENDF/B-VI | JEF2.2 |
|---|---|---|---|
| Resonance Parameter Based on | Derrien & Lucas | Derrien & Lucas | Derrien & Lucas |
| Formalism | Multi-level Breit-Wigner | Single-level Breit-Wigner | Multi-level Breit-Wigner |
| Number of Negative Resonance(s) | 5 | 5 | 1 |
| Energy of Negative Resonance(s) (eV) | -0.50, -0.45, -0.40, -0.32, -0.20 | -0.50, -0.45, -0.40, -0.32, -0.20 | -0.4209 |

lowermost resonance at 0.308 eV and the thermal $1/\upsilon$ cross section, as was shown in **Fig. 4.2**. Although the cross section values are relatively small in this energy range, the fission rate in this energy range increases with spectrum index, which results in a significant difference for well-thermalized cores. The reason for the significant discrepancy at the second resonance at 0.576 eV is under investigatin at present, and a re-examination of the resonance parameters at this resonance might be necessary.

## 4.6 CONCLUSION

In this Chapter, results of the verification of $^{237}$Np and $^{241}$Am fission cross sections based on the integral measurements of $^{237}$Np and $^{241}$Am fission rate ratios relative to the $^{235}$U fission rate performed in thermal systems constructed at the KUCA have been summarized. The fission rates were measured using the back-to-back type double fission chamber at five thermal cores with different H/$^{235}$U ratios so that the neutron spectra of the cores were systematically varied. The fission rate ratios were successfully measured with a typical uncertainty of 2%.

Through the analysis of $^{237}$Np/$^{235}$U fission rate ratio measurements, it was found that the use of JENDL-3.2 gives the C/E values of 0.95 in average, which was the best estimate among the three libraries used. The use of the $^{237}$Np fission cross sections in ENDF/B-VI.5 and JEF2.2 gives approximately 4% smaller $^{237}$Np fission rate compared to the results obtained by using JENDL-3.2. Through the detailed analysis, it is recommended that further improvement be done for the evaluation of both the fast fission and resonance regions in all libraries. Nevertheless, the $^{237}$Np fission cross sections in JENDL-3.2 are considered to be superior to those in the other libraries and can be sufficiently adopted for the use in design calculations for the minor actinide transmutation system of thermal reactors with a prediction precision of $^{237}$Np fission rate within 10%.

Through the analysis of $^{241}$Am/$^{235}$U fission rate ratio measurements, it was found that the use of $^{241}$Am fission cross sections in JENDL-3.2 underestimates the experiment by about 12% and gives the C/E values of 0.88 in average. The C/E values obtained by using $^{241}$Am cross sections of ENDF/B-VI and JEF2.2 were larger than those obtained by using JENDL-3.2 by about 2% and 7 to 9%, respectively. Through the examination of the difference of $^{241}$Am cross sections contained in the evaluated libraries, it was found that cross

section differences at the vicinity of resonance at 0.576 eV were the dominant cause of the C/E difference between JENDL-3.2 and JEF2.2. Contribution of thermal cross section difference, especially in the range of 0.01 eV to 0.2 eV becomes also apparent for well-thermalized cores. It is recommended that both the resonance and thermal energy fission cross sections of $^{241}$Am should be reevaluated in JENDL-3.2.

## References for Chapter 4


[1] "Actinide and Fission Product Partitioning and Transmutation", OECD-NEA (1999).

[2] MOCHIDA, T. and YAMASHITA, J-i. : *Prog. Nucl. Energy*, **29**, 327 (1995).

[3] AZIZ, F. and KITAMOTO, A. : *Ann. Nucl. Energy*, **23**[15], 1239 (1996).

[4] YOKOYAMA, K. *et al.* : *Proc. Int'l. Conf. on Future Nuclear Systems GLOBAL'97*, Yokohama, Kanagawa, Japan, Oct. 5-10, 1997, Vol.**1**, 230 (1997).

[5] WIESE, H. W.: *J. Alloys and Compounds*, **271-273**, 522 (1998).

[6] IWASAKI, T., HORIUCHI, T. *et al.*: *Nucl. Sci. Eng.*, **136**, 321 (2000).

[7] UNESAKI, H., SHIROYA, S. *et al.*: *J. Nucl Sci. Technol.*, **37**, 627 (2000).

[8] UNESAKI, H., SHIROYA, S. *et al.*: *J. Nucl Sci. Technol.*, **38**, 600 (2001).

[9] WHITE, P. H. *et al.*: *Proc. International Conf. on " Physics and Chemistry of Fission"*, Saltzburg, Austria, March 22-26, 1965 (1965).

[10] JIACOLETTI, R. J. and BROWN,W. K.: *Nucl. Sci. Eng.*, **48**, 412 (1972).

[11] HOFFMAN,M. M., SANDERS, W. M. and SEMON, M. D.: *Bull. Am. Phys. Soc.*, **21**, 655 (1975).

[12] PLATTARD, S., BLONS, J. and PAYA, D.: *Nucl. Sci. Eng.*, **61**,.477 (1976).

[13] AUCHAMPAUGH, G. F. *et al.*: *Phys. Rev. C*, **29**, 174 (1984).

[14] YAMANAKA, A. *et al.*: *J. Nucl. Sci. Technol.*, **30**, 863 (1993).

[15] NAKAGAWA, T. *et al.*: *J. Nucl. Sci. Technol.*, **32**, 1259 (1995).

[16] ROSE, P. F. (comp. and ed.): BNL-NCS-17541 (4th Ed.) (1991).

[17] NORDBORG, C. and SALVATORES, M.: *Proc. International Conf. on Nuclear Data for Science and Technology*, Gatlinburg, Tennessee, USA, May 9-13, 1994, Vol. **2**, 680 (1994).

[18] OKUMURA, K., KANEKO, K. and TSUCHIHASHI, K.: JAERI-Data/Code 96-015, Japan Atomic Energy Research Institute (1996) (in Japanese).

[19] IWASAKI, T. *et al.*: *J. Nucl. Sci. Technol.*, **36**, 127 (1999).

[20] YAMAMOTO, S. *et al.*: *Nucl .Sci. Eng.*, **126**, 201 (1997).

[21] WALKER, C. T., NICOLAOU, G.: *J. Nucl. Mat.*, **218**, 129 (1995).

[22] BARBELOT, J. -F. *et al.*: *Proc. Int'l. Conf. on Future Nuclear Systems GLOBAL'97*, Yokohama, Kanagawa, Japan, Oct. 5-10, 1997, Vol.**1**, 676 (1997).

[23] PRUNIER, C. *et al.*: *Nucl. Technol.*, **119**, 141(1997).

[24] PRUNIER, C. *et al.*: *Nucl. Technol.*, **120**, 110(1997).

[25] BARBELOT, J. -F. *et al.*: *J. Alloys Comp.*, **606**, 271 (1998).

[26] NAKANO, Y. *et al.*: *J. Nucl. Mat.*, **274**, 127 (1999).

[27] MUKAIYAMA, T. *et al.*: NEACRP-A-684 (1985).

[28] BEDNYAKOV, S. M. *et al.*: *Proc. Int'l. Conf. on Future Nuclear Systems GLOBAL'97*, Yokohama, Kanagawa, Japan, Vol.**2**, 800 (1997).

[29] YAMAWAKI, M. *et al.*: UTNL-R-0354, 32 (1997) (In Japanese).

[30] DULIN, V. A. *et al.*: *Atomic Energy*, **84**[6], 400 (1998).

[31] UNESAKI, H. and SHIROYA, S.: *Proc. International Conf. on the Physics of Nuclear Science and Technology*, Oct. 5-8, 1998, Long Island, New York, Vol. **2**, 1587 (1998).

[32] OBU, M.: JAERI-M 9757, Japan Atomic Energy Research Institute (1981) (In Japanese).

[33] KOBAYASHI, K. *et al.*: *J. Nucl. Sci. Technol.*, **36**, 20 (1999).

[34] KOBAYASHI, K. *et al.*: *J.Nucl Sci. Technol.*, **36**, 549 (1999).

[35] ANGELONE, M. and D'HONDT, P.: *Nucl. Instrum. Methods in Phys. Res.*, **A286**, 301 (1990).

[36] MORI, T. and NAKAGAWA, M.: JAERI-Data/Code 94-007, Japan Atomic Energy Research Institute (1995) (in Japanese).

[37] HIRAKAWA, N. *et al.*: *J. Nucl. Sci. Technol.*, **30**, 628 (1993).

[38] REMEC, I.: *Trans. Am. Nucl. Soc.*, **77**, 336 (1997).

[39] REMEC, I.: *Trans. Am. Nucl. Soc.*, **81**, 288 (1999).

[40] DERRIEN, H. and LUCAS, B.: NBS-SP-425, 637 (1975).

[41] NAKAGAWA, T.: *private communication* (2000).

# Chapter 5

# Conclusions

The present thesis summarized the results concerning the verification of nuclear data relevant to the neutronics design of next generation thermal reactors. The goal of the present research work is to provide quantitative measures on the validity of the current nuclear data relevant to the nuclear design of next generation thermal reactors, and also to provide suggestions for the anticipated reevaluation of the nuclides of major importance.

The present thesis is composed of the following three topics:

1) Study on the verification of nuclear data for MOX fueled thermal reactors,
2) Study on the verification of nuclear data for thorium-fueled thermal reactors, and
3) Study on the verification of nuclear data for MA incineration system using thermal reactors.

For the first topic, an analysis of benchmark problem devoted for void coefficient predictions in MOX fueled tight-pitch light-water reactor cells has been performed. Detailed analysis of the calculated results obtained by Japanese and French code systems has been performed to investigate the possible causes of the observed discrepancy in $k_\infty$ and void reactivity of MOX fueled light water lattices. Through the study, the following conclusions were obtained:

a) The discrepancy of the $k_\infty$ and void reactivity values obtained by the Japanese SRAC/JENDL-3.2 and French APOLLO-2/JEF2.2 is shown to be caused by a complicated balance of both the negative and positive components. The discrepancy of

$k_\infty$ values is mainly caused by the Pu-239 component, which shows a strong dependence on the void fraction, whereas the void fraction dependence of Pu-241 component strongly affects the overall reactivity discrepancy. The reactivity discrepancy therefore is sensitive to the Pu isotopic composition. Considerable discrepancy due to stainless steel clad and oxygen components is also observed.

b) The discrepancy of void reactivity is also caused by the Pu-239 and Pu-241 components. The difference between SRAC/JENDL-3.2 and APOLLO-2/JEF2.2 for the Pu-239 and Pu-241 components has opposite signs which act as to cancel each other; the overall discrepancy in the void reactivity therefore is sensitive to the isotopic composition of the Pu. Apart from the heavy nuclides, the different treatment of resonance self-shielding of the structure materials in the stainless steel cladding also acts as a cause of the discrepancies.

c) The discrepancies related to the structure materials and oxygen are significant, sometimes having the magnitude comparable to those of the heavy isotopes. The cross section difference for oxygen at high energy region has a considerable impact on cell parameters at the high void fraction. For structure materials, it was found that, not only the treatment of resonance self-shielding is important, but also the energy group structure in the keV region, where the structural material resonance plays an important role in forming the neutron spectrum.

For the second topic, an analysis of thorium loaded thermal reactor critical experiments at the KUCA has been performed. Criticality analysis using $^{232}$Th cross section data from different nuclear libraries has been performed to investigate the reproducibility of $k_{eff}$ values and also to clarify the possible causes of the observed C/E discrepancies. Through the study, the following conclusions were obtained:

a) It was found that JENDL-3.2 overestimates the $k_{eff}$ values of thorium-loaded KUCA cores by about 0.9% to 1.2%. Although approximately 0.7% of the overestimation comes from the $^{235}U$ cross section used in the driver region, the overestimation for thorium-loaded cores is apparently larger than those for cores free from thorium by about 0.2% to 0.5%. This overestimation depends on neutron spectrum and becomes larger for the cores with harder neutron spectrum. The use of $^{232}Th$ cross sections from ENDF/B-VI and JEF2.2 also leads to the overestimation of the $k_{eff}$ values. Compared to JENDL-3.2, $^{232}Th$ cross sections from ENDF/B-VI and JEF2.2 give smaller $k_{eff}$ for the cores with a harder neutron spectrum, leading to reactivity difference up to -0.5% . It became clear that none of the current $^{232}Th$ evaluated cross sections can accurately simulate the criticality of the KUCA experiments.

b) It was demonstrated that the different $^{232}Th$ cross section evaluations may lead to significant difference in criticality predictions of thorium-loaded thermal systems. This difference is mainly attributable to the difference in capture cross section at the thermal region, lower resonance and unresolved resonance regions, where JENDL-3.2 gives significantly smaller cross sections compared to ENDF/B-VI. The contribution of scattering cross section difference in the fast region could be also significant in systems with a harder neutron spectrum.

For the third topic, measurement and analysis of the $^{237}Np$ and $^{241}Am$ fission rate ratios relative to $^{235}U$ in thermal neutron fields of the KUCA have been performed. Analysis using fission cross section data of $^{237}Np$ and $^{241}Am$ from different nuclear libraries has been performed to investigate the reproducibility of fission rate ratios and the possible causes of the observed C/E discrepancies. Through the study, the following conclusions were obtained:

a) By using the back-to-back type double fission chamber at five thermal cores with

different H/$^{235}$U values, the $^{237}$Np and $^{241}$Am fission rate ratios relative to $^{235}$U fission rate were successfully measured within a typical uncertainty of 2%.

b) For the $^{237}$Np/$^{235}$U fission rate ratio, it was found that the use of JENDL-3.2 gives the C/E values of 0.95 in average, which was the best estimate among the three libraries used. The use of the $^{237}$Np fission cross sections in ENDF/B-VI and JEF2.2 gives approximately 4% smaller $^{237}$Np fission rate compared to the results obtained by using JENDL-3.2. It is recommended that further improvement should be pursued for the evaluation of both the fast fission and resonance regions in all libraries. Nevertheless, the $^{237}$Np fission cross sections in JENDL-3.2 are considered to be superior to those in the other libraries and can be sufficiently adopted in design calculations for the minor actinide transmutation system using thermal reactors with prediction precision of $^{237}$Np fission rate within 10%.

c) For the $^{241}$Am/$^{235}$U fission rate ratio, it was found that the use of $^{241}$Am fission cross section in JENDL-3.2 underestimates the experiment by about 12% and gives the C/E values of 0.88 in average. The C/E values obtained by using $^{241}$Am cross sections of ENDF/B-VI and JEF2.2 are larger than those obtained by using JENDL-3.2 by about 2% and 7 to 9%, respectively. Through the examination of the difference of $^{241}$Am cross sections contained in the evaluated libraries, it was found that cross section differences at the vicinity of resonance at 0.576 eV are the dominant cause of the C/E difference between JENDL-3.2 and JEF2.2. Contribution of thermal cross section difference, especially in the range of 0.01 eV to 0.2 eV, becomes also apparent for well-thermalized cores. It is recommended that both the resonance and thermal energy fission cross sections of $^{241}$Am should be reevaluated in JENDL-3.2.

Through the conclusions of the present studies described above, the following recommendations could be made for the improvement of cross section data relevant to the

nuclear design of the next generation thermal reactors;

**Pu isotopes :**

- Cross sections of $^{239}$Pu and $^{241}$Pu.

  Ambiguity of cross section of these two major Pu isotopes should be further reduced for the accurate prediction of nuclear parameters in MOX fueled thermal reactors, especially in cases having hard spectrum.

In order to further enhance our knowledge on the behaviour of plutonium isotopes in MOX fuel cells with hard neutron spectrum, sensitivity studies should be performed as an extension of the studies presented in this thesis. Furthermore, re-analysis of the critical experiments related to void reactivity (for example, the PROTHEUS-HCLWR experiments) would be very useful to directly validate the accuracy of plutonium cross section data, especially performed in conjunction with the sensitivity studies.

**$^{232}$Th :**

- Capture cross sections at the thermal, lower resonance and unresolved resonance regions.

  None of the current $^{232}$Th evaluated cross sections can accurately simulate the criticality of the zone-type experiments performed at the KUCA. Furthermore, the differences among the libraries are significant, and therefore the neutronics characteristics of any thorium-fueled thermal reactor may be considerably different among the libraries used.

- Elastic and inelastic scattering cross sections in the fast region.

  The contribution of these cross section differences could be considerable in systems with a hard spectrum.

As the experimental data directly applicable for the verification of $^{232}$Th cross sections are still limited, sample reactivity and reaction rate measurements of $^{232}$Th in cores with

various neutron spectra will be of great importance. Concerning this study, a series of experiments recently initiated at the KUCA for the sample worth measurement of $^{232}$Th is anticipated to provide valuable experimental data in the near future.

**$^{237}$Np:**

- Fission cross sections in both the fast fission and resonance regions in all libraries.

  The cross section difference is significant and should be reduced to improve the prediction accuracy of $^{237}$Np fission rate in incineration systems.

**$^{241}$Am:**

- Fission cross sections at the giant resonance at 0.576 eV and the thermal region.

  The significant difference among JEF2.2 and other two libraries lead to large difference in C/E of the KUCA experiments. These cross section differences should be reduced to improve the prediction accuracy of $^{241}$Am fission rate in incineration systems.

Experimental data for the MA cross section, especially for $^{237}$Np, are still limited, and accumulation of experimental data is desired to improve the accuracy of MA nuclear data in the evaluated libraries. Together with this, accumulation of integral data, such as reaction rate measurements, is also desired. From this point of view, the systematic experiments performed at the KUCA in this study are considered to be an excellent benchmark data for MA incineration study in thermal neutron reactors. In order to enhance this benchmark data and to merge the results with those from the fast neutron systems, fission rate ratio measurements in intermediate spectrum cores are desired.

It is expected that the improvement of the aforementioned cross section evaluations and related studies will lead to the improvement of the reliability and prediction accuracy of nuclear parameters of next generation thermal reactors.

# Appendix

# Nomenclature

ABBREVIATIONS

| | |
|---|---|
| MA | minor actinide |
| MOX | mixed-oxide |
| TRU | transuranium elements |
| LWR | light water reactor |
| HCLWR | high-conversion light water reactor |
| RMWR | reduced moderation water reactor |
| JENDL-3.2 | Japanese Evaluated Nuclear Data Library, ver. 3.2 |
| ENDF/B-VI | Evaluated Nuclear Data File, B, ver. VI |
| JEF2.2 | Joint Evaluated File, ver. 2.2 |
| KUCA | Kyoto University Critical Assembly |
| BTB | back-to-back type fission chamber |
| C/E | calculated- to-experimental ratio |

DEFINITIONS, UNITS

| | |
|---|---|
| void fraction | volumetric fraction (%) of void in moderator region. In Chapter 2, only the void fraction of infinite array of fuel lattices are treated. |
| void reactivity | reactivity change caused by void in moderator region |
| pcm | 1 pcm = $1 \times 10^{-5}$ $\Delta k / k$ |

MATHEMATICAL EXPRESSIONS

| | |
|---|---|
| $k_{\infty}$ | infinite multiplication factor |
| $k_{eff}$ | effective multiplication factor |
| $g$ | suffix for energy group (fine group structure) |
| $G$ | suffix for energy group (coarse group structure) |
| $i$ | suffix for nuclide |

| | |
|---|---|
| $\phi$ | neutron flux |
| $\rho$ | reactivity |
| $\Delta\rho$ | reactivity difference |
| $\Sigma_f$ | macroscopic fission cross section |
| $\Sigma_c$ | macroscopic capture cross section |
| $\Sigma_{(n,2n)}$ | macroscopic $(n,2n)$ cross section |
| $\nu$ | average number of neutrons produced per fission |
| $P, A, C, N$ | production, absorption, capture and $(n,2n)$ rate in an infinite cell |
| $\Delta P, \Delta A, \Delta C, \Delta N$ | difference of production, absorption, capture and $(n,2n)$ rate in an infinite cell |
| $\overline{P}$, $\overline{A}$ | averaged value of the integrated production and absorption rate in a infinite cell |
| $\overline{k_\infty}$ | averaged value of the infinite multiplication factor |

# Acknowledgments

The author would like to express his gratitude to Professor Seiji Shiroya of Kyoto University for his guidance, generous suggestions and continuous encouragement on this study.

The author expresses his gratitude to Professor Kaichiro Mishima of Kyoto University for his helpful suggestions and continuous discussions on this study.

The author also expresses his gratitude to Professor Nobuhiro Morishima of Kyoto University for his beneficial discussions on this study.

The author is deeply indebted to Associate Professor Tsuyoshi Misawa of Kyoto University for his generous help and suggestions in the course of this study.

The author expresses his gratitude to Associate Professor Yuji Nakamura of Kyoto University for his beneficial discussions on this study.

The author would like to express his gratitude to Prof. Keiji Kanda of Kyoto University for his generous support and encouragement in the course of this study.

The author expresses his thanks to all the members of the KUCA staff, including Prof. Masatoshi Hayashi (present address: Kyushu University of Health and Welfare), Messrs. Keiji Kobayashi, Chihiro Ichihara, Hiroshi Nakamura, Toshimitsu Sagane, Ryusho Ikegawa and Hiroshi Yamamoto for their cooperation in the KUCA experiments and advises during the analysis.

The author expresses his gratitude to Prof. Toshikazu Takeda of Osaka University for his invaluable suggestions and the continuous encouragement in the course of this study.

The author is indebted to the members of the University Association of Japan for the invaluable suggestions on the studies summarized in Chapter 2. The author would like to especially express his gratitude to Prof. Otohiko Aizawa of Musashi Institute of Technology for the invaluable suggestions through the study.

The study summarized in Chapter 2 have been performed during the author's six-month stay as a visiting researcher at Centre d'Etude de Cadarache, CEA, France. The author would like to express his gratitude to Dr. Stephane Cathalau, SPRC/LEPh, CE Cadarache,

CEA, for his generous help and fruitful discussions on the benchmark analysis. The author also should express his sincere thanks to the hospitality of all the staffs of SPRC/LEPh during his stay at CE Cadarache.

Thanks are also due to Drs. Kei-ichiro Tsuchihashi, Takamasa Mori, Keisuke Okumura and Hiroshi Akie of Japan Atomic Energy Research Institute for their invaluable comments on the usage of SRAC and MVP codes.

The study summarized in Chapter 4 was performed within the framework of the KUCA joint study program with Tohoku University and Osaka University. The author expresses his thanks to Dr. Tomohiko Iwasaki of Tohoku University and Mr. Takanori Kitada of Osaka University for their cooperation and fruitful discussions during the experiments and analysis.

The author would like to express their sincere thanks to Prof. Katsuhei Kobayashi and Dr. Shuji Yamamoto for their generous help and advice during the experiment described in Chapter 4, especially for the preparation of BTB chamber and for the instructions in $\alpha$-ray spectrometry measurement of the U sample. The acknowledgment should also be addressed to Associate Professor Hiromu Yamana for his generous instructions and advices for the handling of the MA and $^{235}U$ samples.

Last, but not least, the tireless and warm support of the author's wife, Midori, and the sweetest daughters, Moe and Mio, cannot be thanked enough.

A part of this study was supported by Grant-in-Aid for Scientific Research from the Ministry of Education, Science, Sports and Culture in Japan. A part of this study is also supported by Research for the Future Program from the Japan Society for the Promotion of Science (JSPS). A part of numerical calculations has been performed at the Data Processing Center of Kyoto University.